NOVEL METALLOCALIXARENES AS DISPERSED CATALYSTS FOR HEAVY OIL UPGRADING

BY

TAREQ ALI SALEM AL-ATTAS

A Thesis Presented to the

DEANSHIP OF GRADUATE STUDIES

KING FAHD UNIVERSITY OF PETROLEUM & MINERALS

DHAHRAN, SAUDI ARABIA

In Partial Fulfillment of the
Requirements for the Degree of

MASTER OF SCIENCE

In

CHEMICAL ENGINEERING

NOVEMBER 2018

KING FAHD UNIVERSITY OF PETROLEUM & MINERALS

DHAHRAN- 31261, SAUDI ARABIA

DEANSHIP OF GRADUATE STUDIES

This thesis, written by **TAREQ ALI AL-ATTAS** under the direction of his thesis advisor and approved by his thesis committee, has been presented and accepted by the Dean of Graduate Studies, in partial fulfillment of the requirements for the degree of **MASTER OF SCIENCE IN CHEMICAL ENGINEERING.**

Dr. Mohammad M. Hossain
(Advisor)

Dr. Mamdouh Al-Harthi
Department Chairman

Dr. Md Hasan Zahir
(Co-Advisor)

Dr. Salam A. Zummo
Dean of Graduate Studies

Dr. Mohammed Ba-Shammakh
(Member)

7/2/19
Date

Dr. Zuhair Omar Malaibari
(Member)

Dr. Shaikh Abdur Razzak
(Member)

Dedicated to my parents Allah Almighty blesses them

ACKNOWLEDGMENTS

All Praises and gratitude to Almighty Allah for giving me strength, endurance and patience to complete this work successfully. In addition, I thank my family for their unlimited support that enabled me, after the will of Allah, to reach what I am being on now. Thereafter, I am thankful to King Fahd University of Petroleum and Minerals for offering me the opportunity to pursue my graduate studies.

I would like to express my sincere gratitude and deep appreciation to my thesis advisor, Prof. Mohammad M. Hossain, for the continuous support of my MSc study and research, for his immense knowledge, enthusiasm, and motivation. His guidance had significantly helped me in conducting and composing this thesis. My sincere thanks also go to the co-advisor, Dr. Md Hasan Zahir, for his excellent guidance, motivation and inspiration. I would like to extend my gratitude and appreciation to the thesis committee members, Dr. Mohammed Ba-Shammakh, Dr. Zuhair Omar Malaibari and Dr. Shaikh Abdur Razzak, for their immense assistance and invaluable suggestions.

I wish to thank Dr. Syed Ali from the Center for Refining and Petrochemicals (CRP) at KFUPM and Dr. Saad Al-Bogami from the Research and Development Center (R&DC) of Saudi Aramco Company for their contributions to this project. My grateful thanks are also extended to my senior colleagues, Dr. Sagir Adamu, Mr. Emad Bdwi and Mr. Ahmed Alrashidy, for their assistance and support throughout my research work. Also, I would like to thank all the staff in the Department of Chemical Engineering including Mr. Sarath Unnikrishnan, Mr. Syed Amanullah, and Mr. Mohammed Elgzoly for their collaboration. Finally, I want to express my deepest appreciation to the Department of Chemistry, Center for Engineering Research (CER), Center of Research Excellence in Renewable Energy (CoRE-RE) and Center of Research Excellence in Nanotechnology (CENT) for their collaborations in helping me to perform some of the material characterizations in this study.

TABLE OF CONTENTS

LIST OF TABLES

LIST OF FIGURES

LIST OF ABBREVIATIONS

^{1}H NMR	:	Proton Nuclear Magnetic Resonance
AR	:	Atmospheric Residue
C/O	:	Catalyst to Oil ratio
CUS	:	Coordinatively Unsaturated Sites
DSC	:	Differential Scanning Calorimetry
DTA	:	Differential Thermal Analysis
DTG	:	Differential Thermogravimetric Analysis
EDX	:	Energy-Dispersive X-ray
EXAFS	:	Extended X-ray Absorption Fine Structure
FBP	:	Final Boiling Point
FCC	:	Fluid Catalytic Cracking
FID	:	Flame Ionized Detector
GC	:	Gas Chromatography
HDC	:	Hydrocracking
HDM	:	Hydrodemetalation
HDN	:	Hydrodenitrogenation
HDS	:	Hydrodesulfurization

HGO	:	Heavy Gas Oil
HVGO	:	Heavy Vacuum Gas Oil
I	:	dimensionless catalytic activity parameter
IBP	:	Initial Boiling Point
ICP	:	Inductively coupled plasma
PAHs	:	Polycyclic Aromatic Hydrocarbons
R	:	Universal gas constant
SEM	:	Scanning Electron Microscopy
T	:	Temperature of reaction
TBC[4]	:	*p-tert*-butylcalix[4]arene
TBP	:	True Boiling Point
TCD	:	Thermal Conductivity Detector
TEM	:	Transmission Electron Microscopy
TGA	:	Thermogravimetric Analysis
UV-Vis	:	Ultraviolet-Visible
VGO	:	Vacuum Gas Oil
VR	:	Vacuum Residue
XPS	:	X-ray Photoelectron Spectroscopy
XRD	:	X-Ray Diffraction

ABSTRACT

Full Name : Tareq Ali Salem Al-Attas

Thesis Title : Novel Metallocalixarenes as Dispersed Catalysts for Heavy Oil Upgrading

Major Field : Chemical Engineering

Date of Degree : November 2018

This study investigates the potential of applying metal-based *p-tert*-butylcalix[4]arenes (TBCs[4]) as oil-soluble dispersed catalyst precursors to enhance catalytic hydrogenation reactions involved in the upgrading of vacuum gas oil (VGO). Co- and Ni-TBC[4] were synthesized and characterized by SEM-EDX, ICP, XRD, UV-Vis, FT-IR, and ^{1}H NMR to confirm the coordination of the cations with the TBC[4] ligand to form organometallic compounds. The thermogravimetric and calorimetric behaviors of the synthesized complexes, which are key properties of dispersed hydrocracking catalysts, were also observed. The differential scanning calorimetry (DSC) profile of Ni-TBC[4] and Co-TBC[4] showed that the organometallic structure has diminished thermal stability compared with that of the parent TBC[4]. The performance of the synthesized catalyst precursors was evaluated using an autoclave batch reactor with varying concentrations of catalyst precursors at 390-450°C. The results show that the synthesized metal-based TBC[4] dispersed catalysts evidently boosted the hydrogenation reactions and suppressed coke deposition. The addition of 500 ppm Co-TBC[4] and Ni-TBC[4] as standalone dispersed catalysts produced distillate yields of 45.7 wt% and 49.7 wt% and a coke laydown of 2.6 wt% and 2.3 wt%, respectively. A co-catalytic system was further applied by introducing the synthesized Ni-TBC[4] dispersed catalyst precursor in addition to a presulfided, commercial, first-stage hydrocracking supported catalyst named KC-2710. The results showed that the yields of coke and gases decreased upon introducing the dispersed catalyst along with the supported solid catalyst by 35.86 % and 13.90 %, respectively. The yields of naphtha increased from 15.27 wt% to 16.36 wt%, and those of distillate increased from 52.17 wt% to 53.57 wt% compared with the use of the supported catalyst, where the conversion of VGO was comparable at ~83.20 %. The value of the dimensionless catalytic activity parameter proved the existence of the synergy between the two catalysts since it is much higher than that acquired through the algebraically calculated yields. A five lump discrete kinetic scheme was developed based on the experimental data governed from both the standalone supported catalyst and the mixed-phase catalyst. The model incorporated the VGO conversion to middle distillate, naphtha, and C1-C5 gaseous hydrocarbons in addition to coke deposition. The activation energy of the distillate was markedly reduced from 65.39 kcal/mol to 57.32 kcal/mol by adding a Ni-TBC[4] catalyst precursor in addition to the supported catalyst.

GRAPHICAL ABSTRACT

Full Name : Tareq Ali Salem Al-Attas

Thesis Title : Novel Metallocalixarenes as Dispersed Catalysts for Heavy Oil Upgrading

Major Field : Chemical Engineering

Date of Degree : November 2018

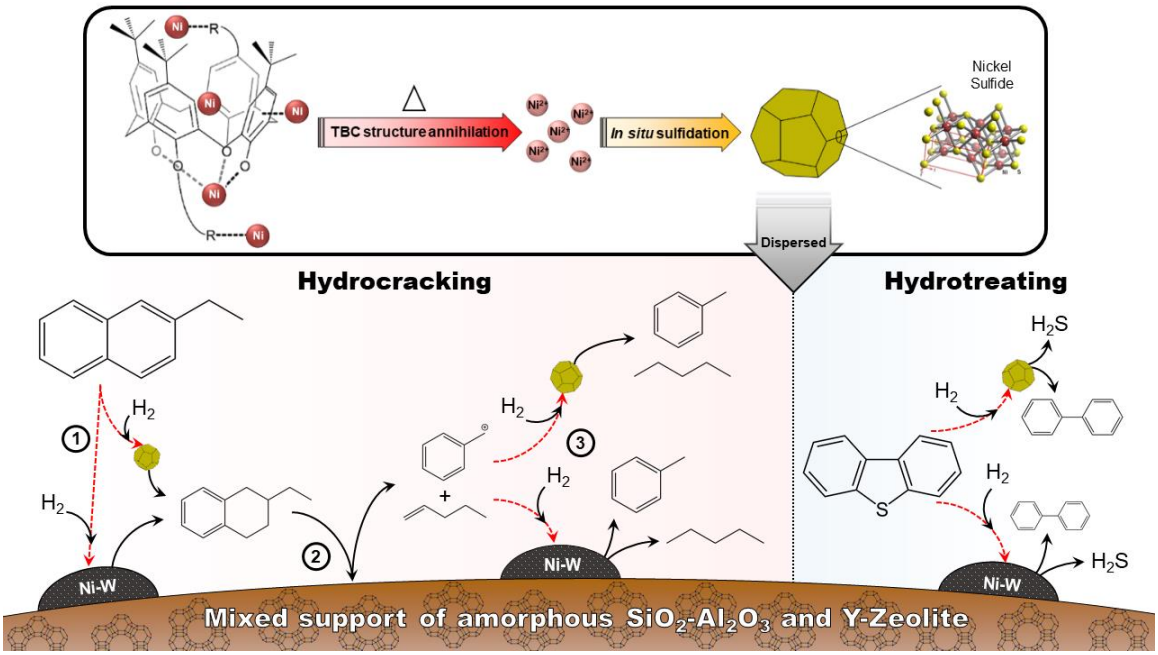

ملخص الرسالة

الاسم الكامل: طارق بن علي سالم العطاس

عنوان الرسالة: استخدام كاليكسارينات معدنية كمحفزات مشتَّتة لترقية الزيت الثقيل

التخصص: هندسة كيميائية

تاريخ الدرجة العلمية: نوفمبر 2018

تتطرق هذه الدراسة لإمكانية استخدام البارا-ثالثي-بيوتيل الكاليكس[4]-ارين (TBC[4]) المستند بالفلزَّات كسلائف لمحفّزات قابلة للذوبان في الزيت لتعزيز تفاعلات الهدرجة المتضمّنة في عملية التكسير الهيدروجيني لزيت الغاز الفراغي (VGO). تم توليف مركّبات الكاليكسارين المعدنية مع الكوبالت والنيكل والتي تم توصيفها فيما بعد من خلال إجراء تقنيات تحليلية مختلفة للتحقق من تنسيق الكاتيونات مع هيكل البارا-ثالثي-بيوتيل الكاليكس[4]-ارين لتشكيل معقَّدات تناسقية والتي هي: مجهر إلكتروني ماسح مقترِن بمطيافية تشتت الطاقة بالأشعة السينية (SEM-EDX) ومطيافية البلازما المقترنة حثيًا (ICP) وحيود الأشعة السّينية (XRD) ومطيافية الأشعة المرئية وفوق البنفسجية (UV-Vis) ومطيافية تحويل فوريه للأشعة تحت الحمراء (FT-IR) ومطيافية الرنين المغناطيسي النووي للبروتون (^{1}H NMR). بالإضافة لذلك، تم تحليل السلوكيات الحرارية والمسعرية للمركبات الفلزية العضوية والتي تعتبر من الخصائص الرئيسة لسلائف المحفزات المشتَّتة المستخدمة في التكسير الهيدروجيني. أظهرت المنحنيات الناتجة عن مسعر المسح التباييني (DSC) لكلا المركّبين المحضّرين أن إنْشاء البنية الفلزية العضوية قد قلل من ثباتها الحراري مقارنة مع الربيطة العضوية الأصلية. تم تقييم القدرة التحفيزية للسلائف المركّبة باستخدام مفاعل دفعي موصد عن طريق تغيير ظروف التفاعل كدرجة الحرارة (390 إلى 450 درجة مئوية) وفترة التفاعل (نصف ساعة إلى ساعة ونصف) وتركيز سلائف المحفز. أوضحت النتائج أن المحفزات المشتَّتة قد حسَّنت أداء تفاعلات الهدرجة وساعدت في تقليل تكوُّن فحم الكوك البترولي. إن إضافة 500 جزء من المليون من الكوبالت والنيكل زاد من إنتاجية المقطّرات الوسطَى إلى 45.71% بالوزن و49.66% بالوزن بينما انخفضت ترسبات فحم الكوك إلى 2.60% بالوزن و2.26% بالوزن، على التوالي. كما تم تطبيق نظام تحفيزي ثنائي عن طريق إدخال سلائف النيكل المحفز مع محفز تكسير هيدورجيني تجاري صلب مدعوم. أظهرت النتائج أن إضافة الكاليكسارين المعدني قد عزّزت نشاط تفاعلات الهدرجة وخفّضت بشكل ملحوظ تكوّن الغازات وفحم الكوك. علاوة على ذلك، تحّسنت جودة المنتج السائل عن طريق تعزيز نسبة الهيدروجين إلى الكربون وكذلك تقليل محتويات الكبريت والنيتروجين. أظهرت النتائج أن عوائد فحم الكوك والغازات قد انخفضت عند إدخال المحفز المشتّت مع المحفّز الصلب المدعوم بنسبة 35.86% و13.90%، على التوالي. ارتفع ناتج النافثا من 15.27% بالوزن إلى 16.36% بالوزن، وتقطير من 52.17% بالوزن إلى 53.57% بالوزن مقارنة باستخدام المحفّز المدعوم حيث أظهرت نسبة تحوُّل لزيت الغاز الفراغي مقاربةً عند 83.20%. أثبتت قيمة معامل النشاط الحفزي بلا أبعاد وجود التآزر بين المحفزين حيث أنها أعلى بكثير من تلك المكتسبة من خلال الغلَّة المحسوبة جبريًا. تم تطوير آلية تفاعل حركي ذو خمسة كتل منفصلة استنادًا إلى البيانات التجريبية المستقاة من خلال تطبيق المحفز المستقل المدعم بذاته ومقارنته بنظام تحفيزي الثنائي المشتمل على سلائف محفّز النيكل المشتَّت. يفترض النموذج تحويل زيت الغاز الفراغي إلى كلٍّ من مقطّرات وسطى ونافثا وغازات هيدروكربونية إلى جانب مرسّبات فحم الكوك. شهدت طاقة التنشيط الخاصة بإنتاج المقطرات انخفاضًا ملحوظًا من 65.39 كيلو كالوري/مول إلى 57.32 كيلو كالوري/مول بعد إضافة نيكل البارا-ثالثي-بيوتيل الكاليكس[4]-ارين بجانب المحفز المدعوم.

ملخص تصويري للرسالة

الاسم الكامل: طارق بن علي سالم العطاس

عنوان الرسالة: استخدام كاليكسارينات معدنية كمحفزات مشتَّتة لترقية الزيت الثقيل

التخصص: هندسة كيميائية

تاريخ الدرجة العلمية: نوفمبر 2018

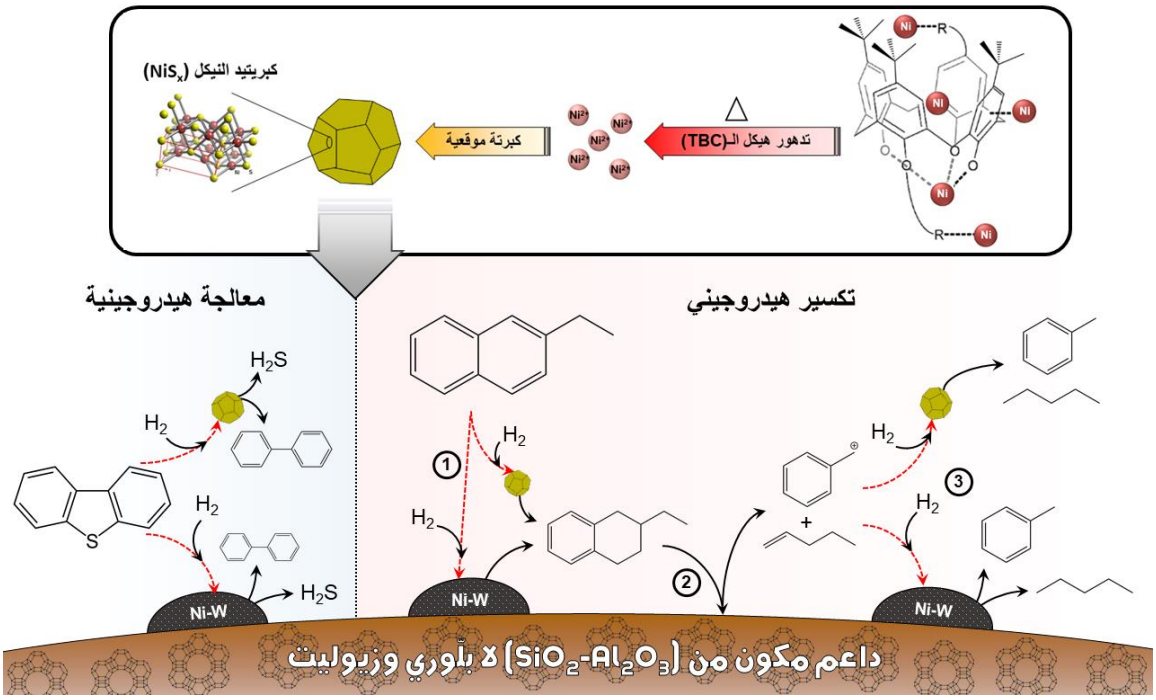

CHAPTER 1

INTRODUCTION

1.1 Background

The depleted supply of light crude oil and the increasing demand for high-value fuels has encouraged petroleum refiners to process low-value feedstocks, such as fuel oil, bitumen and residual oils (Figure 1-1). Some of the most important issues that alarmed the problem is the fact that the decrease in the availability of conventional crude due to the massive dependence on light oil [1]. Consequently, the utilization of every part of heavy petroleum feedstocks represents the facile challenge to solve the issue of the increased demand of light fuels and to reduce the dependency on conventional crude oil reserves. One of the most favorable techniques that used to be carried out is the optimized utilization of the heavy oil through different processes that are conducted in refineries. Heavy oil is found either in nature or due to thermal/catalytic processes inside within refineries. Naturally, heavy oil is found either in the form of heavy crude oil or extra-heavy crude that could be referred to as bitumen. Moreover, the heavy oil could be part of the problem inside the petroleum refining due to the non-destructive physical separation processes that take place in the atmospheric distillation as well as the vacuum distillation to give heavy residues, such as vacuum residue (VR), vacuum gas oil (VGO) and atmospheric gas oil (AGO) [2].

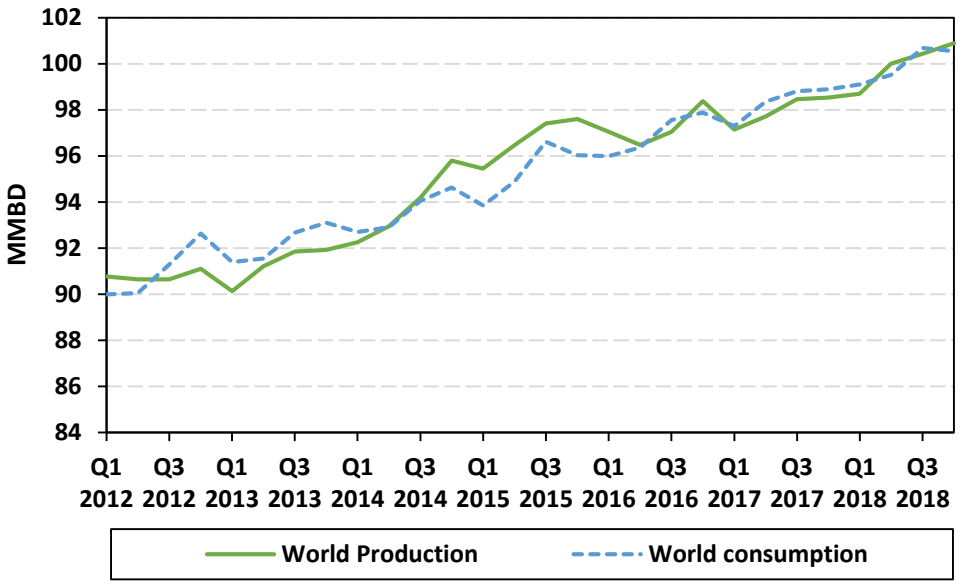

Figure 1-1 World's production and consumption capacity of liquid fuels. Adapted from Ref. [1].

Several technologies were invented in the refining industry to upgrade the heavy oil and this job was mainly done by two means; either by thermal processes or catalytic processes. The thermal processes include some techniques, such as delayed-coking, flexi-coking, visbreaking and fluid-coking [2]. On the other hand, the catalytic upgrading of the heavy oil is conducted through either catalytic hydrocracking or fluid catalytic cracking (FCC). In order to get rid of the most problematic issue in heavy oil, which is the condensation of the polynuclear aromatics the cause the formation of coke, catalytic cracking conducted by utilizing hydrogen was a revolutionary leap and it was referred to as “Hydrocracking”. Catalytic hydrocracking has become an important component for the petroleum refining industry for upgrading low-value feedstocks [3–5]. The first appearance of hydrocracking was In Germany in 1915 to provide light valuable liquids that could be derived from their coal resources. In 1927, the first attempt to build a commercial hydrocracking unit was

begun in Leuna, Germany [6, 7]. After that, this technology of converting coal to liquid fuels started to spread to other countries such as Great Britain and France. Between 1925 and 1930, a collaboration was initiated between I.G. Farben Industrie of Germany and Standard Oil of New Jersey to develop catalytic hydrocracking unit that is more efficient in converting heavy petroleum oils into fuels [2]. Unfortunately, the invented process was very expensive because it needs high pressure that reaches 200.0 to 300.0 bar and a temperature of 375 °C. In Germany in 1929, the first hydrogenation process of coal was commercially employed in only two units. Then, during the world war II, the feed was converted to vacuum residue (VR) where it was working on only two units until 1964 [7]. Later in 1939, the British Imperial Chemical Industries company created a new technology of hydrocracking which is the two-stage hydrocracking. This technology has played a significant role in producing aviation gasoline in World War II for the United States, Great Britain and Germany. Due to the abundance of crude petroleum that had been discovered in the Middle East, the importance of hydrocracking became lesser [3]. After that, a new catalytic cracking technology, i.e. the fluid catalytic cracking (FCC), was considered to be a more attractive alternative to hydrocracking in terms of the economics for converting heavy oils to high-value fuels. Nevertheless, later in the 1960s, the importance of catalytic hydrocracking had been reestablished due to several reasons [3, 8, 9]:

- High-octane gasoline that is produced in hydrocracking started to become more important due to the development in the automobile industry that requires this type of gasoline.

- Although that fluid catalytic cracking can produce high-octane gasoline, its gasoline effluent contains cycle oil, high-boiling oil, which is challenging to be recycled back

for further cracking. However, cracking of such heavy feedstock could be achieved by hydrocracking.

- The demand for jet fuel and diesel oil showed an increased due to the switch from steam engines to engines operating on diesel public transportations. Hydrocracking flexibility of producing either diesel oil, jet fuel, or gasoline made the refineries to favor hydrocracking.

During the late 1960s, the hydrocracking units in the United States became a mature process and after that its development has kept proceeding at a slow pace. Nevertheless, this wasn't the situation for many countries and regions that faced huge growth in the Middle East, the Asia-Pacific and Europe. In 2001, the number of hydrocracking units reached 155 worldwide with a feedstock capacity of four million barrels (550,000 metric tons) per day [2]. Catalytic hydrocracking has become a promising technology for upgrading the value of heavy petroleum feedstocks since the past three decades. Figure 1-2 shows the capacity of different catalytic processes in Saudi Arabian refineries.

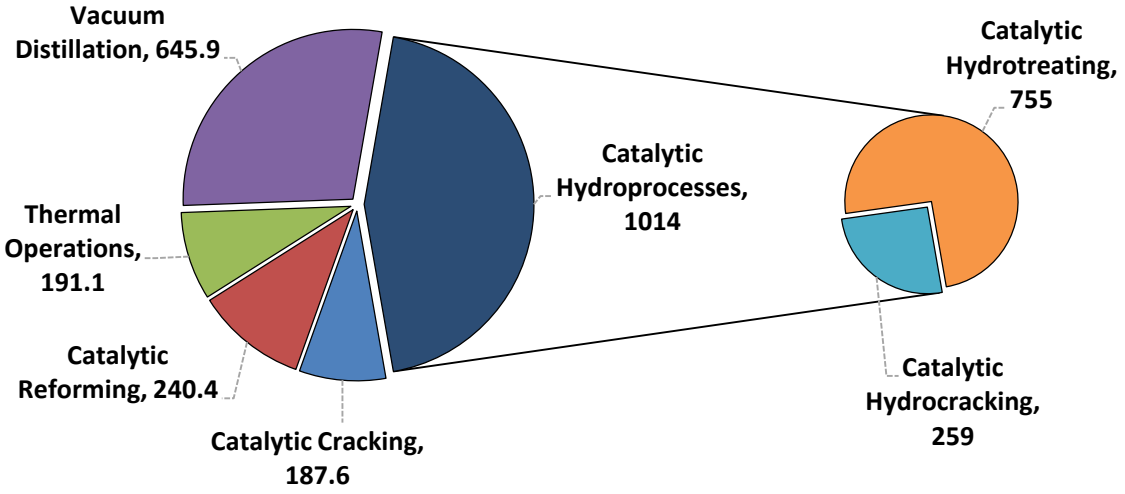

Figure 1-2 Petroleum refining units' capacity of OPEC countries in 2016 (1000 b/cd). Source (2017's OPEC annual statistical bulletin).

1.2 Slurry-Phase Hydrocracking

Different technologies for hydrocracking process were developed and they were still widely used for heavy oil upgrading by employing different reactor types, such as fixed-bed, moving-bed, slurry-phase and ebullated-bed. In principle, all these types of process work on the same techniques, however, they differ in some technical operations and their capability of handling impurities [2]. Moreover, the adoption of a proper technology for upgrading heavy oil depends on the nature of the feed and the reaction conditions where every technology has its own specifications and type of catalyst.

In terms of hydrotreating process, fixed-bed reactors are the most widely used for treating middle distillates or feed with high API, however, for heavy feed the case is different because of the regeneration of the deactivated catalyst limitation. Hydrotreating of heavy oil causes the catalyst to be deactivated fast, so continuous withdrawal and regeneration of the catalyst are required in this case [9]. Fortunately, moving-bed reactor and ebullated-bed reactor are alternatives to solve this problem. The deactivated catalyst in the moving-bed reactors is continuously leaving the reactor from the bottom for regeneration while the fresh catalyst is fed from the top of the reactor [8]. Also, the pressure drop in moving-bed reactors is decreased to some extent because that the catalyst, unlike the fixed-bed reactors, is simultaneously expanded with the flow. In terms of the hydrocracking process, heavy oil could be fed to the fixed-bed reactor where the different catalysts must be either mixed or packed in multiple beds. However, for very heavy feed combination of fixed-bed with either moving-bed ebullated-bed or reactors could be an effective choice [10].

Different parameters should be considered when using hydrocracking processes such as the size of the particles, the intraparticle mass transfer between solid and liquid phases, and the amplitude of agitation speed. There are some limitations commonly occur while using ebullated-bed, moving-bed and fixed-bed reactors for heavy oil upgrading such as pressure drop, mass transfer limitations, and diffusion of feeds [10]. The slurry-phase reactor is an alternative technology that could be efficiently employed to overcome one of the most important issues which is the mass transfer [6, 10]. The intraparticle mass transfer limitation arises between the solid (supported catalyst) and the liquid (heavy oil) could be diminished by implementing slurry-phase process that applies high agitation speed leading to enhance the turbulence of the fluid [5].

Among the available technologies of hydrocracking, the slurry-phase hydrocracking technology is considered as the most recently developed and where the research is still going on it widely due to its features. It is capable to convert more than 95% of the heavy oils [6, 7, 10]. Additionally, the utilization of slurry-phase hydrocracking assures the formation of lower amounts of coke compared to other processes, which leads to maintain the amount of liquid product produced from being lost in the sediment [6]. Figure 1-3 shows a schematic diagram of a typical slurry-phase hydrocracker [11].

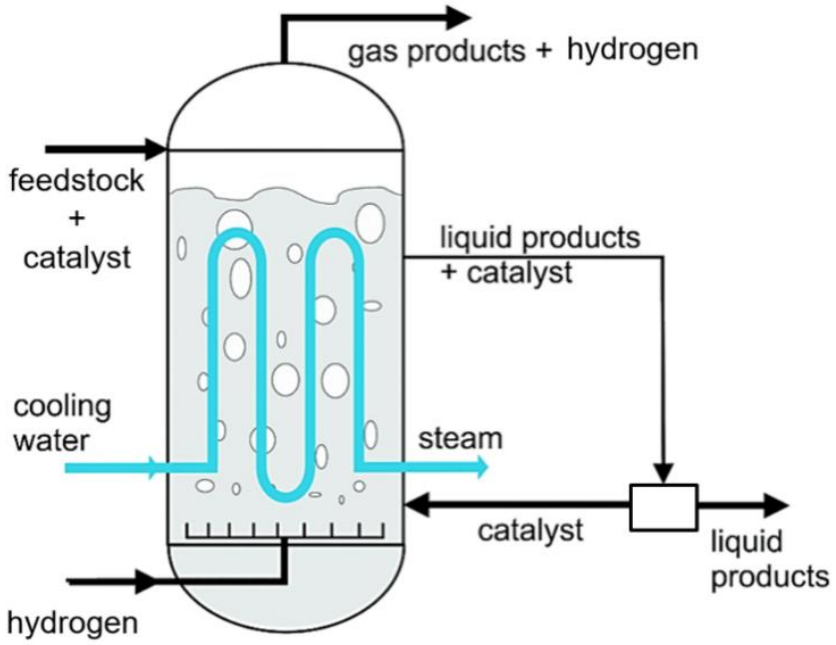

Figure 1-3 A schematic diagram of a typical slurry-phase hydrocracker [11].

Keeping the above into consideration, the present research has been focused on investigating Co- and Ni-based *p-tert*-butylcalix[4]arenes (TBC[4]s) organometallic complexes as potential oil-soluble dispersed catalyst precursors for boosting hydrogenation activity during slurry phase hydrocracking processes. Following are the major contributions of this research:

i. Developed new Co- and Ni-based TBC[4]s catalyst precursors suitable for in-situ activation (sulfiding) in slurry phase hydrocracking reaction conditions.

ii. Demonstrated promising performances of the developed Co- and Ni-based TBC[4]s catalyst precursors, both as stand-alone catalysts and co-catalyst (with a commercial Ni-W/SiO_2-Al_2O_3-(Y-zeolite) catalyst) in slurry phase hydrocracking of heavy vacuum gas oil (HVGO).

iii. Developed the kinetics model and estimated the kinetics parameters that clearly showed the synergy between Ni-based TBC[4]s and Ni-W/SiO_2-Al_2O_3-(Y-zeolite) catalyst in hydrocracking of HVGO.

CHAPTER 2

LITERATURE REVIEW

The researches on the slurry-phase hydrocracking of heavy oil are mainly categorized according to the type of catalyst precursor used, that is either in finely powdered form or soluble form. The nature of the catalyst precursors affects their catalytic activity in terms of the degree of dispersion and the catalyst particle sizes. The activation of the dispersed catalysts is accomplished through *in situ* or *ex situ* sulfidation. The catalytic activity of the metal sulfides (active form of the catalyst) is understood by studying their crystalline structures. Moreover, studies have suggested the simultaneous application of homogeneously dispersed catalysts along with solid supported catalysts for studying their synergic effects on the hydrocracking of heavy oils. Kinetic modeling is a major tool to further commenting on the enhancement of the catalytic hydrogenation/dehydrogenation reactions governed upon introducing the dispersed catalyst. This chapter presents the literature review that covers the types of catalysts/catalyst precursors used for slurry-phase hydrocracking, the nature of the dispersed catalyst and the kinetic modeling.

2.1 Catalysts for Slurry-Phase Hydrocracking

The catalyst used for slurry-phase hydrocracking are categorized into two general types, i.e. supported catalyst and unsupported dispersed catalyst. The supported catalyst is referred to systems where the reactants and the catalyst are being in different physical phases. It consists of at least one metal (e.g. molybdenum, cobalt, Iron, nickel, etc.) that

is/are either impregnated on a supporting material, e.g. silica-alumina, alumina and carbon nano-tubes, or being in the salt form [12]. The disadvantage that faces the development of the solid supported catalyst involves the deposition of high molecular weight reactants on the active sites resulting in blocking the pores on the surfaces of the solid catalyst. This results in shortening the catalyst life and through the formation of a high number of solid particle and building up of the pressure [12]. The dispersed catalysts, on the contrary of the conventional supported catalysts, are unsupported catalysts transition metals in the form of sulfides or oxides. They are derived either in finely powdered form or in water/oil soluble form. The slurry-phase process is considered as one of the top hydrocracking processes in terms of promoting the activity and selectivity toward the product. This activity depends primarily on the catalytic behaviour of the used catalyst that may exhibit decreasing due to different factors. The deactivation of the catalyst takes place either because of the deposition of undesirable products or the formation of coke or because of physical effects such as attrition or sintering. The used catalyst in slurry-phase process hydrocracking can be both supported solid catalyst and unsupported dispersed catalyst. Figure 2-1 shows the general classification of the catalysts used for the slurry-phase hydrocracking process for heavy oils.

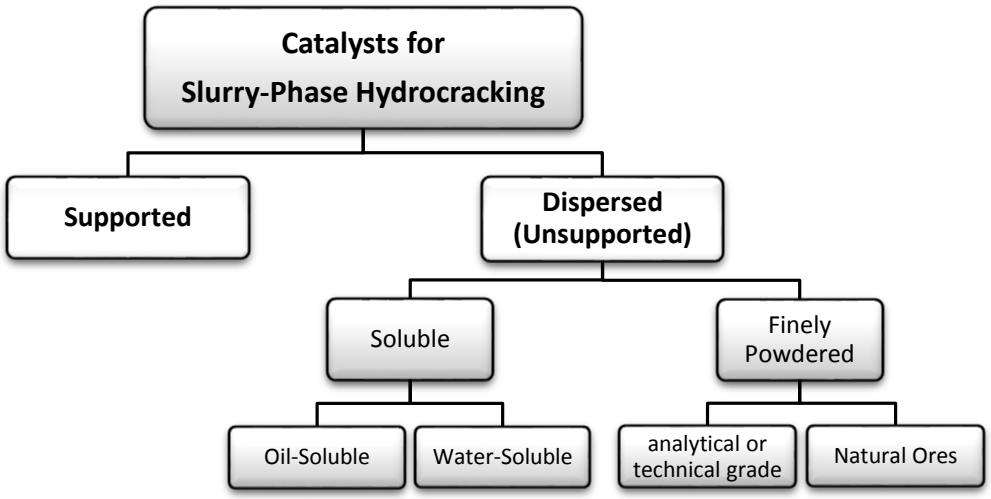

Figure 2-1 Catalyst types applied for hydrocracking in slurry-phase reactors.

2.1.1 Finely Powdered Dispersed Catalysts

The finely dispersed catalysts are prepared either by analytical/technical means or from natural ores. These catalysts are synthesized based on various transition metals, such as cobalt, molybdenum, nickel, iron, titanium, chromium, etc. They are prepared to be in the form of salt, sulfide or oxides with the size of a micron or even less [9, 13].

Al-Marshed *et al.* [14] studied the heavy oil upgrading for different transition metals unsupported catalyst which are based on molybdenum, nickel, and iron. Different particle sizes of Iron (II), nickel (II) and molybdenum oxides and their sulfides were investigated. Generally, the product distribution, the quality of the products and the properties are similar for both cases. It was expected that the 50 nm particles will show higher overall activity because of their higher surface area/volume ratio, however, it was concluded that over the range of 50 nm and 5 μm there was no significant effect of the particle sizes. Molybdenum-based dispersed catalysts were studied by using its oxide and sulfide at different sizes.

Figure 2-2 shows the particle size effects in product distribution and product quality for hydrocracking over MoS_2 and MoO_3.

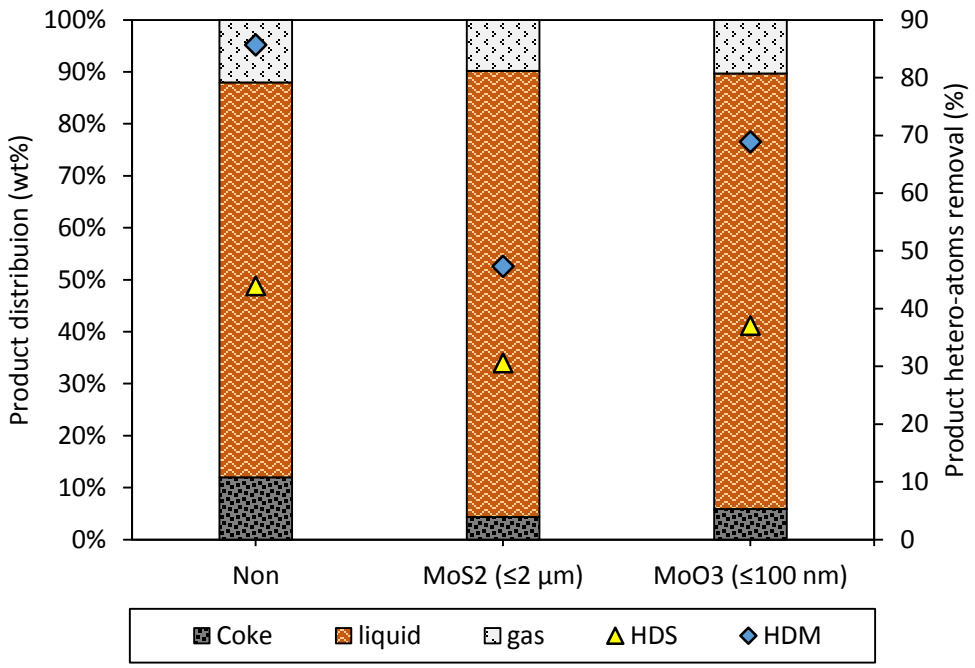

Figure 2-2 Product distribution and quality of hydrocracking over Mo-based catalysts. Adapted from Ref. [14].

It was noticed that MoS_2 proved better yield than MoO_3. The liquid yield boosted to reach up to 85.84 wt% for MoS_2 compared with 83.81 and MoO_3. Furthermore, MoS_2 showed better inhibition of coke formation with 4.35 wt% compared with 5.9 for MoO_3. This study suggests that the sulfide form for the dispersed catalysts (Ni, Mo, and Fe) formed by *in situ* sulfidations of metal oxides enhances the hydrogen uptake that helps in preventing the condensation and polymerization reactions caused from the free radicals. This takes by forming active hydrogen molecules that are created due to the sulfur-deficient sites in metal sulfide catalysts. The finely dispersed catalysts could also be derived from natural ores,

which are being widely used practice in the industrial applications of slurry-phase hydrocracking due to their availability as well as their low cost. According to the studies found in the literature, different ores are available and have been implemented for hydrocracking processes of heavy oil, for example, magnetite, limonite, molybdenite, hematite, ferrite and laterite [13, 15, 16]. They are prepared by grinding, milling, sieving, and drying of pieces of minerals [13].

The use of red mud for vacuum residue (VR) hydrocracking in a batch slurry-phase mode was investigated by Nguyen-Huy and coworkers [17]. The red mud contains different metal oxides that include hematite, Fe_2O_3. The experiments showed that the conversion was lower than the thermal cracking; the coke formation was sufficiently inhibited. The characterization of the spent catalysts proved that the hematite crystalline is activated *in situ* by the sulfur content released after thermal cracking to form pyrrhotite ($Fe_{(x-1)}S_x$). The formed compound boosts the hydrogenation reactions, so the pretreatment step of the feed could be abandoned. Figure 2-3 shows the *in situ* sulfidation mechanism for the red mud during the hydrocracking reaction.

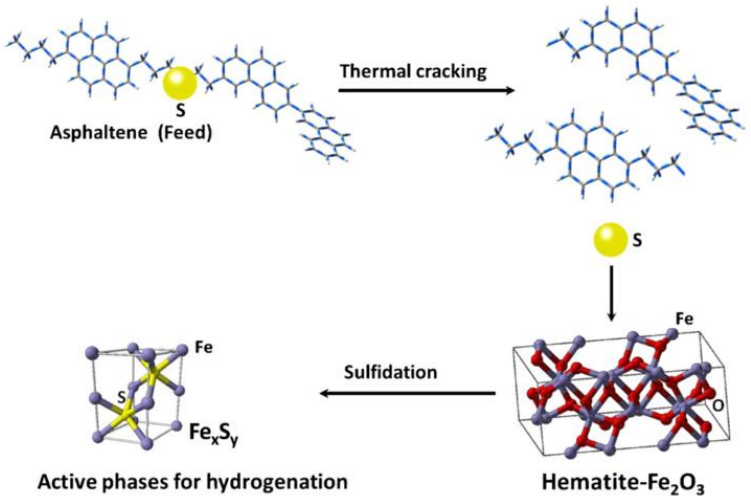

Figure 2-3 Red mud activation during the hydrocracking reaction due to the sulfur content of the feed [17].

Matsumura *et al.* [18] studied the use of an iron ore which is natural limonite that is derived from two locations, which are Brazilian (BL) and Australian (AL) limonites. Their catalytic performances were compared with the hydrocracking over the commercial $NiMo/Al_2O_3$. The $NiMo/Al_2O_3$ presents higher activity than limonites in terms of suppressing coke and gas as well as hydrogenation. However, in terms of conversion, limonites showed higher values.

The slurry-phase hydrocracking was firstly proposed by implementing solid powder catalysts. Examples of these technologies are the VEBA Combi Cracking (VCC) process, the HDH technology and the Canadian CANMET process. Although that these technologies proved high conversion, the drawback of producing large solid particles was considered as the main issue.

The Hydrocracking Distillation Hydrotreating (HDH). The HDH technology is one of the technologies that were developed to utilize natural ores, such as iron laterite. The

catalyst is prepared by crushing and fining the ore then it is fed to this process in a huge amount relative to the feed. Hence, the separation process of the catalyst and the unconverted solid fraction is presented in a complex manner [6, 19]. The previous studies showed that the catalyst loading of mineral ores used for hydrocracking between 0.5 and 2.0 wt% with particle sizes of 5 to 100 μm [13]. Unlike soluble dispersed catalysts (oil-soluble and water-soluble) the dispersion and suspension of the finely dispersed catalysts in the feeds are not efficient, so this reflects a drawback in terms of overall activity. Fortunately, the activity of the finely dispersed catalysts could be boosted by preventing precipitation of the catalysts during the process by applying higher agitation speed that results in keeping the catalysts effectively in suspension [13].

The Veba Combi Cracker (VCC). The VCC technology was first invented for coal liquefaction in Germany and started to be commercially adopted from 1927 until 1945 [6]. Later from 1981 until 2001 where it was shut down again, the feed of the VCC process was switched to heavy oil and it was reconstructed in Bottrop (Germany) refinery to process 3500 barrel/day. The process was developed to be operated at high of 220-250 bar and temperature of 440-485 °C with a catalyst of red mud, which is a solid containing iron, and powder of Bovey coal with a high dosage of 5.0 wt% raw materials. The VCC slurry-phase hydrocracking technology proved a reasonable value of conversion that could reach up to 60% of the feed [6, 10]. Nevertheless, later developments applied to this process have made success in terms of increasing the conversion to 90-94% at a higher capacity of 4000 barrel/day [5].

The Canada Centre for Minerals and Energy Technology (CANMET). The process was developed for processing heavy oils by utilizing a solid powder catalyst which is

$FeSO_4$ a high concentration of (1.0 to 5.0%) [6]. The solid powder catalyst enhances the hydrocracking reactions by preventing the coke formation thus allowing a higher yield of the low boiling point products. The process takes place in a vertical reactor at reaction temperatures ranging between 440 °C and 460 °C and a pressure of 10.0–15.0 MPa. The reactor contains no internal parts and the mixture of the feed with the suspended catalyst particles is getting contact with the hydrogen by bubbling. Along 15 years starting from 1986, the Petro-Canada refinery in Montreal started the use of this technology by processing the visbreaking effluent which was 5000 barrel/day [10]. Although that the conversion of this process is efficient, the hydrotreating reactions such as hydrodesulfurization and hydrodenitrogenation are not that high. The disadvantage of this technology is the separation issue of the spent catalyst from the unconverted heavy parts [6].

In 2006, UOP started a collaboration with the Natural Resources Canada to develop the CANMET Slurry Hydrocracking technology. UOP benefited from that by developing its own technology which was based on CANMET and it was named UOP Uniflex (Figure 2-4). The new technology used a nanoscale catalyst that is blended with feed that helped in enhancing the residue conversion to reach above 90% and effectively reducing the coke formation. The conversion was also enhanced by operating the process at a higher temperature and that was attained by maintaining near-isothermal conditions. The near-isothermal conditions are approached by making the reactor at its full capacity and bubbling the hydrogen-rich which also enhances the back-mixing [10].

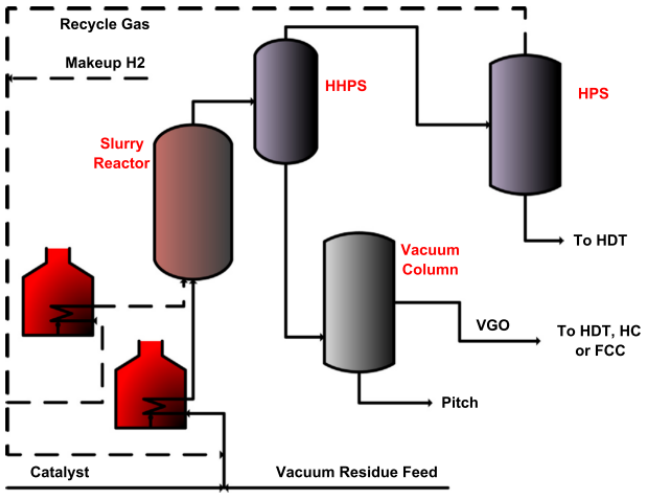

Figure 2-4 UOP Uniflex Slurry Hydrocracking process [10].

The Super Oil Cracking (SOC). The SOC technology was invented by Japanese Ashi Kasei Industrial Company. This technology uses horizontal furnaces as reactor where the feed and the catalysts are fed in the form of a slurry. The process takes place at a temperature of 480 °C and a high H_2 pressure that exceeds 20.0 MPa. This sever conditions makes the SOC process under some limitations due to the high investment cost required. The catalysts used in this process is highly dispersed powdered catalyst which provides high activity in terms of hydrogenations and as such reducing the coke formation. The process used to be applied on vacuum residue at processing scale of 3500 barrel/day [6, 8].

2.1.2 Soluble Dispersed Catalysts

The hydrocracking reactions using soluble dispersed catalyst have become a hot area of research since that it could be used alone or besides a solid supported catalyst to inhibit the prominent drawback of excessive coke formation that is associated with using standalone heterogeneous catalysts. Unsupported or homogeneously soluble dispersed catalysts are

classified into two types: oil-soluble dispersed catalysts and water-soluble dispersed catalysts. Indeed, both soluble catalyst precursors contain metals that are selected from group IV B-VIII and they are usually Mo, Co, Cr, Ni, etc. These metals are either be in the salt form or they could be chemically linked with organic compounds in the form of ligands. Figure 2-5 shows examples of oil-soluble and water-soluble dispersed catalyst precursors that are used in applications of heavy oil upgrading. The soluble catalyst precursors are catalytically activated by *in situ* sulfidation through reactions with H_2S, that is released during the hydrodesulfurization reactions, to form active metal sulfide crystals [9, 20]. The dispersed catalysts are activated *in situ* to form infinitesimally small particulates that reach up to a molecular level which ensure high contact with the molecules and dispersion in the heavy oil, ideal utilization of catalyst could be achieved [9].

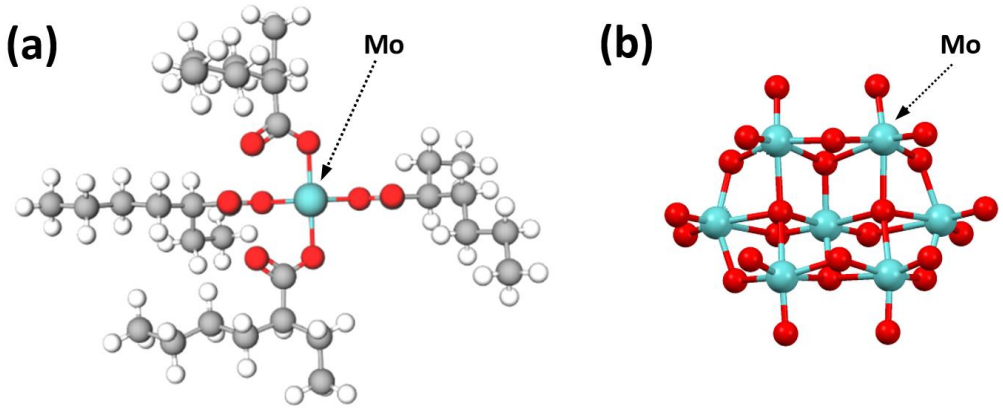

Figure 2-5 (a) oil-soluble molybdenum 2-ethylhexanoate and (b) water-soluble ammonium heptamolybdate.

Water-Soluble Dispersed Catalysts

Water-soluble dispersed catalyst precursors are categorized into two typical types which are ammonium molybdates and phosphomolybdic acids. The use of water-soluble dispersed catalyst precursors necessitates performing pretreatment steps that involve emulsion and dispersion followed by dehydration [5]. The dispersed catalyst is prepared by an emulsion that is formed by dissolving metal salts is water. Prior to mixing with the feedstock, the dispersed catalyst is dehydrated and sulfided. Water or heteropoly acid is fed together with the water soluble precursors to form organometallic compounds that has a combined effect which enhances their catalytic activity [5]. Water-soluble dispersed catalyst precursors are considered as good choices in terms of economics since they are synthesized from inexpensive inorganic compounds. However, their overall catalytic activity is lower compared to the oil-soluble precursors due to the fast evaporation of the water followed by sintering of the *in situ* formed active sites, forming large particles that lower its capability to disperse into the tiny particles of the feed.

Ortiz-Moreno *et al.* [21] studied the slurry-phase upgrading of Maya heavy crude oil using molybdenum sulfide catalyst that is obtained by two different water-soluble dispersed catalyst precursors which are ammonium tetrathiomolybdate and ammonium heptamolybdate. The catalyst precursors were activated *in situ* to obtain MoS_2. Several experiments were conducted by varying the conditions of temperature, pressure and catalyst concentration to verify their effects on the product distribution. It was found that the use of low concentration of catalyst (330 ppm Mo) showed similar results with the thermal run. However, increasing the catalyst loading (1000 ppm Mo) at a high reaction temperature of 400 °C showed promising results in terms of promoting gasoline and gases

yields. Applying the same catalyst concentration at a low temperature of 390 °C gave results in favor of middle distillate than gases and gasoline. An attractive result was noticed while operating the process at a low temperature for a long time. Although the feedstock conversion was not that high, the coke inhibition, as well as the valuable liquid yield, were enhanced. This was attributed to the fact that more part of the asphaltene fraction was transformed to the liquid which its yield was increased from 12.0 % to 23.0 %.

The reactivity and composition of dispersed nickel catalyst derived from a water-soluble precursor were studied by Liu and coworkers [22]. The studied catalyst was used for the slurry-phase hydrocracking of vacuum residue in a batch mode. Several experiments were conducted by varying the reaction time (1.0, 2.0, 3.0, and 4.0 hours) at a fixed temperature and pressure of 420 °C and 5.0 MPa. BET analysis was performed for the runs at different times and the results showed that the surface area of the nickel catalyst changed versus the reaction time according to the following order 1 h>2 h>4 h>3 h. This result was verified by conducting XRD which proved that at different reaction times the precursor is sulfided in different mechanism to give different metal sulfides. It was proved that between at reaction time of 1.0 and 2.0 hours the precursor activated to be in the form of NiS and Ni_3S_2. For three hours reaction time, the Ni_3S_2 started increasing and Ni_9S_8 started to appear while the NiS decreased. After 4.0 hours of reaction, the analysis showed that most of the nickel is sulfided in the form of Ni_9S_8. The coke inhibition was reported to be promising for reaction times of 1.0, 2.0, and 4.0 hours while it sharply reduced for when processing for 3.0 hours. This was attributed to the reactive centers which are different for each metal sulfide.

The effect of mixing two water-soluble catalyst precursors was investigated by Luo and coworkers [23]. A mixture of nickel sulfate and ferrous sulfate was utilized to provide dispersed catalysts for the slurry-phase hydrocracking Liaohe vacuum residue (LHVR) under batch mode. The blend of precursors was presulfurized with ammonium sulfide solution in order to assure its conversion into the active sulfides. The factors studied were the interfacial tension between the catalysts precursor solution and the vacuum residue, stirring rate, and the concentration of the catalyst. The interfacial tension was measured by a specialized meter and it was tuned by of nonionic surfactants. Figure 2-6 showed that the when the interfacial tension was lowered the dispersion of the catalysts improved, so the coke formation was inhibited, and the gas yield reduced. Applying a high stirring speed on process resulted in improving the dispersion of the catalyst, however, there was a critical point where increasing the stirring rate could not help in promoting the dispersion of the catalyst [24]. Also, decreasing the catalyst concentration was found to be effective in promoting the dispersion of the catalyst and through inhibiting the coke formation, however, this effect was not comparable with the huge effect of decreasing the interfacial tension between the precursor and the feedstock.

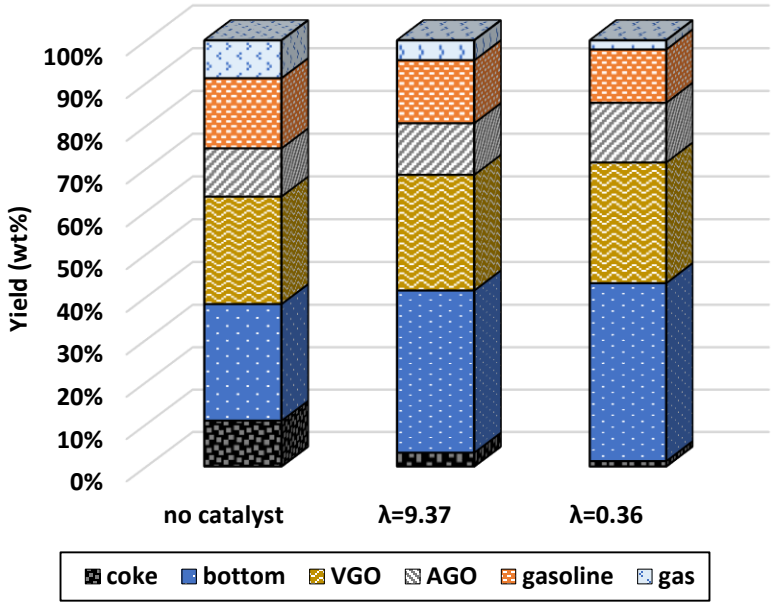

Figure 2-6 Interfacial tension effect on the product distribution of hydrocracking of LHVR. Adapted from Ref. [23].

The summary of other published literature on heavy oil upgrading over water-soluble dispersed catalysts is presented in Table 2-1.

Table 2-1 Summary of literature on heavy oil upgrading over water-soluble dispersed catalysts.

Reference	Feedstock	Catalyst precursor	Operating conditions	Key findings
Ortiz-Moreno *et al.* [25]	Maya crude oil	ammonium heptamolybdate (AHM)	Parr batch reactor. Conditions: 390 °C, 1400 Psi, 700 rpm, catalyst concentrations of 0-1000 ppm and a reaction time of 1.0-11.0 h.	1. The naturally occurring asphaltenes of Maya crude were catalytically directed to yield liquid fractions. 2. The formation of asphaltene-like components and coke depositions were inhibited. 3. The yield of middle distillates was enhanced.
Martinez-Grimaldo *et al.* [26]	Maya crude oil	ammonium heptamolybdate (AHM)	Parr batch reactor. Conditions: 390-410 °C, 1400 Psi, 700 rpm, catalyst concentrations	The liquid yield increased and the amounts of solid and gases decreased by increasing the catalyst

			of 0-1000 ppm and a reaction time of 0.0-8.0 h.	concentration from 300 ppm Mo to 1000 ppm Mo.
Liu *et al.* [27]	Gudao vacuum residue	ammonium phosphomolybdate (APM), ammonium heptamolybdate (AHM) and ammonium terathiomolybdate (ATTM)	a 165 cm^3 high pressure internally stirred autoclave. Conditions: 350-420 °C, 7.0 MPa, 950 rpm, catalyst concentrations of 1000-5000 ppm Mo and reaction times of 0.0-3.0 h.	1. The adopted dispersion method of the catalyst precursors improved the catalytic activity. 2. SEM and TEM show that the *in situ* formed active phase by using the high dispersion method appears with particles sizes less than 2 µm.
Petrukhina *et al.* [28]	model hydrocarbon feedstocks, i.e. (10% solutions of bicyclic aromatic hydrocarbons (BCAHs) in n-hexadecane) and (5% solution of dibenzothiophene (DBT) in benzene)	nickel–molybdenum and cobalt–molybdenum complexes with citric, oxalic, succinic, glutaric, and tartaric acids as precursors	a 20-mL steel autoclave. Conditions: 380 °C, 5.0 MPa, a BCAH:Mo molar ratio of 60:1 and a DBT:Mo molar ratio of 20:1 and a reaction time of 1.0-10.0 h.	1. Bimetallic CoMoS and NiMoS were *in situ* synthesized by the decomposition of bimetallic water-soluble precursors 2. The synthesized catalysts showed high activity in hydrodesulfurization and hydrogenation. 3. The optimum medium that ensures high dispersion of the dispersed catalysts is water.
Tian *et al.* [29]	low sulfur waxy residual oil	a mixture of nickel chloride and ammonium molybdate	a 300 mL batch autoclave reactor. Conditions: 340 °C, 7.0 MPa, 1000 rpm, a catalyst precursors molar ratio of 0.5 and reaction times of 0.0-4.0 h.	1. The catalytic activity of the water-soluble dispersed Ni-Mo catalyst was comparable to the presulfided Co-Mo supported commercial catalyst. 2. The dispersed catalyst showed better performance in terms of hydrodenitrogenation compared the supported catalyst.
Luo *et al.* [23]	Liaohe vacuum residue (LHVR)	a mixture of nickel sulfate ($NiSO_4 \cdot 6H_2O$) with ferrous sulfate ($FeSO_4 \cdot 7H_2O$) as a sulfiding agent	FDW-01 autoclave. Conditions: 430 °C, 7.0 MPa, 1000 rpm, a catalyst precursor of 0.04 g/mL, ammonium sulfide [$(NH_4)_2S$] as sulfiding agent and a reaction time of 1.0 h.	The dispersion of catalyst could be improved by lowering the interfacial tension between the feedstock and the precursor solution.
Jian *et al.* [30]	Gudao vacuum residue	ammonium heptamolybdate (AHM), ammonium paramolybdate (APM), phosphomolybdic acid hydrate (PMA), iron pentacarbonyl	a 500 mL steel batch autoclave reactor. Conditions: 420 °C, 7.0 MPa, a catalyst precursor of 500 ppm, sulfiding agent fed at a ratio of 3:1 sulfur-to-metal and a reaction time of 1.5 h.	A lower yield of <200 °C fraction and a higher yield of 300–500 °C fractions were observed by adding 500 ppm of the PMA catalyst precursor.

		and ammonium terathiomolybdate (ATTM)		
Afanasiev [31]	a model feedstock of thiophene	ammonium tetramolybdate (ATM)	a fixed-bed flow microreactor. Conditions: 280-320 °C, a 50 mL/min H_2 flow, catalyst precursor loadings of 50-500 mg and reaction times of 1.0-80.0 h.	1. Over-stoichiometric sulfur present in the catalyst in the form of S_2^{-2} edge-located species has an important role in terms of MoS2 activity. 2. The stacking degree of MoS_2 slabs has a less important role for the selectivity of thiophene HDS.
Liu *et al.* [22]	Karamay atmospheric residue (KLAR)	water-soluble Ni salts	a 500 mL batch autoclave reactor. Conditions: 420 °C, 5.0 MPa, the mass fraction of nickel was 0.1-1.0% and reaction times of 1.0-4.0 h.	1. An optimum coke inhibition was achieved at reaction times 1.0-2.0 h. 2. The catalyst precursors turn into NiS and N_3S_2 after 1.0 or 2.0 h. After three hours, the Ni_3S_2 increases while the NiS diminishes. After that, Ni_9S_8 start forming. 3. The coke inhibiting catalytic ability is different for each kind of nickel sulfide crystals.
Al-Rashidy *et al.* [32]	light vacuum gas oil (LVGO)	mixtures of iron(III) nitrate nonahydrate ($Fe(NO_3)_3{\cdot}9H2O$) and nickel(II) nitrate hexahydrate ($Ni(NO_3)_2{\cdot}6H2O$) with ammonium heptamolybdate ($(NH_4)_2MoO_4$)	a 300 mL batch autoclave reactor. Conditions: 400-430 °C, 8.0 MPa, 1000 rpm, a dispersed catalyst concentration 250 ppm for each precursor and reaction times of 0.0-1.0 h.	The injection of 500 ppm water-soluble Fe-Mo resulted in the most reduction of coke formation from 0.75 wt% to 0.46 wt%, compared to the thermal hydrocracking run.

Oil-Soluble Dispersed Catalysts

Oil-soluble dispersed catalyst precursors are more popular because of their high activity and capability of dispersion in heavy oil, which results in preventing the coke formation. The dispersed catalysts decomposing from oil-soluble precursors report appreciable results in terms of boosting the hydrogenation reactions. Consequently, it hinders the mesophase,

i.e. an intermediate phase formed during the cracking reactions of heavy oil [33], from coalescence to larger domains that eventually deposit as coke [34].

Different compounds are used to get oil-soluble precursors that have the ability to disperse in the hydrocarbon environment on the heavy oil such as metal salts of organic amines, organic acids (acetic, naphthenic, octoic, oxalic, etc.), metal-containing quaternary ammonium compounds, etc [35]. The oil-soluble dispersed catalyst has a unique trait that is its capability to highly dispersed in the heavy oil with a greater surface-area-to-volume ratio. Furthermore, during the reaction the metal sulfide, which is the active species for the reaction, is formed *in situ* from the oil-soluble precursors. However, their cost of synthesis and its difficulty to be recovered impede their development for a slurry-phase hydrocracking process [5].

Many molybdenum compounds are utilized as dispersed catalysts because that molybdenum is considered as the most preferred candidate compared to other metals due to its high hydrogenation activity in the sulfide form, MoS_2 [12, 20]. In term of coke suppressing and product upgrading, molybdenum-based dispersed catalysts generally show the most promising results. However, iron-based dispersed catalysts are still the most used oil-soluble dispersed catalysts because of their low cost [36].

Watanabe *et al.* [37] conducted several slurry-phase hydrocracking experiments on Arabian heavy vacuum residue to study the activities of oil-soluble catalyst precursors of Mo-dithiophosphate (Mo-DTP) and Mo-dithiocarbamate (Mo-DTC). The study showed that Mo-DTC was proved that it decomposes at 350^{o}C to give definite MoS_2 while Mo-DTP start decomposing at 200^{o}C and yet it did not give definite MoS_2 even when raising the temperature up to 500^{o}C. Thus, it was concluded that Mo-DTC is better than Mo-DTP

in terms of sulfiding efficiency. Also, the dispersion of both complexes in the asphaltene was observed by TEM to be good. As a result, at room temperature, both Mo-DTC and Mo-DTP give solid fine particles that are dispersed in the feed with low crystallinity.

As an attempt to study the effect of utilizing different precursors for molybdenum-based dispersed catalysts, Rezaei and coworkers [39–41] did a performance comparison of dispersed MoS_2 that is prepared from oil-soluble molybdenum octoate and molybdenum micelle precursors. The conversion of vacuum residue was conducted in in batch and semi-batch modes at reaction temperature ranging between 415 °C and 445 °C, a pressure of 13.8 MPa and a reaction time of 1 h. The experiments that utilize Mo-micelles as catalyst precursor were conducted at different concentrations of the Mo-based precursor in the heavy oil [40]. In the same manner, the experiments were done at the same concentrations of the oil-soluble molybdenum octoate catalyst precursor which consists of 15.3 wt% Mo as molybdenum 2-ethylhexanoate which added directly to the residue oil. Both catalyst precursors showed the same catalytic activity of MoS_2 in terms of hindering coalescence of coke precursors, VR conversion, and hydrogen uptake. At a concentration of 100 ppm Mo, the coke yield decreased from 22.0 wt% to 4.8 wt% [41]. The maximum conversion of residue (84.0 wt %) and the minimum coke yield (2.9 wt %) were found to be at a molybdenum concentration of 600 ppm. Figure 2-7 shows the coke yield and conversion of residue (TIOR) during the hydroconversion of CLVR as a function of molybdenum-based concentration for the molybdenum octoate and molybdenum micelle catalyst precursors.

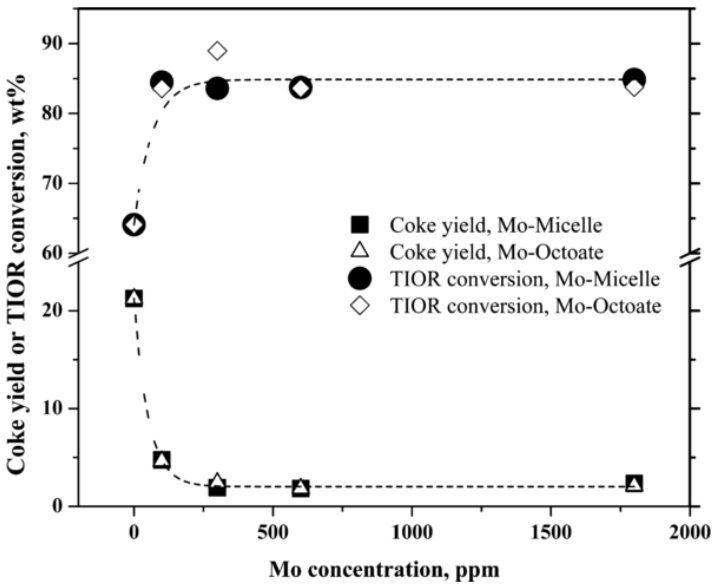

Figure 2-7 The conversion of residue and the yield for hydrocracking over molybdenum octoate and molybdenum micelle [39].

Kim *et al.* [42] the hydrocracking of vacuum residue (VR) in batch mode by using an oil-soluble molybdenum hexacarbonyl precursor. The catalyst is activated *in situ* to form MoS_2 at an amount of 0.113 mmol Mo. Different experiments were conducted in a batch autoclave reactor by changing the operating conditions which are reaction time, reaction temperature, and hydrogen pressure. Standard conditions of temperature, pressure, and catalyst loading were chosen to be at 673 K and 9.5 MPa, respectively to study thoroughly the yields of the process. It was found that after operating the process for 4.0 hours at standard conditions, the yields of liquid, gas and coke were 77.0, 12.0, and 11.0%, respectively. It was found that at the same standard reaction temperature when hydrogen pressure of the process exceeds 15.0 MPa the yield of the light oil products reaches its maximum value at 90%. Analysis conducted by TEM and Extended X-ray absorption fine structure (EXAFS) proved an abundance of exposed sites as the active phase. This

conclusion brought by analyzing the spent catalyst which showed that the MoS_2 particles were developed from $Mo(CO)_6$ from the beginning of the reaction, where Mo-S and Mo-Mo coordination is low, which allowed them to be having more exposed and defect sites as active phases.

Nickel-based oil-soluble catalyst precursors for dispersed catalysts were also proposed for heavy oil upgrading due to its catalytic activity relative to molybdenum-based precursors. Zhang *et al.* [34] studied the slurry-phase hydrocracking of Liaohe atmospheric residue using a nickel-based dispersed catalyst that was formed by the decomposition of the oil-soluble precursor *in situ*. The catalyst precursor structure used is represented in Figure 2-8. The "A" represents an aromatic ring containing six carbon atoms while the X in an independent linker group. The R is an independent functional group containing twelve carbon atoms while the (n) is at least one or equal to the number of position available by the aromatic ring, which is six. The nickel compound is an amphipathic molecule and it consists of two active parts: the aromatic ring (A) and the nickel atom. Since that the aromatic ring is a flat molecule, so it gives enough Van der Waal's interactions that are responsible for attaching the precursors on the similar aromatic asphaltene [34]. Since that the cracking reaction takes place by only thermal means, conversion of the feed to distillates is found to be independent of dispersed catalyst loading and hydrogen pressure. However, by increasing the catalyst concentration it was found that both the coke formation and the light oil (naphtha + atmospheric gas oil) yields were decreased. On the contrary, increasing the reaction temperature found to increase the yield of coke and light oil. The effect of increasing the hydrogen pressure realized to be positive for both coke inhibition and promoting the light oil yield.

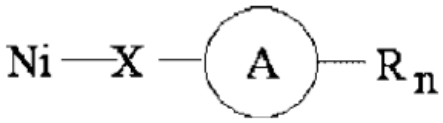

Figure 2-8 A sketch of the oil-soluble precursor (Ni-based) proposed by Zhang *et al.* [34].

Different studies have investigated the influence of metals on the catalytic hydrogenation performance of the dispersed catalyst precursors. Bearden [43] had discussed the hydroconversion of Jobo and Cold Lake crudes over different metal-based catalyst precursors of iron naphthenate, molybdenum resinate, nickel octoate, cobalt resinate, chromium resinate and vanadium resinate that are homogeneously activated *in situ*. The results showed that all the metals used present promising values in terms of coke suppressing as well as hydrotreating that was depicted from the desulfurization and demetallization results. The molybdenum-based dispersed catalyst showed the best yields of liquid that ranges between 95.8 to 97.2 wt% and it gave the lowest values for the coke formation yield at a range between 0.50 and 0.80 wt%. Although that Fe-based dispersed catalyst is considered as the most appropriate choice in terms of economics, it showed the least effective values in term of coke suppressing that reaches up to 5.2 wt%.

Similarly, the effect of different metals, i.e. nickel, cobalt, molybdenum, iron, and vanadium, studied with various oxidation states, was studied for upgrading of the heavy Arabian vacuum residue by Dabkowski and coworkers [44]. For each run, the autoclave batch reaction was loaded with 1000 ppm of the catalyst with severe conditions where hydrogen pressure was 14.0 MPa and temperature of 713 K for 1.0 hour of reaction. After doing the experiments, the results showed that the degree of coke formation was varying

in the order of Ni^{+2} > Mo^{+6} > V^{+4} ~ Co^{+2} > Fe^{+3}. In terms of coke suppressing, Co^{+2} naphthenate, Mo^{+6} naphthenate, and Ni^{+2}octoate showed the most promising results.

The catalytic activity of different oil-soluble compounds was investigated thoroughly by comparison in terms of products quality and yields by Panariti *et al.* [45]. The upgrading of the vacuum residue of Belayim crude by applying different dispersed metals derived from different oil-soluble precursors. Molybdenum was studied by using molybdenum naphthenate (MoNaph), molybdenum acetylacetonate (MoAA), phosphomolybdic acid (PMA), dithiocarbamate complex Mo_3S_7–$(dtc)_4$ (SP2), (MoO_2)–LB^* (RMV12) and (MoO_2)–LA_2^* (RMV6), where LB^* represents $(Ph–CH)_2$–$C(COOEt)PO_3H_2$ and LA^* represents $(O_2N–Ph–CH_2)_2$–$C(COOH)PO_3H_2$. Cobalt, nickel, iron, ruthenium, and vanadium were derived from the oil-soluble precursors of cobalt resinate (CoRe), nickel naphthenate (NiNaph), iron naphthenate (FeNaph), ruthenium acetylacetonate (RuAA), and vanadium resinate (VRe), respectively. The performance of the catalysts was studied by processing 10 grams of the feedstock at a 30-mL autoclave batch reactor at 460 °C with hydrogen pressure at 9.0 MPa in the presence of 1000 ppm of metal for each run. Figure 2-9 shows some of product yields for hydrocracking over each dispersed catalyst. It was noticed that, as it was mentioned earlier by Shen *et al.*[36], the performance of the dispersed catalysts is independent on the organic group bonded to the metal except at small ranges where it could be attributed to the variation in the thermal liability for each precursor. The comparison of the catalytic performances of the different metal-based dispersed catalysts showed that they arranged in order of activity as Mo>Ni~Ru>Co>V>Fe.

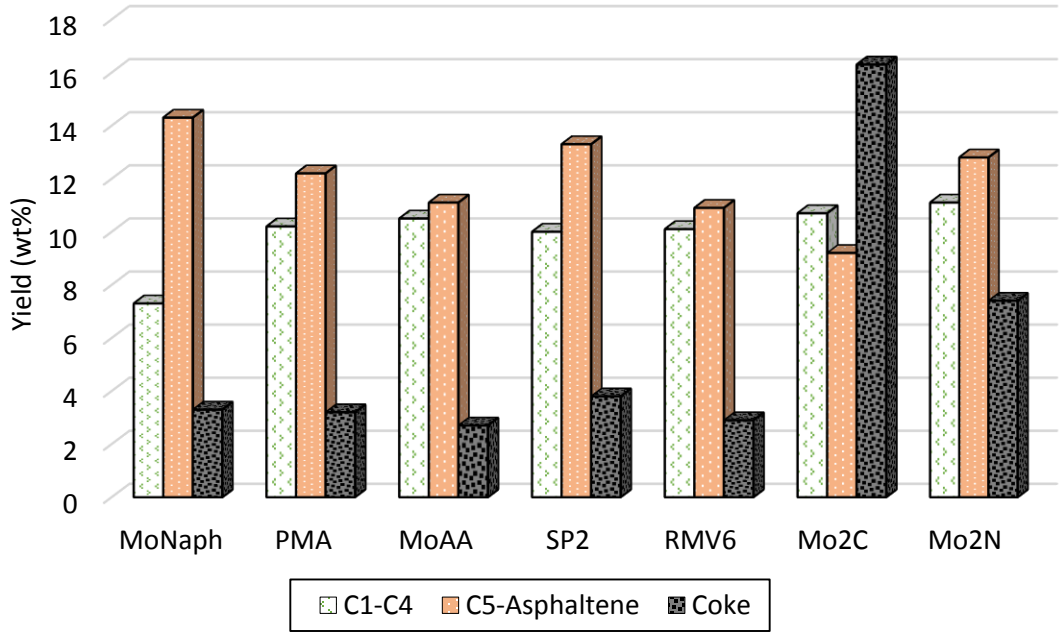

Figure 2-9 Compound type of the dispersed catalyst versus some of product yields at a reaction temperature of 460 °C. Adapted from Ref. [45].

The rate of catalyst activation through decomposition and sulfidation strongly affect the reaction pathways. Therefore, if the rate of catalytic activation is slow, the hydrogenation reactions will be suppressed and the system will be thermally controlled [45]. Coke inhibition and sulfur removal are the most obvious reactions that can tell about the rate of catalysts activation since they are highly dependent on hydrogenation. To study this issue, ultrafine powdered dispersed catalysts were investigated in order to compare their activity with the oil-soluble dispersed catalysts [45]. The powdered dispersed catalysts were chosen to be molybdenum-based and they were molybdenum nitride (Mo_2N) and molybdenum carbide (Mo_2C). Figure 2-10 shows a comparison of the product yield and quality for using the oil-soluble molybdenum naphthenate (MoNaph) precursor and the powdered molybdenum nitride (Mo_2N) dispersed catalyst. The powdered dispersed catalysts showed

poor results in term of coke inhibition, gas yield reduction, and middle distillate yield promotion compared with the oil-soluble precursor. A suggested solution to enhance the catalytic activity of the powdered catalysts is done by pre-treatment step that could partially improve their performance.

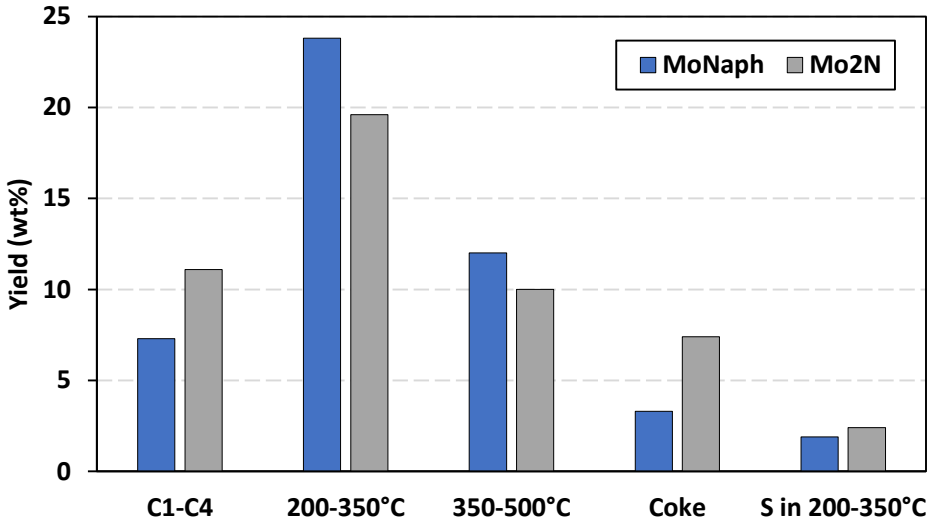

Figure 2-10 Product yield and quality for oil-soluble MoNaph and powdered Mo_2N. Adapted from Ref. [46].

The synergic effect of physically mixing two oil-soluble precursors on the hydroconversion of an atmospheric residue (AR) was investigated by Nguyen *et al.* [47]. The study adopted catalyst precursors of molybdenum naphthenate (MoNaph), nickel octoate (NiOcto), and vanadium acetylacetonate (VAcac). The mixtures of the catalyst precursors were described by a factor called r, where r=M/(M+Mo) and M is either V or Ni. The experiments were conducted in a 250 cm^3 autoclave batch reactor where it was loaded for each run with 100.0 g of the feed with 100.0 µL dimethyl disulfide (DMDS) that is used as a sulfiding agent. The mixture of MoNapth and NiOcto precursors showed collaborative behavior once they

sulfide to form MoS_2 slabs and Ni_3S_2 nanoparticles. The high-resolution TEM images confirmed the occurrence of interactions between the weakly stacked MoS_2 slabs and the Ni_3S_2 particles which appear like supports. Although that this catalytic combination still has less activity in terms of hydroconversion compared to the bimetallic catalyst of Ni-Mo-S (or Co-Mo-S), it showed sort of favoring the hydrodesulfurization reactions. On the other hand, the mixture of Mo and V precursors did not show any synergic effect. The sulfiding of the precursors lead to produce separate metal sulfides of V and Mo, so the promotional effect of mixing Mo with V is considered to as only an additive effect.

Shen *et al.* [36] studied hydrocracking of vacuum residue with mixed oil-soluble precursors. At first, the oil-soluble monometallic precursors used for this study were molybdenum dithiocarboxylate (MoDTC), nickel naphthenates (NiNaph) and iron naphthenates (FeNaph). The study was performed by studying each precursor alone and while for the bimetallic case mixtures of molybdenum dithiocarboxylate (MoDTC) was mixed with nickel and iron naphthenate respectively. For both mixtures of oil-soluble bimetallic catalyst studied, (Mo with Ni) or (Mo with Fe), it was noticed that the yields of coke and light gas were lower than those when nickel naphthenates or iron naphthenates were used alone as catalyst precursor. Although that X-ray analysis under the hydrocracking conditions led to the conclusion that no Ni-Mo sulfide or Fe-Mo sulfide was formed, the results of suppressing coke and light gas showed promoted results. These results of the bimetallic catalysts formed by simply mixing the monometallic precursors may be attributed to the enhancement of the dispersion of catalysts that were detected by microscopy and transmission electron microscopy (TEM) to be improved by introducing the second metal.

The use of physically mixed oil-soluble precursors was further investigated by introducing a hydrogen donor [48]. The slurry-phase hydrocracking of Liaohe VR was studied with cobalt naphthenate and nickel naphthenic oil-soluble precursors to get the dispersed catalysts while the hydrogen donor was tetralin (THN). The study divided into three phases; first, each dispersed catalyst was studied alone as monometallic dispersed, then studying mixing of the two precursors to form bimetallic and finally study the effect of hydrogen donor addition to this bimetallic catalyst. The result showed that use of either monometallic dispersed improve the upgrading of the VR, however, of the Ni-based precursor gives higher values than Co-based precursor the in terms of conversion yield. The addition of both catalysts precursors to getting bimetallic Ni-Co combination gave a mathematical addition effect in terms of coke inhibition and VR conversion. Moreover, the addition of the THF hydrogen donor to the bimetallic Ni-Co provided sort of synergism effect that promoted the suppressing of coke formation.

From the previous literature discussed it is noticed that the use of oil-soluble molybdenum-based precursors for hydrocracking process in the most common. Other studies suggest that the use of inexpensive promotors, such as nickel, cobalt or iron, could be a practical choice because these promoters may decrease the cost of the catalyst by enhancing the hydrocracking activity. However, most of the studies imply the use of bimetallic dispersed catalyst by simply physically mixing two monometallic catalyst precursors to get collaborative catalytic combination [46, 49]. Other relatively recent studies were done by researchers, such as Jeon *et al.* [49, 50] and Petrukhina *et al.* [28], suggest the use of a chemically bonded bimetallic dispersed catalyst as a single catalyst. Bellussi *et al.* [10]

proposed that the transition metal, such as cobalt or nickel, utilized beside molybdenum could be considered being as a promoter.

Jeon and coworkers [49] presented a novel technique of synthesizing a bimetallic oil-soluble dispersed precursor by coating of layered ammonium nickel molybdate ($(NH_4)HNi_2(MoO_4)_2(OH)_2$), termed Ni-LTM, with oleic acid. The organic ligand, i.e. oleic acid, is chemisorbed on the Ni-LTM to form the oil-soluble bimetallic dispersed catalyst which is Ni-Mo oleate complex. The prepared catalyst was characterized using X-ray photoelectron spectroscopy and the catalytic activity was tested by comparing it with was compared with two monometallic dispersed catalysts, i.e. molybdenum octoate (MoOcto) and nickel naphthenate (NiNaph). Since that the hydrogenation reactions are associated to cracking reactions during hydrocracking process, the consumption of hydrogen is considered as a characteristic parameter to tell which catalyst favors the hydrogen uptake and hinders the excessive formation of hydrocarbon gases. From Figure 2-11, it is noticed that the NiNaph and MoOcto show comparable results, however, Ni-Mo oleate complex experiences rapid hydrogen consumption which is attributed to its high catalytic hydrogenation capability.

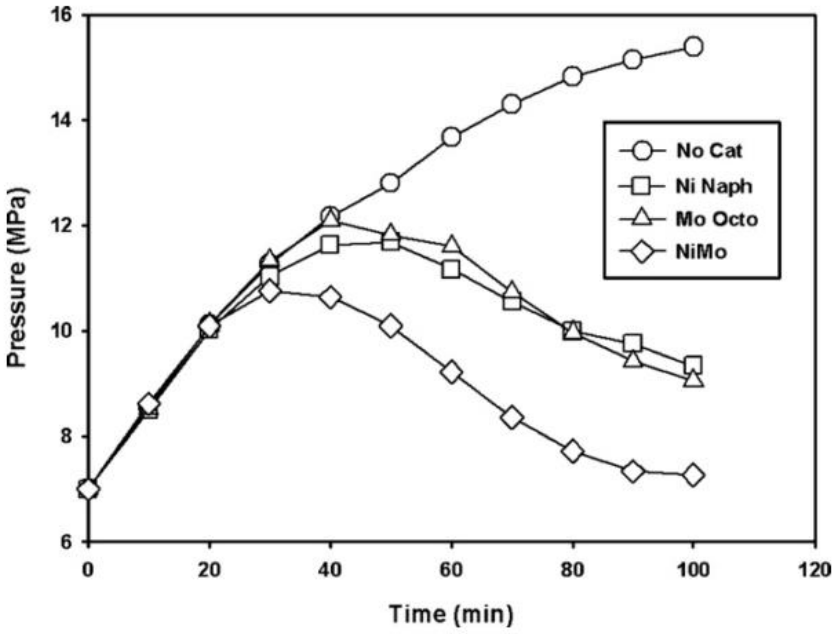

Figure 2-11 Pressure profiles for different dispersed catalysts during the hydrocracking [49].

Following the same experimental procedure that was proposed by Jeon *et al.*[49], the precursor for bimetallic Co–Mo dispersed catalyst was prepared using the layered ammonium cobalt molybdate (Co-LTM) [50]. Its catalytic performance was investigated using a batch autoclave reactor for the hydrocracking process of oil sand bitumen. The activity of the bimetallic oil-soluble Co-Mo dispersed catalyst was screened by comparing its activity with monometallic cobalt naphthenate (CoNaph) and Mo octoate (MoOcto) catalyst precursors as well as physically mixing them at a molar ratio of Co to Mo of 1:1. Figure 2-12 shows that Co-Mo bimetallic dispersed catalyst is the highest in terms of hydrogen consumption. Additionally, it is shown that the product distribution of hydrocracking reactions with different catalyst combination. It is expected that the thermal cracking run showed the poorest yield while for other catalysts the conversion was highly

enhanced, and it follows the order of CoNaph < MoOcto < CoNaph + MoOcto < CoMo bimetallic catalyst.

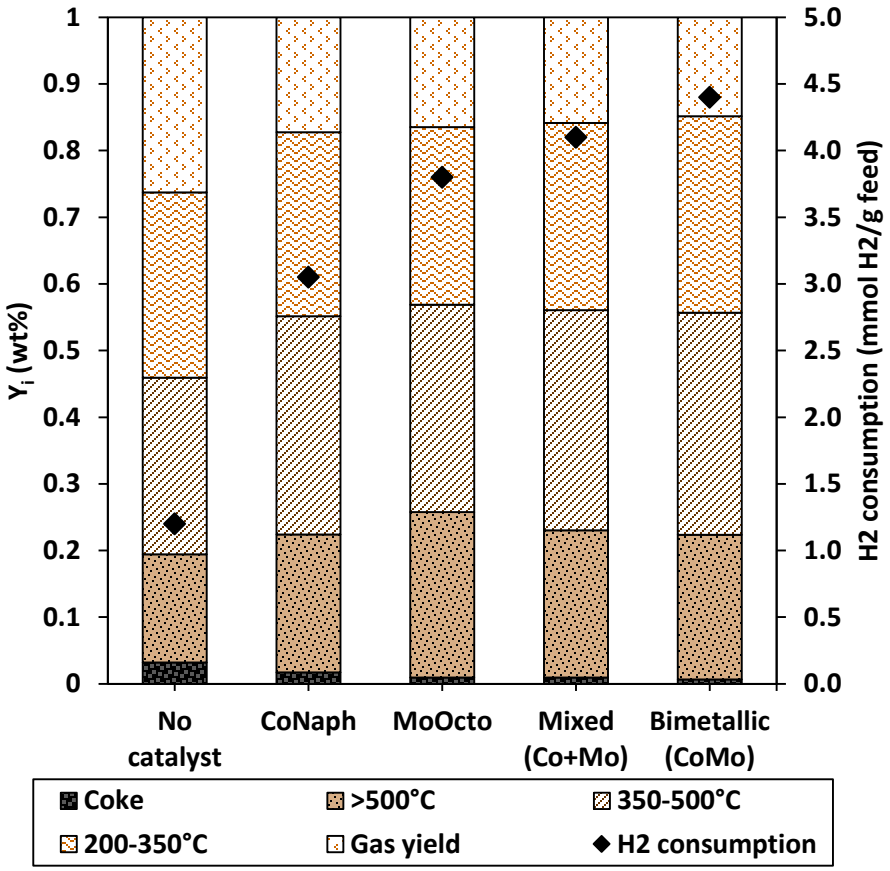

Figure 2-12 Distribution of products and H_2 consumptions after hydrocracking using different catalyst precursors. Adapted from Ref. [50].

The physical mixture of Co and Mo showed a better performance in terms of suppressing the yields of coke formation and light gas, however, compared with bimetallic Co-Mo the results showed much better catalytic activity in term of asphaltene conversion. This conclusion attributed to the same idea in the supported catalyst that is sulfided to be in the form of a binary sulfide, such as MoS_2 or WS_2, where the addition of a second transition

metal, e.g. nickel or cobalt, could highly promote its catalytic activity [51]. In order to get the most benefit the bimetallic dispersed catalyst, a chemically stable bond must be achieved, $CoMoO_4$, to prevent the decomposition of the catalyst to be simply a mixture of Co and Mo which results in losing its high catalytic activity. The oil-soluble bimetallic catalyst has a high surface area which could contribute to enhancing the catalytic activity [49]. In term of sulfur conversion through hydrodesulfurization, the bimetallic catalyst also showed higher activity than Co + Mo mixture. This reaction is highly favored by the active metal sulfide that is formed by a chemical structure, such as Co-Mo-S. Thus, the catalytic activity of sulfur conversion is low for Co + Mo because of the possibility of forming Co-Mo-S since that the two metals are separately dispersed in the feed.

Panariti *et al.* [45] also studied the catalytic activity of different forms of bimetallic dispersed catalysts. The catalyst precursors used were $Co(MoO_2)$–LB^* and $Ni(MoO_2)$–LB^*, where LB^* stands for $(Ph–CH)_2–C(COOEt)PO_3H_2$, that are named RMV14 and RMV15, respectively. The objective of this work was to generate finely dispersed binary sulfide bimetallic catalyst that could be applied for the hydrocracking process. However, for both Co-Mo and Ni-Mo, the XRD analysis indicated that MoS_2 and CoS_x and NiS_x were found in the process while there was no evidence that bimetallic sulfide was formed. Despite this conclusion, compared with similar Mo-based catalyst precursor, the bimetallic Co-Mo precursor still showed a slight synergetic effect in terms of sulfur conversion.

A recent invention showed that the chemically bonded bimetallic dispersed catalyst structure could be achieved *in situ* by introducing a mixture of two monometallic precursors [52]. Zhou *et al.* [52] discussed the implementing of mixed catalyst precursors of hydrocarbon-soluble metal salts that can form a signal cobalt-molybdenum sulfide

catalyst *in situ* for hydrocracking of heavy oil. Cobalt precursor was mixed with the molybdenum precursor at molar ratios varied from 1:98 to 1:10. The study showed that the active species present during the hydrocracking of the vacuum residue were CoMoS and CoS. It was found that the combination of catalyst precursors reduced sediment and enhanced asphaltene conversion. From the above discussion, the use of bimetallic dispersed catalysts in heavy oil upgrading still in its early stages. However, from a future point of view, the possibility of switching to including the use of the bimetallic dispersed catalyst in heavy oil upgrading is very expectable.

Metallocalixarenes. Metal-based calixarenes are good candidates for dispersed oil-soluble catalyst precursors and have not been studied previously for such systems. Calixarenes are defined as macrocyclic oligomeric phenolic compounds formed through the condensation of *para*-substituted phenols at a certain temperature in the presence of formaldehyde under alkaline conditions and are capable of forming complexes with metal ions, anions and neutral molecules [53–55]. The formation reaction of calix[n]arenes (R=alkyl, n=number of p-substituted phenols) is shown in Equation (2-1) [56]:

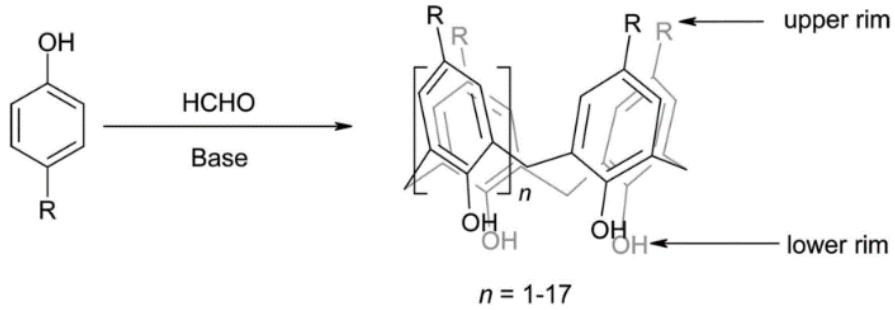

(2-1)

The synthesis procedure was developed to achieve the targeted calixarene with different configurations involving tetrameric, hexameric, or octameric phenolic ring systems bridged by methylene (-CH_2-) spacers by varying either temperature or amount of base

used [55, 57]. It is worth monitoring that the calix[4]arene could exist in other different conformations besides the cone that is a partial cone, 1,3-alternate and 1,2- alternate. The probability of forming the other possible structures stems from the limited steric bulkiness of the R groups if they are smaller or equal to ethyl [58]. Although that this class of macromolecular compounds had been studied earlier by Baeyer and Zinke, the name was proposed by C. D. Gutsche who suggested an analogy between cyclic tetramers and a type of Greek vase known as calix crater, so it was titled as "calix[n]arene" where the n represents the number of phenolic residues involved in the structure [55, 59].

The conical configuration of calix[n]arene is stabilized through hydrogen-bonding interactions, while the upper rim creates an electron-rich hydrophobic cavity owing to the presence of benzene rings. This structure enables the calix[n]arene to host a wide range of different "guests", particularly cations, at different positions [60, 61]. The presence of phenoxy groups in calix[4]arenes enables transition metal cations to form metal phenolate complexes by substituting for one to four hydrogen atoms [62].

One of the most potential applications of calixarenes is to use for heavy metal extraction [57, 63–66]. The modification of the lower rim through substitution results if expanding the cavity which facilitates the complexation with bigger moieties such as heavy metals and organic molecules. The substitution of diphenylphosphoryl acetamide moieties on either the lower rim and upper rim results in a highly efficient extractant for Pu^{+3}, Eu^{+3}, Th^{+3}, Am^{+3}, and Np^{+3} [67–70]. Moreover, the introduction of thiazole azo groups for all four positions of calix[4]arene forms a complex that is applicable for heavy metal ion recognition [71]. Extensive researches were conducted on calix[4]arene with various *para*-substituents to utilize the hydrophobic cavity generated by the wide upper-rim as a storage

for small gas molecules [72–83] or even H_2O which made Hontama *et al.* [84] to assign his formed cluster as the world's smallest cup of water. Nevertheless, the inclusion of transition metals such as Fe and Cu at the lower-rim found to enhance the binding of the guest molecules stored in the upper-rim cavity by providing additional possible binding sites and because of their magnetic properties where a range of polymetallic clusters is being formed [85, 86]. Murphy *et al.* [60] had investigated theoretically the effects of including metal i.e. Mn^{3+} (quintet) and Fe^{3+} (quartet) on the binding energy of small guest molecules i.e. H_2, O_2, N_2, H_2O, CO_2, N_2O, NH_3, H_2S, HCN, and SO_2 using Density Functional Theory. It was found that the coordination to lower-rim of the *p-tert*-butylcalix[4]arene with both metals strengthens the binding energy towards all guest molecules considered compared with the use of parent calixarene.

The use of metal-based calixarenes was extended to catalytic applications for a wide range of reactions, such as olefin polymerization [87–89], hydrogenation/dehydrogenation [90–92], oxidative dehydrogenation [93–95], hydroformylation [96, 97], alkylation [98–100], and cyclopropanation [101]. Based on previous studies, the use of calix[4]arene, particularly the *p-tert*-butyl derivative, for metal-based catalysis represents the majority of applications, at 75%; the rest is for calix[6]arene, calix[8]arene, oxacalixarene, and other ligand systems [56].

Table 2-2 summarizes the features and the acquired benefits that advocate the use of calixarenes as ligands in metal-base catalysis. Marson *et al.* [92] studied the hydrogenation of dimethylitaconate and R-(acyl-amino)acrylate at mild conditions (i.e. 25°C and 5 bar H_2) using rhodium-based *p-tert*-butyl-calix[4]arene functionalized at the lower-rim through chiral diphosphite ligands where complete conversion was achieved after four

hours of reaction time. Palermo *et al.* [102] proposed another approach for the use iridium-base calixarene by anchoring the metallocalixarene intact on a support for ethylene hydrogenation in a flow reactor at 313 K. The catalyst, which is $Ir_4L_3(CO)_9$, composed of a closed Ir_4 carbonyl cluster with tetrahedral metal frame and three sterically bulky L that is tert-butyl-calix[4]arene$(OPr)_3(OCH_2PPh_2)$ (Ph = phenyl; Pr = propyl) supported on porous silica and the cluster is being bonded exclusively to the basal plane by the bulky calixarene phosphine ligands. The Ir_4 cluster has high structural stability and full characterization in the crystalline state which is considered to be key advantages for application as a catalytic platform. The results show that synthesizing the cluster at ethylene atmosphere gave advanced turnover frequency at TOF = 1.2 h^{-1} and reaction orders of 0.66 in H_2 and -0.27 in ethylene.

Table 2-2 The features and advantages offered by using calixarene ligands [56].

Features	Subsequent advantages
inexpensively and easily synthesized	multigram quantities
ability to be functionalized	solubility control (including water)
ability to incorporate chirality	enantio-discrimination
presence of a cavity	multiple-substrate recognition
multiple binding sites	cooperative effects
ability to be fixed on solid supports	heterogeneous catalysis

The low solubility of calix[n]arenes in an organic solvent can be enhanced by forming derivatives of the parent molecule, such as hexaacetate *p*-methylcalix[6]arene [103, 104]. The thermal stability of calixarenes is a crucial factor since that they have various applications that require high temperatures such as ink-jet printing, dyeing of textile fibers,

and photocopying and also in other technologies such as lasers and electro-optical devices [105]. Calix[n]arenes have relatively high thermal stability (T_m > 300°C) and do not degrade in various chemical environments [104]. The coordination of metal with calixarene will affect its thermal stability based on the study conducted by Deligöz *et al.* [105] on calix[n]arene-Fe^{3+} complexes (n=4, 6, 8) by performing thermogravimetric analysis under flowing nitrogen gas at atmospheric pressure. It was observed that the complexes are starting to degrade beyond 200°C. This concludes that at this temperature thermal stability is vanished gradually because of the decomposition of the complexes as reported in other previous studies [106–108]. However, for processes operated under relatively severe conditions (e.g., ~400°C), such as heavy oil upgrading, the low thermal stability can be exploited by employing calixarenes as a carrier of the metal, where the active sites are formed by the destruction of the organometallic complex upon reaching the desired reaction conditions. Hence, the present research investigates the potential of applying metal-based calixarenes as precursors to enhance the catalytic hydrogenation reaction in vacuum gas oil (VGO) upgrading.

Table 2-3 Summary of literature on heavy oil upgrading over oil-soluble dispersed catalysts.

Reference	Feedstock	Catalyst precursor	Operating conditions	Key findings
Kennepohl and Sanford [109]	Athabasca bitumen	Molyvan-L and molybdenum naphthenate	a 1.0 L batch autoclave reactor. Conditions: 400 °C, 1000 psi, 600 rpm, catalyst concentrations of 0-6000 ppm and a reaction time of 4 h.	Only low molybdenum concentrations showed the reduction of coke formation.
Nguyen *et al.* [47]	atmospheric residue (AR)	molybdenum naphthenate (MoNaph), nickel octoate (NiOcto) and	a 250 cm^3 batch autoclave reactor. Conditions: 450 °C, 9.0 MPa, catalyst concentrations of	1. Mixing of Mo and Ni catalyst precursors proved improvements in terms of hydrodesulfurization (HDS) and total conversion of the

		vanadium acetylacetonate	300–900 ppm and a reaction time of 1 h.	AR which indicates a notable synergy between the catalysts. 2. In the case of Ni-Mo combination, the weakly stacked MoS_2 slabs act as supports for the *in situ* formed nanoparticles of Ni_3S_2. However, for the sulfide phase do not experience any sign of affinity in the case of V–Mo combination.
Rezaei *et al.* [39–41]	cold lake vacuum residue (CLVR)	molybdenum octoate	a 250 mL stirred semibatch. Conditions: 415−445 °C, 13.8 MPa, catalyst concentrations of 100-1800 ppm Mo and a reaction time of 1 h.	1. The optimum Mo concentration in terms of minimizing coke formation (2.9 wt%) and maximizing the conversion of residue (84.0 wt%) was found to be at 600 ppm Mo. 2. Short reaction times and high catalyst concentration, i.e. >600 ppm Mo, yielded amorphous coke with high H/C ratio.
Kim *et al.* [42]	vacuum residue (VR)	molybdenum hexacarbonyl	a 150 mL batch autoclave reactor. Conditions: 623-683 K, 9.5-10.0 MPa, 700-4000 rpm, a catalyst concentration of 360 ppm and reaction times of 0.0-6.0 h.	1. The formation of light oils was strongly related to operating conditions, such as hydrogen pressure, reaction time and reaction temperature. 2. EXAFS analysis shows that the MoS_2 phase was *in situ* formed with shorter Mo-S and coordinated Mo-Mo which indicates the abundance of the active sites.
Du *et al.* [20, 38]	Venezuelan atmospheric residue (V-AR), Karamay vacuum residue (KLVR) and Karamay vacuum gas oil (KLVGO)	molybdenum naphthenate	a 500 mL batch autoclave reactor. Conditions: 420 °C, 8.0 MPa, 500 rpm, a catalyst concentration of 300 ppm and a reaction time of 1.0 h.	1. The conversion of the feedstocks enhanced in the presence of the dispersed catalyst. 2. The presence of the dispersed active sites increases the hydrogen free radical concentration which boosts the cracking reactions of the naphthenic and aromatic hydrocarbons, however, it suppresses the formation of isomerization products.
Nguyen *et al.* [110]	Arabian light atmospheric residue (AR)	molybdenum naphthenate	a 250 cm^3 batch autoclave reactor. Conditions: 420 and 430 °C, 15.0 MPa, 600 rpm, a catalyst concentration of 600 ppm Mo and reaction times of 0.0-1.0 h.	The presence of *in situ* formed MoS_2 catalysts activates the hydrogen species to catalytically react with atmospheric residue fractions to yield. This results in yielding lighter fractions, i.e. gas oil and naphtha, with an infinitesimally small amount of coke.
Jeon *et al.* [49, 50]	oil sand bitumen	layered ammonium	a 200 mL batch autoclave reactor.	1. Synergistic effect of the CoMo bimetallic dispersed catalyst was noticed.

		cobalt molybdate	Conditions: 420 °C, 7.0 MPa, 500 rpm, a catalyst molar ratio of Co/Mo of 1 and a reaction time of 1.0 h.	2. The presence of the dispersed catalysts promoted the yield of the liquid product and enhanced the conversion of the asphaltene and sulfur 3. It is suggested that the bimetallic effect arises due to the chemical bonding between the two metals to form a single catalyst.
Bdwi *et al.* [24]	heavy vacuum gas oil (HVGO)	iron naphthenate, molybdenum 2-ethylhexanoate and cobalt 2-ethylhexanoate	a 300 mL batch autoclave reactor. Conditions: 390-450 °C, 8.5 MPa, 950 rpm, catalyst concentrations of 300-1000 ppm and a reaction time of 1.0 h.	1. The dispersed catalysts enhanced the catalytic hydrogenation by generating reactive hydrogen. 2. High concentration of the dispersed catalyst precursors led to retreat in the catalytic performance due to the formation of larger metal crystals. 3. Co dispersed catalyst showed the best hydrogenation activity compared to Fe and Mo.
Li *et al.* [111]	a kind of coal from Anhui (AHC) and an atmospheric residue from Merey (MRAR)	molybdenum naphthenate and synthesized iron-nickel bimetallic catalyst precursor	a 500 mL stirred autoclave. Conditions: 400 °C, 8.0 MPa, catalyst concentrations of 500-1000 ppm, a 3:1 oil-to-coal ratio and a reaction time of 1.0 h.	1. The hydrogenation activity of the synthesized catalyst precursor was found to be better than that of the molybdenum naphthenate catalyst. 2. The synthesized catalyst precursor contributed in enhancing the conversion of coal.
Liu *et al.* [27]	Gudao vacuum residue	molybdenum dithiocarboxylate (MoDTC) and molybdenum dithiophosphate (MoDTP)	a 165 cm^3 high pressure internally stirred autoclave. Conditions: 350-420 °C, 7.0 MPa, a catalyst concentration of 5000 ppm Mo and reaction times of 0.0-3.0 h.	1. The activation of the catalyst precursor requires certain conditions of temperature and time period. 2. High dispersion of the precursor facilitated the conversion the catalyst precursors to their active phase that occurs in the presence of sulfur-containing species of external H_2S.
Shi and Que [48]	Liaohe vacuum residue	cobalt naphthenic and nickel naphthenic	a 100 mL magnetic stirred autoclave. Conditions: 436 °C, 7.0 MPa, catalyst concentrations of 0-200 ppm, 3.4 g tetralin (THN) hydrogen donor and a reaction time of 1.0 h.	1. Simple mathematical addition effect is governed by combining of Ni and Co oil-soluble precursors. 2. A synergy between the dispersed catalyst and the hydrogen donor was observed in terms of inhibiting coke formation.
Shen *et al.* [36]	Liaohe vacuum residue	mixtures of molybdenum dithiocarboxylate (MoDTC) and	a 100 mL magnetic stirred autoclave. Conditions: 430 °C, 7.0 MPa, a catalyst	1. XRD of the spent catalyst showed no evidence of the formation of a Ni-Mo (or Fe-Mo) sulfide.

		nickel or iron naphthenate (NiNaph or FeNaph)	concentration of 200 ppm of metal based and a reaction time of 1.0 h.	2. The presence of the second metal improved the dispersion of the catalysts.
Li *et al.* [112]	Venezuela fuel oil (VFO)	molybdenum naphthenate with iron(III) dodecylbenzenesulfonate (IDBS) additive	a 500 mL stirred autoclave. Conditions: 420 °C, 7.0 MPa, 750 rpm, a catalyst concentration of 50 ppm of metal-based, IDBS concentrations of 0-1500 ppm and a reaction time of 1.0 h.	1. The catalytic performance of the Mo catalyst could be enhanced by increasing their sulfidity. 2. The synergy between the Mo catalyst and IDBS resulted in hindering the formation of coke deposits and preventing their agglomeration.
Inukai [113]	coal with petroleum atmospheric residue (AR)	molybdenum dithiophosphate (MoDTP)	a 40 cm^3 minireactor. Conditions: 375-450 °C, 6.0-7.8 MPa, catalyst amounts of 0.5%-1.0% Mo as metal, 1:1 and 1:2 coal-to-AR ratios and reaction times of 0.5-1.5 h.	low yields of solvent-insoluble were observed by using the oil-soluble Mo compared to the Ni-Mo/Al_2O_3 catalyst.
Rankel [114]	Arabian heavy vacuum residue	tungsten hexacarbonyl and nickel naphthenate	a 300 ml stirred autoclave. Conditions: 340 °C, 13.4 MPa, 0.2 L/min H_2 flow was maintained throughout the process, a catalyst precursors molar ratio of 0.5 and reaction times of 0.0-4.0 h.	The dispersed oil-soluble Ni-W inhibited the coke formation. However, it produced less gasoline range material, CCR conversion, demetallation and desulfurization compared to the presulfided Ni-W/Al_2O_3 catalyst at the same conversion.
Panariti *et al.* [45, 46]	vacuum residue of Belayim crude	molybdenum acetyl acetonate (MoAA), molybdenum naphthenate (MoNaph), iron naphthenate (FeNaph), phospho-molybdic acid (PMA), nickel naphthenate (NiNaph), ruthenium acetyl acetonate (RuAA), cobalt resinate (CoRe),	a 30 mL autoclave with a swinging capillary stirring device. Conditions: 460 °C, 9.0 MPa, a catalyst concentration of 1000 ppm of metal-based and reaction times of 0.0-1.5 h.	1. The catalytic performance of the metals tested is as follows: Mo>Ni~Ru>Co>V>Fe. 2. The catalytic performances of the tested precursors found to be nearly independent of the organic ligand. 3. No evidence of the bimetallic sulfide formation

		and vanadium resinate (VRe)		
Jian *et al.* [30]	Gudao vacuum residue	molybdenum dithiocarboxylate (MoDTC), nickel naphthenate (NiNaph), cobalt naphthenate (CoNaph) and nickel acetate ($Ni(Ac)_2$)	a 500 mL steel batch autoclave reactor. Conditions: 420 °C, 7.0 MPa, a catalyst precursor of 500 ppm, sulfiding agent fed at a ratio of 3:1 sulfur-to-metal and a reaction time of 1.5 h.	1. The catalytic performance of the catalyst precursors tested is as follows: MoDTC>NiNaph>CoNaph>$Ni(Ac)_2$. 2. The optimum concentration of catalyst precursors was 500 ppm.
Al-Rashidy *et al.* [32]	light vacuum gas oil (LVGO)	layered ammonium of cobalt molybdate (Co-LTM) and layered ammonium of nickel molybdate (Ni-LTM)	a 300 mL batch autoclave reactor. Conditions: 400-430 °C, 8.0 MPa, 1000 rpm, a dispersed catalyst concentration 250 ppm for each precursor and reaction times of 0.0-1.0 h.	1. The coke formation was significantly reduced in the presence of dispersed active metal sites that enhance the catalytic hydrogenation reactions 2. The bimetallic oil-soluble Ni-LTM catalyst precursor hindered coke deposition without affecting the naphtha yield, in contrast to the thermal run.
Jeong and Lee [115]	Vacuum residue (VR)	hexacarbonyl tungsten ($W(CO)_6$) and hexacarbonyl molybdenum ($Mo(CO)_6$) with dimethyl disulfide (DMDS) as a sulfiding agent	a 150 mL autoclave. Conditions: 692 K, 9.5 MPa, 1500 rpm, a dispersed catalyst concentration 0.113 mmol metal for each precursor, 5.3 mmol sulfiding agent and a reaction time of 0.5 h.	1. Smaller WS_2 crystals were formed during the VR hydrocracking with aid of DMDS. 2. TEM and EXAFS analysis showed that both W and Mo catalyst precursors formed nano-scaled mono-slab of MoS_2 and WS_2. 3. The high oil-solubility of the *in situ* formed WS_2 crystals improved their catalytic performance compared to MoS_2.

Due to their unique property of high ratio of surface area to volume, dispersed catalysts are considered as an alternative for the solid powder catalysts. Dispersed catalysts have proven high catalytic activity that made it desirable for slurry-phase hydrocracking of heavy oil. Since that the oil-soluble dispersed catalysts proved superior catalytic performance compared to the water-soluble dispersed catalysts, they had a better chance to be commercialized. Examples of these technologies are the Canadian $(HC)_3$ technology, the EST technology, the M-coke technology and the Microcat-RC technology.

The HighConversion HydroCracking HomogeneousCatalyst $(HC)_3$. The $(HC)_3$ was developed by the Canadian Alberta Research Company. The process implemented oil-soluble dispersed catalyst that either based on iron or molybdenum, where the precursors are either molybdenum 2-ethylhexanoate or iron pentacarbonyl. The precursor is mixed in the reactor with stripping to ensure forming well-dispersed colloidal particles that work on promoting the conversion of the heavy oil and inhibiting coke formation through enhancing the hydrogenation reactions. It is proposed that the active colloidal particles are formed by sulfiding the catalyst precursor *in situ* by benefiting from the sulfur content of the heavy oil itself. The wetting property of the formed colloidal particles enables them to be attached with the coke spheroids, so this will reduce coke formation by preventing the coke precursors from being coalesced. The catalyst colloidal particles sizes were investigated by doing chemical analysis on the coke formed after the reaction and they were found to be less than 0.1 nm [116]. Later, the same principle of the $(HC)_3$ technology of using homogeneous catalyst was utilized by Headwaters Technology Innovation Group (HTIG). The dispersed catalyst is being in either colloidal or molecular form and its size was close to the asphaltenes within the heavy oil. The process is conducted in a pilot scale slurry-phase reactor on Cold Lake bitumen AR while the catalyst is being sulfided *in situ* and fed at a concentration of 300 ppm [6].

The Eni Slurry Technology (EST). The Italian Eni company has invented a new slurry-phase hydrocracking technology that has the ability to improve the conversion, even for the heaviest feeds, to almost complete conversion. This development was achieved by following a specific way of recycling the unconverted fraction as well as implementing an organic oil-soluble dispersed catalyst. The process is conducted at a temperature of 400-

450 °C and at a pressure of 150.0 bar. The hydrogen is fed from the bottom of the reactor with the catalyst precursor, i.e. molybdenum naphthenate, that is mixed with the feed to ensure good mixing and then fed to the reactor where the catalyst is sulfided *in situ* to give the active phase of MoS_2. Other metal-based dispersed catalysts were studied for this process such as Fe, Co, Ni, and V, however, the Mo-based dispersed catalyst showed the highest catalytic activity in terms of hydrogenation [6, 117].

The EST technology show very high conversion of 98 to 99% and high hydrotreating, e.g., hydrodesulfurization > 80% and hydrodemetalation > 99% [8]. Some improvements have made EST one of the best slurry-phase hydrocracking technologies such as its capability to handle different types of feeds as well as its high efficiency of hydrogen utilization. EST technology considered as the only hydrocracking technology that can accomplish complete conversion and this is attributed to its specialized technique of recycling the unconverted fraction and dispersed catalyst (Figure 2-13) [6, 8].

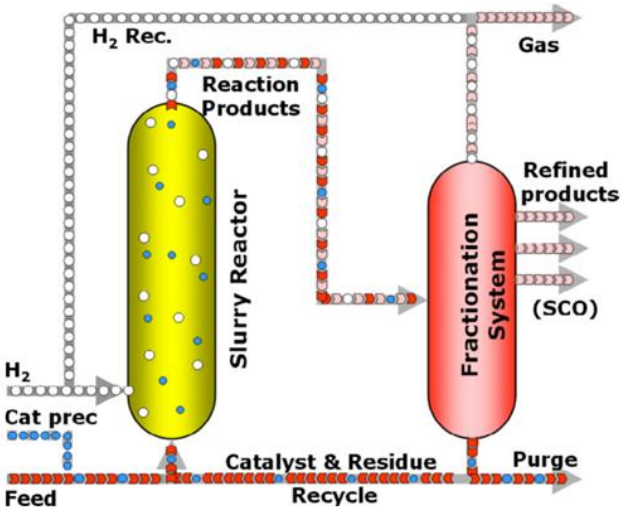

Figure 2-13 Demonstration of the Eni Slurry Technology (EST) [10].

The ExxonMobil M-coke technology. The M-coke was developed by employing molybdenum dispersed catalyst from a mixture of two types of oil-soluble precursors which were phosphomolybdic acid and molybdenum naphthenate. The process was conducted on an experimental scale of one drum per day at 440 °C and a pressure of 170.0 bar. The conversion of this process reaches up to 90%, however, this process still could not be applied for industrial scale because of the high synthesis cost of the catalyst precursors [6].

2.2 The Nature of the Dispersed Catalysts

2.2.1 Sulfidation

Prior to contacting with the feed, the dispersed catalysts, i.e. nanosized transition metal sulfide crystals, are activated from the precursors by sulfidation. As mentioned earlier, the preparation of water-soluble dispersed catalyst requires pretreatment steps that involve emulsion and dispersion followed by dehydration, so its activation procedure is delimited to *ex situ*. However, the oil-soluble precursors could be sulfided either *in situ* or *ex situ*. In the case of oil-soluble precursors, the organometallic compounds decompose upon reaching a suitable process/preparation temperature to release cations that form the active metal sulfide crystals by reacting with sulfur source molecules. Previous studies on oil-soluble precursors proved that albeit the ligands provide thermal liability as well as efficient dispersion for the *in situ* formed dispersed active sites, they has almost no effect in terms of catalyst performance [36]. To promote the rate of the reaction, sufficient hydrogen pressure must be maintained [5].

The sulfur sources present in the petroleum feedstocks as organosulfur compounds. The *in situ* sulfidation occurs by reacting the released cations with H_2S molecules that evolve by hydrodesulfurization reactions. The number of coordinately unsaturated active sites (CUS) could be greatly affected by the ratio of hydrogen to hydrogen sulfide [35].The sulfidation occurs at a temperature ranging between 300 and 400 °C under a pressure of about 1000–2500 psig [12, 118].

As attempts to ensure optimum sulfidation, different researches have suggested the implementation of liquid sulfiding agents, such as elemental sulfur [30] IDBS [112] and DMDS [115]. Jeong and Lee [115] showed the effect of employing dimethyl disulfide (DMDS) as a sulfidation agent to effectively get WS_2 dispersed catalyst for VR hydrocracking at 692 K under a hydrogen pressure of 9.5 MPa. It was observed that the addition of the DMDS caused a notable H_2 consumption compared to the run of its absence (Figure 2-14).

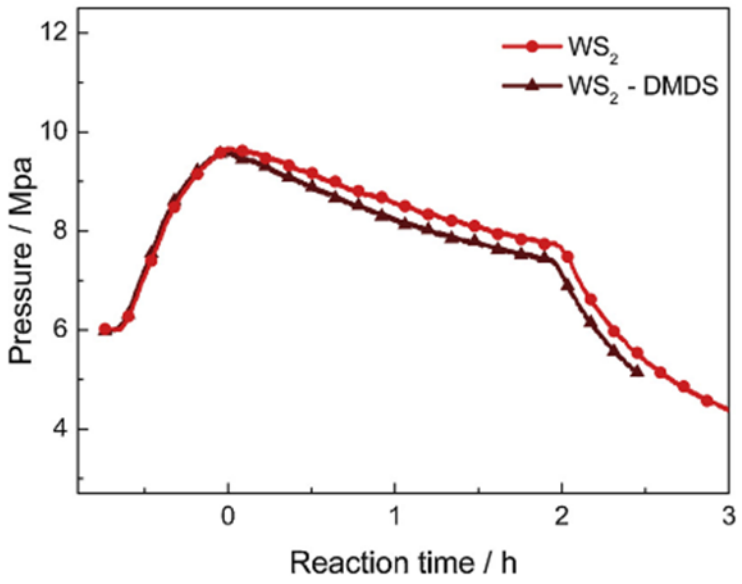

Figure 2-14 Pressure profile of VR hydrocracking over WS_2 and WS_2-DMDS at 692 K and 9.5 MPa [115].

Additionally, the TEM images showed that the sulfiding agent resulted in reducing the average particle size of the WS_2 catalyst from 13.9 nm to 10.6 nm. Therefore, the sulfiding agent could boost the catalytic performance of the dispersed catalyst which is reflected in enhancing the hydrogenation and increasing the asphaltene conversion. A similar observation was reported by Li *et al.* [112] where the employment of the sulfiding agent showed synergy effect with the dispersed catalysts that helped in hindering the formation of coke deposits and preventing their agglomeration.

2.2.2 Catalytic Activity

The crystalline structure of the active metal sulfides dispersed catalysts appear as trigonal prisms of sulfur coordinated to the metal. The formed trigonal prisms are strongly bonded to form S-Mo-S that extends to form a single layer structure. Figure 2-15 shows the structure of a single layer of MoS_2 that is formed by first the reduction of Mo IV to Mo III.

The reduced Mo III is bonded with another Mo III to form distorted octahedral with respect to the molybdenum coordination that extends to form a single layer structure of MoS2 [117].The hexagonal coordination displayed by the unsupported metal sulfides is considered as the most significant factor responsible for the hydrogen uptake function.

The available coordinately unsaturated sites (CUS) and/or sulfur ion vacancies and become active sites for hydrogenation by the Lewis acid characteristic. The presence of the Lewis acid character permits the CUS to adsorb molecules with the unpaired electrons present in the feed. Moreover, they are considered as sites for hydrogen activation. The functionality of a catalyst is accredited by its ability for activating hydrogen. The hydrogen molecules are activated by moving to the surface of the catalyst followed by heterolytically and homolytically splitting to yield the S-H and Mo-H moieties, respectively [119]. The formed moieties are unstable, so they could react easily with the free radicals evolved by thermal cracking of the hydrocarbon, which inhibit the condensation of polycyclic aromatic hydrocarbons (PAHs). Moreover, the catalytic hydrogenation offered by the dispersed transition metal sufides plays an important role in facilitating the hydrotreating reactions, such as hydrodesufurization where the free radicals formed after breaking the C-S bonds are hydrogenated thereof. Surprisingly, the dispersed catalysts could have cracking ability that is attributed the S-H groups [12]. A research conducted by Petit and coworkers [120] proved that the Brønsted acid sites present in sulfided Mo, NiMo, and CoMo phases.

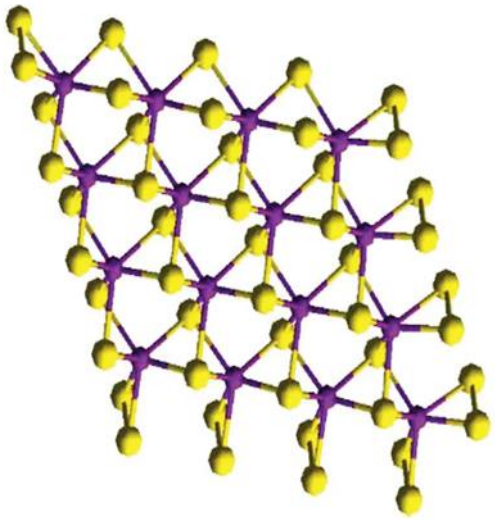

Figure 2-15 The single layer structure of MoS_2 [117]. (The purple spheres stand for Mo and the yellow ones stand for S).

Kim *et al.* [42] implemented Extended X-ray absorption fine structure (EXAFS) analysis to study the structural behavior of the dispersed MoS_2 during the reaction. Analysis of the spent catalysts by EXAFS and TEM demonstrated that the nanosized MoS_2 phase was well developed from $Mo(CO)_6$ in the early stage of the reaction with lower Mo-S and Mo-Mo coordination verifying the small MoS_2 particles having more exposed and defect sites as active phases (Figure 2-16).

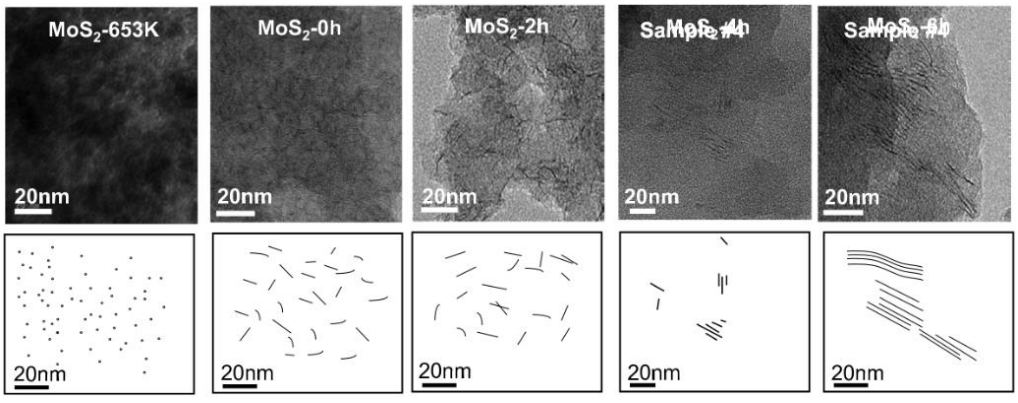

Figure 2-16 Effect of reaction time on dispersed MoS_2 catalysts depicted by TEM [42].

To understand the bulk activity of the metal sulfides, hypothesized models were suggested, i.e., brim sites model and rim-edge model.

Brim sites model. The brim sites model was developed by the Topsøe group [121–124] through combining the results of surface studies governed from scanning tunneling microscopy (STM) with *ab initio* theoretical calculations based on the density functional theory (DFT). The commonly described way of molecular binding to occur is that coordinately unsaturated sites (CUS) are required to achieve binding, however, the brim sites model suggests that the binding sites are one dimensional metallic brim sites as found by the DFT calculations. In other words, the active sites are located on the rim as well as on the brim on the basal plane close to the rim as per characterized by a continuous electronic structure having ‘‘metal-like’’ conduction properties. The rim sites could be utilized to enhance the catalytic activity by altering their morphology through incorporating promoters, e.g. Co-Mo-S and Ni-Mo-S, and/or varying synthesis conditions. Figure 2-17 shows the STM image of MoS_2 brim where the brim sites present to be bright yellow.

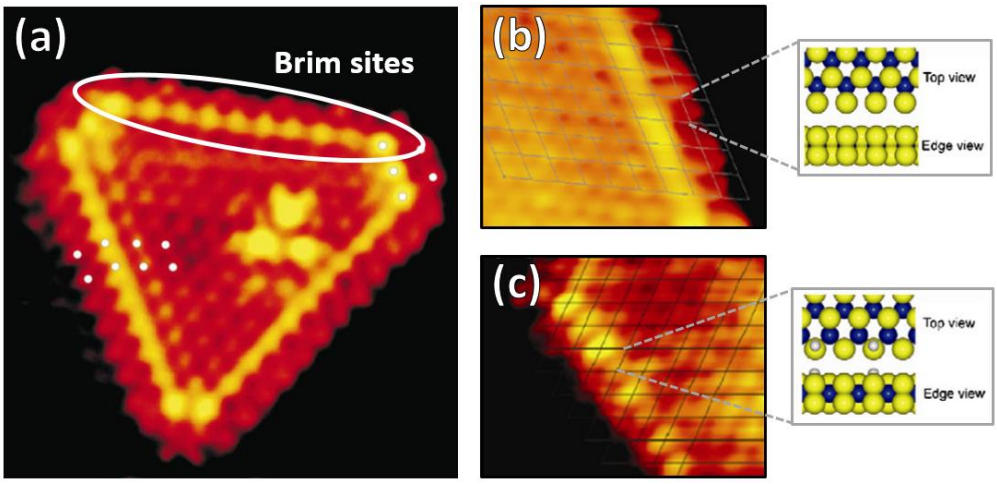

Figure 2-17 (a) STM images of single-layer MoS_2 nanocrystals. (b) Left: Atom-resolved STM image showing the atomic-scale structure of Mo-edge on a multilayer cluster. Right: A ball model (top and side view, respectively) of the Mo-edge fully saturated with sulfur dimers. (c) Left: Atom-resolved STM image showing the atomic-scale structure of S-edge on a multilayer cluster. Right: A ball model (top and side view, respectively) of the fully sulfided S-edge and with a fractional coverage of S–H groups. (S: yellow; Mo: blue; H: gray). Adapted from Refs. [121, 124].

Rim-Edge model. The catalytic activity of the metal sulfide was plainly described by Daage and Chianelli [125] through proposing the "Rim-Edge" model. The activity is suggested to be attributed mainly to the disordered nature of the edge plane. Figure 2-18 shows a schematic description of the planes where the edge planes have the high activity and the basal planes considered as inert. The model suggests two kinds of sites based on their position over the stacked lamellae of metal sulfides. The rim sites, located on the first lamella of the stacking, are active for hydrogenation reactions as well as C-S bonds session. Nevertheless, for the internal lamellae of the stacking, only edge sites are active for breaking C-S bonds [117]. Additionally, the selectively of the unsupported metal sulfide is affected by the height of stacking planes.

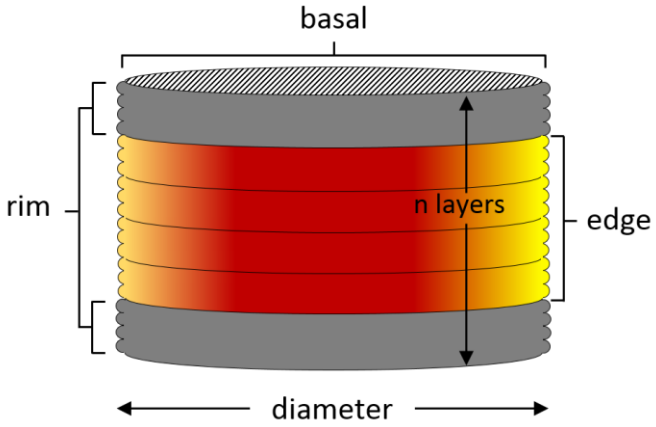

Figure 2-18 Rim-edge theory. Adapted from Ref. [125].

Second metal as a promoter. The use of other transition metal, such as cobalt or nickel, beside molybdenum could be considered being as a promoter. The incorporation of a second metal could modify the sulfur–metal binding energy. Therefore, the catalytic activity is enhanced by shifting the binding energy, referring to the volcano curve, towards an intermediate position [10]. Zhou *et al.* [52] presented that the *in situ* formed CoMoS active species were highly affected for hydrocracking of heavy oil in terms of reducing sediment and enhancing asphaltene conversion. The promotional effect governed was ascribed to the synergetic effect between cobalt and molybdenum which is explained by their electronic configurations. Cobalt ([Kr] 4d55s1) has a stronger attraction to sulfur than molybdenum ([Ar] 3d74s2). Accordingly, the molecular structure of the bimetallic catalyst is formed by considering the cobalt as a promoter that attracts the sulfur and then transfers it to its nearby molybdenum.

2.3 Synergy between Dispersed and Supported Catalysts

Most of the technologies studying the use of dispersed catalysts suggest that the cracking reactions take place thermally while they are immediately followed by the hydrogenation reactions that are enhanced catalytically by the presence of the dispersed metal. The supported catalysts are used commercially for providing the catalytic activity for both reactions at once, so such catalysts considered to be as bifunctional catalysts because that the supports, which are usually mixed alumina oxide (Al_2O_3–ZrO_2, Al_2O_3–MgO, etc.), provide the acidity needed for the cracking reactions while the active metal sites provide the hydrogenation function.

The use of supported catalysts for heavy oil upgrading is more likely to be implemented for fixed-bed or ebullated-bed reactors rather than slurry-phase reactors. The catalytic activity of supported catalysts depends on both the support and the active sites. A comparison between different hydrocracking supported catalysts was made by Ghosh *et al.* [126] concluded that zeolites and silica-alumina are widely used supports due to their high efficiency in term of ability to load different metals and also cracking catalytic activity. Figure 2-19 shows the ascending arrangement of some of the commercially used supports and metals in terms of their catalytic activity.

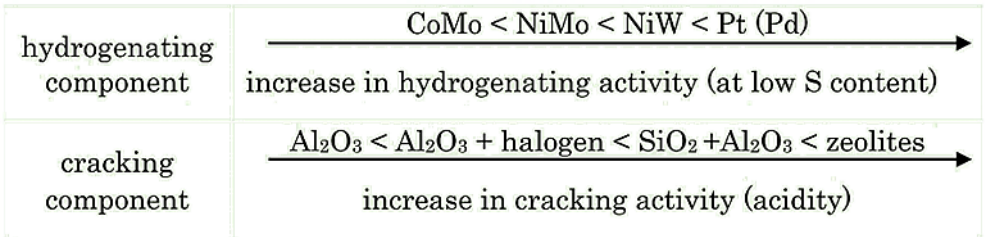

Figure 2-19 Bifunctional hydrocracking catalytic activity [127].

The supported catalysts used in heavy oil upgrading are synthesized by either wet or incipient wetness impregnation methods where the active metal sites are deposited on the support. The impregnation of the active sites takes either on the support which is classified, depending on the commercially used catalysts for heavy oil upgrading, into two general categories which are microporous (zeolites) and mesoporous materials. In order to make the metal supported sites active for the hydrogenation, the catalyst is converted to its sulfide form by pretreatment with a sulfiding agent is conducted either *ex situ* or *in situ* [5].

Very few studies have investigated the idea of using both homogenous oil-soluble dispersed catalyst and solid supported catalyst to study its synergic effects. Kennepohl and Sanford [109] conducted the research on this idea in order to overcome the problem of coke formation during the hydrocracking process of Athabasca bitumen. The study was conducted in the absence and presence of the supported catalyst, i.e. Co-Mo/γ-Al_2O. The dispersed catalyst was derived from a mixture two oil-soluble precursors which are molybdenum naphthenate and Molyvan-L, a mixture of 80 wt% sulfurized oxymolybdenum (V) dithiophosphate and 20 wt% of aromatic petroleum oil. The experiments conducted utilizing the standalone dispersed molybdenum catalyst showed high ability in prevent the coke formation. However, the coke deposition decreased as the concentration of molybdenum dispersed catalyst in the feed increased up to approximately 800 ppm where the solid deposits start increasing again. It was explained by the fact that the dispersed MoS_2 could favors the formation of coke by either stabilizing the coke precursors through hydrogen transfer of by enhancing the precipitation of solids. The other phase of the experiments was conducted using the solid catalyst where the formation of solid deposits increased sharply. The dispersed molybdenum catalyst works on hindering

the catalytic performance of the supported catalyst by depositions on the active sites. As such, although introducing the dispersed catalyst together with the solid supported catalyst suppresses the formation of coke, it actually diminishes its overall catalytic performance.

Other research was done by Emad *et al.* [24] to study thoroughly the synergic effects of implementing dispersed catalysts with a supported catalyst. In this study, not like Kennepohl & Sanford [109], where the dispersed catalyst used is only Mo, different oil-soluble dispersed catalysts were utilized by considering different metal precursors. The study focused on the promotional effects of the oil-soluble dispersed catalysts on the slurry hydrocracking of vacuum gas oil (VGO). Different metal precursors were investigated, i.e. oil-soluble iron naphthenate, molybdenum 2-ethylhexanoate and cobalt 2-ethylhexanoate. The effect of the nature of the dispersed metal was studied by testing each oil-soluble precursor alone. The sulfiding of the catalyst was performed *in situ* to get the active phase, i.e. the metal sulfide. The formation of the active sites was proved by conducing FTIR analysis of the spent catalyst.

This study showed that the introduction of the dispersed catalysts reduced the formation of coke by boosting the catalytic hydrogenation activity through generating reactive hydrogen. Nevertheless, applying high concentration of the dispersed catalyst led to reduce the hydrogenation activity by forming large metal crystals that result in losing the surface area (active sites per unit amount). Among all oil-soluble dispersed catalysts observed, cobalt showed the optimum catalytic performance in terms of hindering coke deposition and maximizing distillate yield. Figure 2-20 shows the percentage of coke formed over different concentration of Mo, Co and Fe standalone catalysts.

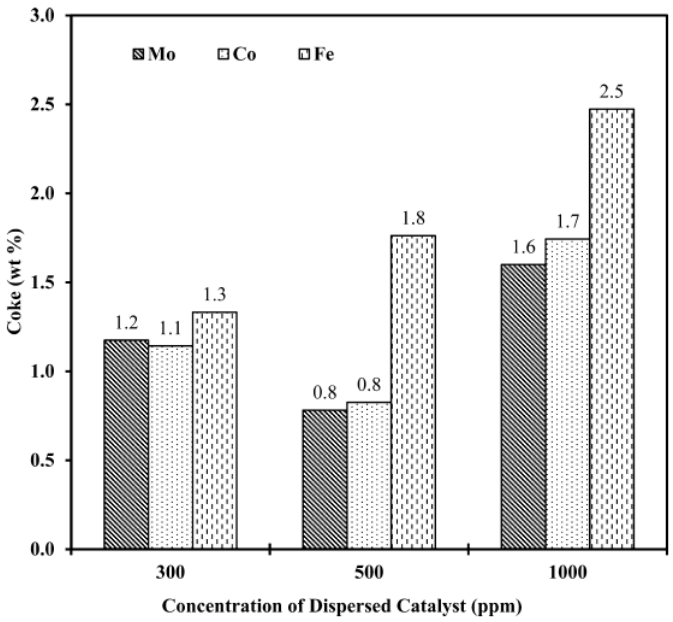

Figure 2-20 Amounts of coke formed over different concentration of Mo, Co and Fe standalone catalysts [24].

A compilation of previously studied systems of co-catalytic slurry-phase hydrocracking of heavy oils is presented in Table 2-4.

Table 2-4 Summary of literature on heavy oil upgrading over mixed (dispersed+supported) catalysts.

Reference	Feedstock	Dispersed catalyst precursor	Solid supported catalyst	Operating conditions	Key findings
Rankel [114]	Arabian heavy vacuum residue	a mixture of tungsten hexacarbonyl and nickel naphthenate	presulfided Ni-W/Al_2O_3	a 300 ml stirred autoclave. Conditions: 340 °C, 13.4 MPa, 0.2 L/min H_2 flow was maintained throughout the process, a dispersed catalyst precursors molar ratio of 0.5, a 1:100 supported-catalyst-to-oil ratio and reaction times of 0.0-4.0 h.	No apparent effects were observed on coke formation and distillation boiling ranges upon mixing the two catalysts.

Kennepohl and Sanford [109]	Athabasca bitumen	Molyvan-L and molybdenum naphthenate	Co-Mo/γ-Al_2O_3	a 1.0 L batch autoclave reactor. Conditions: 400 °C, 1000 Psi, 600 rpm, dispersed catalyst concentrations of 0-6000 ppm, a 1:4 supported-catalyst-to-oil ratio and a reaction time of 4.0 h.	The presence of the solid supported catalyst caused an increase in coke formation and an overall reduction in catalytic performance as a function of dispersed MoS_2 concentration.
Bdwi *et al.* [24]	heavy vacuum gas oil (HVGO)	cobalt 2-ethylhexanoate, molybdenum 2-ethylhexanoate, and iron naphthenate	W−Ni/Al_2O_3−SiO_2	a 300 mL batch autoclave reactor. Conditions: 390-450 °C, 8.5 MPa, 950 rpm, dispersed catalyst concentrations of 300-1000 ppm, 1:40 and 1:10 supported-catalyst-to-oil ratios and reaction times of 0.5-1.5 h.	1. VGO conversion can be controlled by varying the supported catalyst loading, however, the coke formation is delimited by controlling adjusting the dispersed active sites concentration. 2. SEM of the spent supported catalyst showed that the active metal sites are deposited on the support. 3. A lower amount of coke deposition was formed when a lower amount of supported catalyst (1:40 supported-catalyst-to-oil ratio) was applied.
Al-Rashidy *et al.* [32]	light vacuum gas oil (LVGO)	layered ammonium of nickel molybdate (Ni-LTM)	W−Ni/Al_2O_3−SiO_2	a 300 mL batch autoclave reactor. Conditions: 400-430 °C, 8.0 MPa, 1000 rpm, a dispersed catalyst concentration 250 ppm for each precursor, a 1:10 supported-catalyst-to-oil ratio and reaction times of 0.0-1.0 h.	1. SEM images showed that injecting the dispersed catalyst, as an additive, has significantly decreased the coke deposition on the solid supported catalyst surface 2. The acidic support of the solid catalyst is responsible for the cracking of the heavy molecules; however, hydrogenation of intermediate carbanion ions take

					place over the supported metals as well as on the dispersed active metal sites that suppress coke formation.

2.3.1 Reaction Kinetics

The heavy oil contains wide ranges of different hydrocarbon components that makes it very complex in terms of characterization. Modeling such feeds, that involve producing a huge network of interconnected reactions; require sophisticated analytical and numerical techniques. Fortunately, alternative methods of kinetic modeling have been suggested in the literature in order to solve this issue by simplifying the reactions through different techniques to get predictable results of the big distribution of the product. Due to its practicality, discrete or traditional lumping technique is considered the most used [128]. In the discrete lumped approach, the chemical components involved in the process are distributed in lumps in which they are assigned as psedocomponents. The lumps are formed by various manners depending on different factors. The distillation ranges technique is considered as the most practical way of apply the discrete lumping in which the chemical components are divided based on boiling point ranges depending on the products of interests, for example naphtha [IBP—204°C], middle distillates [204°C–343°C], vacuum gas oil [343°C–538°C], and vacuum residue [538°C+] [8]. Figure 2-21 shows some of previously proposed discrete lumped kinetic models based on boiling points ranges. Additionally, discrete lumping approach could be attained by considering the idea of assigning psedo-components that are formed either based on the carbon number (Paraffins, …) or based on their chemical structure which could be qualified by using special well

known crude characterization method such as SARA (saturates, aromatic, resins, and asphaltenes) and PIONA (n-paraffins, iso-paraffins, olefins, naphthenes, and aromatics). Table 2-5 shows a compilation of studies adopted the discrete lumping approach to estimate the kinetic parameters the reactions involved in heavy oil upgrading.

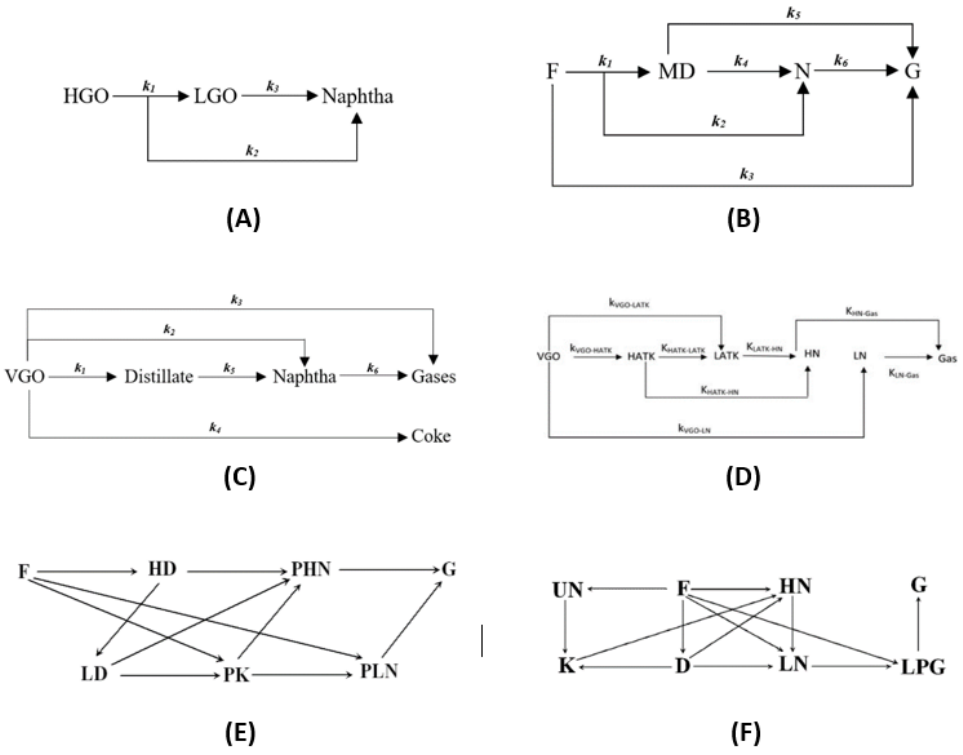

Figure 2-21 Different lumps proposed; A. 3-lump [129], B. 4-lump [130], C. 5-lump [24], D. 6-lump [131], E. 7-lump [132], F. 8-lump [133].

Table 2-5 List of some proposed discrete lumped models from literature.

n-Lump	Feed	Catalyst(s)	Lumps	Operating mode	Reference
3	HGO	Ni-Mo/Al_2O_3	heavy gas oil (HGO), light gas oil (LGO) and naphtha.	continuous (trickle-bed reactor)	Yui and Sanford [129]
3	AR	Ni-Mo/γ-Al_2O_3	atmospheric residuum (AR), light oils and gases.	continuous (autoclave stirred tank reactor)	Callejas and Martínez [134]

4	VGO	Ni-Mo over mixed support of USY-zeolite and alumina-silica	VGO, middle distillates, naphtha and gas.	continuous (fixed-bed reactor)	experimental data collected by Ali *et al.* [135], kinetic modeling performed by Valavarasu *et al.* [130]
4	VGO	Ni-Mo/γ-Al_2O_3	VGO, middle distillates, naphtha and gas.	continuous (trickle-bed reactor)	Sadighi *et al.*[136]
4	VR	$NiMo/Al_2O_3$ and $NiMo/Al_2O_3$-Cr (alumina doped with chromium)	products boiling point > 450 °C (L+), products boiling point < 450 °C (L-), gas and coke.	batch (microbomb batch reactor)	Puron *et al.* [137]
5	VR	Ni-Mo/γ-Al_2O_3	VReasy (VR-MCR), microcarbon residue (MCR), gasoil, diesel and naphtha+gas.	batch (Parr autoclave stirred reactor)	De Almeida and Guirardello [138]
5	HVGO	Co-based dispersed catalyst + Ni-W over mixed support of Y-zeolite and SiO_2-Al_2O_3	HVGO, distillate, naphtha, coke and gas.	batch (batch autoclave reactor)	Bdwi *et al.* [24]
5	residue	Ni-Mo/ Al_2O_3	residue, VGO, middle distillates, naphtha and gases.	continuous (fixed-bed reactor)	Sánchez and Ancheyta [139]
5	VGO	a commercial amorphous bifunctional catalyst	VGO, diesel, kerosene, naphtha and gas.	continuous (trickle-bed reactor)	Sadighi [140]
5	LVGO	bimetallic Ni-LTM dispersed catalyst + Ni-W over SiO_2-Al_2O_3 support	LVGO, distillate, naphtha, coke and gas.	batch (batch autoclave reactor)	Al-Rashidy *et al.* [32]
5	residue	Ni-W-Mo dispersed catalyst	residue, VGO, middle distillates, naphtha and gases.	batch	Hassanzadeh and Abedi [141]
5	residue	Mo-based dispersed catalyst	residue, VGO, middle distillates, naphtha and gases.	batch (Parr autoclave stirred reactor)	Nguyen *et al.* [110]
5	VR	Mo-based dispersed catalyst	Unconverted oil (UCO), vacuum gas oil (VGO), distillates (DIST), gas and coke	batch (batch autoclave reactor)	Kim *et al.* [42]
6	VGO	a commercial amorphous	VGO, heavy aviation turbine kerosene (HATK), light aviation turbine kerosene	continuous (fixed-bed reactor)	Elkilani and Fahim [131]

		bifunctional catalyst	(LATK), heavy naphtha (HN), light naphtha (HN) and gas.		
6	VGO	a commercial amorphous bifunctional catalyst	wild VGO (WV), wild diesel (WD), wild kerosene (WK), wild heavy naphtha (WHN), wild light naphtha (WLN) and gas	continuous (trickle-bed reactor)	Sadighi *et al.* [132]
7	VGO	a commercial amorphous bifunctional catalyst	VGO (F), heavy diesel (HD), light diesel (LD), kerosene (PK), heavy naphtha (PHN), light naphtha (PLN) and gas (G)	continuous (trickle-bed reactor)	Sadighi *et al.* [132]
8	VGO	a commercial amorphous bifunctional catalyst	VGO (F), recycle (UN), diesel (D), kerosene (K), heavy naphtha (HN), light naphtha (LN), LPG and gas	continuous (trickle-bed reactor)	Sadighi and Ahmad [133]

A limited number of researches were carried out for investigating the reaction kinetics of hydrocracking of heavy oils over standalone water-soluble [25, 142] or oil-soluble [42, 110] dispersed catalysts. The previous studies agreed in the conclusion that the introduction of the dispersed catalyst enhances the catalytic hydrogenation, which was manifested by observing the variations in the estimated reaction rate constants. Kim *et al.* [42] performed a kinetic study on hydrocracking of vacuum residue (VR) over dispersed MoS_2 catalyst derived from oil-soluble molybdenum hexacarbonyl ($Mo(CO)_6$) precursor. The reaction scheme proposes five lump that are categorized as unconverted oil (UCO, >833 K), vacuum gas oil (VGO, 593–833 K), and distillates (Dist, 323–593 K) besides gas and coke (Figure 2-22).

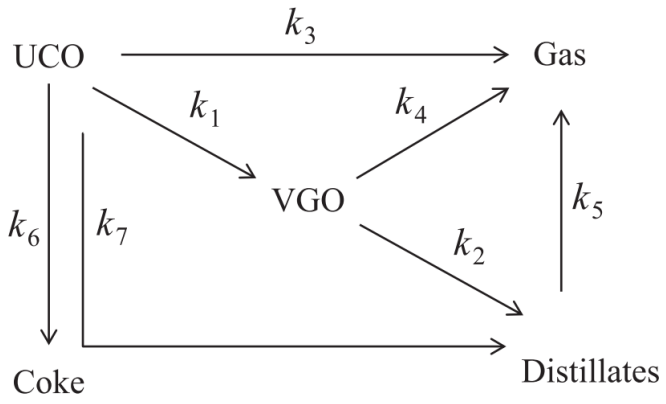

Figure 2-22 Proposed reaction mechanism of VR hydrocracking [42].

On the basis of the proposed 5-lump reaction scheme, the rate of reaction for each reacting species can be written as the following:

Rate of UCO conversion:

$$r_{UCO} = -(k_1 + k_3 + k_6 + k_6){Y_{UCO}}^2 \tag{2-2}$$

The reaction rates of formation of the pseudoproducts, i.e., VGO, distillate, gas, and coke, are as follows:

$$r_{VGO} = k_1{Y_{UCO}}^2 - (k_2 + k_4)Y_{VGO} \tag{2-3}$$

$$r_{Dist} = k_2 Y_{VGO} + k_7 Y_{UCO} - k_5 \tag{2-4}$$

$$r_{Gas} = k_3{Y_{UCO}}^2 + k_4 Y_{VGO} + k_5 \tag{2-5}$$

$$r_{Coke} = k_6{Y_{UCO}}^2 \tag{2-6}$$

A Levenberg–Marquardt algorithm encoded in MATLAB were conducted to estimate the kinetic parameters at reaction temperatures of 673 and 653 K. The estimated reaction rate constants suggest that the process takes place dominantly by hydrocracking of VR to yield VGO followed by distillates. The gas is formed mainly from distillates or VGO by cracking

rather than the direct of VR, however, the formation of coke is mostly occurring due to VR cracking. Therefore, the coke formation could be avoided by properly controlling the direct VR cracking pathways to enhance the liquid fractions and minimize condensation of heavy fractions such as asphaltenes.

A few recent studies were devoted to investigating the synergy between the solid supported catalysts and dispersed catalyst by performing kinetic studies [24, 32]. Unlike the previous studies, Bdwi *et al.* [24] estimated the apparent kinetic triplets by solving the differential equation and fitting the experimental data simultaneously. The model adopted five lumps. The feed, vacuum gas oil (VGO), was processed in batch mode, so experiments were conducted at different residence times of 0.5, 1.0, and 1.5 in order get time relation with products yield required for applying the model. The experiments were conducted at a range of temperature, as well as a range of time, which resulted in 45 data points with a degree of freedom of 33. The kinetic parameters estimation shows that the activation energy of VGO hydrocracking to form distillate had required the least activation energy (1.5 kcal/mol) compared to the other competing reactions. Hence, it was concluded that VGO is most likely cracked to form distillate then distillate is cracked to form naphtha, and naphtha is cracked to gases.

CHAPTER 3

OBJECTIVES

The main objective of this study is to investigate nickel- and cobalt-based *p-tert*-butylcalix[4]arenes (TBC[4]s) as oil soluble dispersed catalysts to minimize coke formation and enhance liquid product yields by facilitating the hydrogenation/dehydrogenation reactions during hydrocracking of heavy vacuum gas oil (HVGO). In order to achieve the main objectives, following are identified as specific objectives of this study:

i. Synthesis of nickel and cobalt- based TBC[4]s catalyst precursors using a precipitation technique.

ii. Characterization of the synthesized catalyst precursors to confirm the Ni and Co compositions and coordination of the cations with the ligand forming organometallic compounds. In this regards, ICP, SEM-EDX, UV-Vis, FT-IR, XRD and ^{1}H NMR have been employed.

iii. The thermal decomposition behaviors of the synthesized catalyst complexes (to ensure leaching of the Ni-, Co- cations) are determined by thermogravimetric (TGA) and calorimetric analysis.

iv. Figure 3-1 shows a possible mechanism of thermal decomposition followed by *in situ* sulfidation (active form of the catalyst) of Ni- and Co- based TBC[4]s catalyst precursors.

v. The catalytic performance of the synthesized Ni- and Co- based TBC[4]s catalyst precursors are evaluated in a batch autoclave reactor using heavy vacuum gas oil (HVGO) as a feedstock. In this regard, the Ni- and Co- based TBC[4]s are employed both as a (a) standalone catalysts and (b) co-catalysts with a commercial Ni-W catalyst supported on mixed SiO_2-Al_2O_3-(Y-zeolite).

vi. The synergy between Ni-based TBC[4]s and the commercial Ni-W catalyst is further investigated by conducting the kinetics analysis of the co-catalytic hydrocracking experiments.

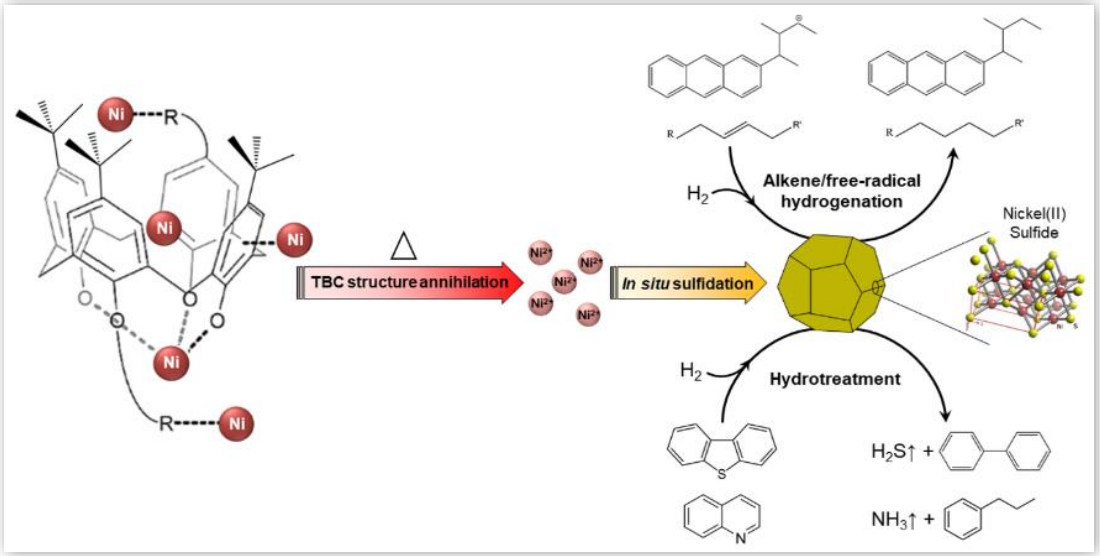

Figure 3-1 The proposed *in situ* sulfidation mechanism and catalytic reaction mechanism of dispersed catalyst derived from the metal-based calixarene precursor.

CHAPTER 4

MATERIALS AND METHODS

This chapter presents the materials and methodologies employed for synthesizing and evaluating the Co- and Ni-based TBC[4]s. The synthesis procedure of the catalyst precursors was presented, in detail. The textural and structural of the commercial Ni-W/SiO_2-Al_2O_3-(Y-zeolite) solid catalyst used for the synergy study were discussed. Prior to conducing the process with the supported catalyst, it was sulfided *ex situ* using a standard presulfiding procedure with dimethyl disulfide (DMDS) in a fixed-bed reactor. The feedstock to the process, i.e. heavy vacuum gas oil (HVGO), was provided from an ongoing operation in a Saudi Aramco refinery. The nature of feedstock was demonstrated and its physical and chemical properties were listed. The catalytic performance evaluation was performed in a batch autoclave reactor. Finally, the quantitative and qualitative product analysis techniques were discussed.

4.1 Chemicals

For synthesizing the metal-based calixarene, 4-tert-butylcalix[4]arene ($C_{44}H_{56}O_4$, ≥99.0%), cobalt(II) nitrate hexahydrate ($Co(NO_3)_2{\cdot}6H_2O$, reagent grade, ≥98.0%), nickel(II) nitrate hexahydrate ($Ni(NO_3)_2{\cdot}6H_2O$, 99.999% trace metals basis), N,N-dimethylformamide ($HCON(CH_3)_2$, anhydrous, 99.8%), dimethyl sulfoxide ($(CH_3)_2SO$, reagent grade, 99.5%), triethylamine ($(C_2H_5)_3N$, ≥99.5%), and methanol (CH_3OH anhydrous, 99.8%). Nickel(II) 2-ethylhexanoate (78% in 2-ethylhexanoic acid, 10-15% Ni)

and cobalt(II) 2-ethylhexanoate (65 wt% in mineral spirits, 12 wt% Co) were used as oil-soluble dispersed organometallic catalyst precursors to compare their catalytic behaviors against the analogous synthesized metal-based calixarenes. All chemicals were obtained from Sigma-Aldrich, USA and used without further purification. Hydrogen and nitrogen gases used in the catalyst evaluation were procured from a local supplier with a purity of 99.999%.

4.2 Supported Catalyst

A commercial supported catalyst for first-stage hydrocracking was used to study the synergic effects of its application along with the synthesized dispersed catalyst. The catalyst was composed of tungsten and nickel metal oxides anchored on a mixed support of amorphous Al_2O_3−SiO_2 (55 wt%) and Y zeolite (45 wt%). The textural and structural properties of the supported commercial catalyst are listed in Table 4-1. The catalyst was crushed and sieved to obtain particle sizes between 0.5 mm and 1.0 mm, which are suitable for slurry-phase hydrocracking in the batch autoclave reactor. To transform the metal sites to their active sulfided form, the catalyst was sulfided *ex situ* in a fixed-bed reactor [143].

A standard presulfiding procedure was followed using a straight-run gas oil spiked with dimethyl disulfide (DMDS). The volume of catalyst loaded in the fixed-bed reactor was 25.0 mL. The sulfur content of the spiked feed was adjusted to 2.5 wt% by the addition of DMDS. Hydrogen was first introduced at 10.0 L/h to pressurize the reactor system to 40 MPa at room temperature. Then, the flow of white kerosene was started at approximately 50 mL/h (~42 g/h) under hydrogen pressure. The reactor temperature was increased from room temperature to 175°C at a rate of approximately 25°C/h. The spiked feed was

introduced at this point while the temperature was increased to 200°C. The temperature was held at 200°C for one hour before increasing it to 350°C at a rate of approximately 25°C/h. These conditions were maintained overnight (16.0 hours) to ensure complete presulfiding.

Table 4-1 Properties of Commercial Hydrocracking Catalyst (KC-2710).

Property	Unite	Value
BET specific surface area	m^2/g	346
Specific pore volume	mL/g	0.37
Average pore diameter	nm	4.3
Specific total acidity	µmol/g	844
Chemical composition:		
SiO_2	wt%	33
Al_2O_3	wt%	38
WO_3	wt%	23
NiO	wt%	6
Support phase		amorphous SiO_2-Al_2O_3 and Y-Zeolite (45 wt%)

4.3 Feedstock

The feedstock for the hydrocracking process is vacuum gas oil (VGO) (Figure 4-1). Gas oil is considered as a group of a mixture of organic chemicals produced via distillation of petroleum and it has a boiling point range between kerosene and lubricating oil. The vacuum gas oil is a more viscous form of gas oil and is produced through vacuum distillation of the atmospheric residue that is the bottom effluent of the atmospheric distillation column in the refinery (Figure 4-2) [2, 144].

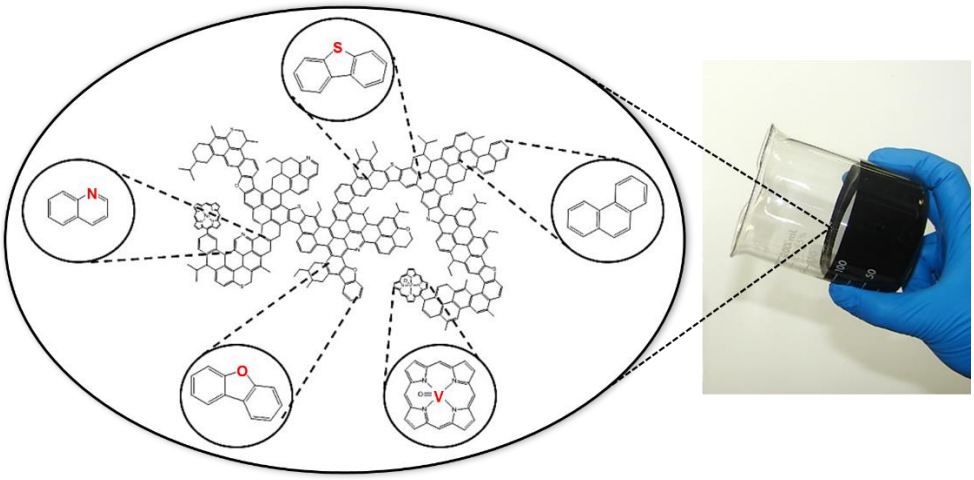

Figure 4-1 Examples of chemical species contained in HVGO.

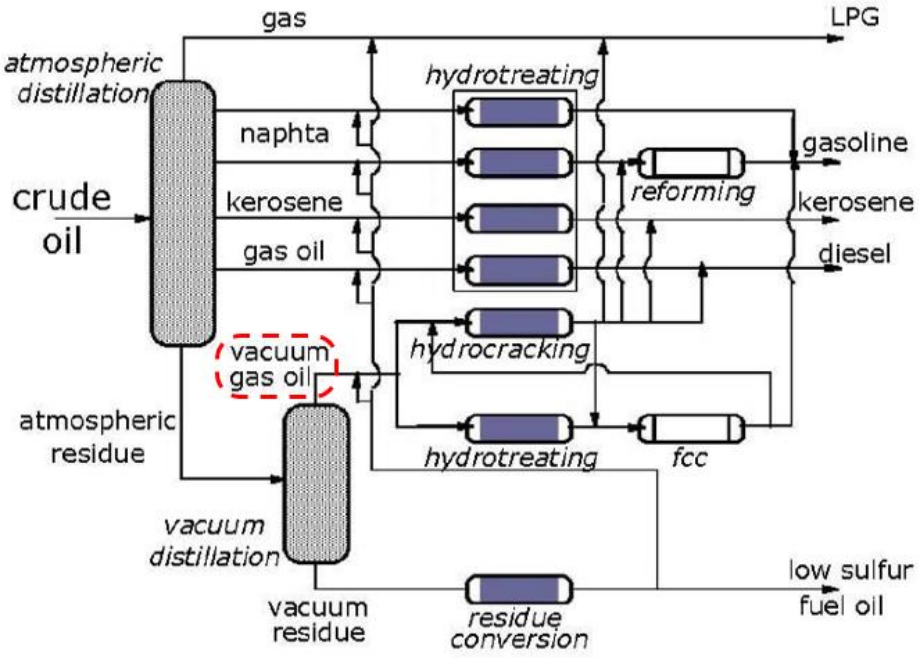

Figure 4-2 Simplified process scheme of an oil refinery [144].

In this study, heavy vacuum gas oil (HVGO) feedstock for the hydrocracking process was obtained from a Saudi Aramco Refinery. Table 4-2 shows the physical and chemical properties of the heavy vacuum gas oil.

Table 4-2 Physical and chemical properties of the heavy vacuum gas oil (HVGO).

Properties	Value
Appearance	soft but solid at room temperature
Color	greenish dark brown
Density (g/cm^3 at 15°C)	0.892
Molecular weight	442.7
The initial boiling point, IBP (°C)	343
The final boiling point, FBP (°C)	641
Elemental analysis (wt%)	
Carbon	85.10
Hydrogen	11.95
Sulfur	2.667
Nitrogen	0.215
HPLC analysis (wt%)	
Saturates	13.3
Aromatics	68.1
Polars	18.6

4.4 Experimental

4.4.1 Synthesis of Metal-Based *p-tert*-Butylcalix[4]arenes

The dispersed catalysts (nickel-*p-tert*-butylcalix[4]arene (Ni-TBC[4]) and cobalt-*p-tert*-butylcalix[4]arene (Co-TBC[4])) were synthesized from the parent TBC[4]. The metal precursors for Ni and Co were nickel(II) nitrate hexahydrate and cobalt(II) nitrate hexahydrate. The host calixarene structure was prepared by adding 100 mg of TBC[4] to 10.0 mL of dimethylformamide (DMF) and then heating to 60°C with stirring until conversion to a colloidal solution was achieved. Then, 0.6 mL of triethylamine was added dropwise to the mixture until the solution became transparent again. Cobalt(II) nitrate

hexahydrate and nickel(II) nitrate hexahydrate precursors were used for incorporation of the metal. Two grams of metal precursor was added to 10.0 mL of methanol, followed by the dropwise addition of 1.5 mL of dimethyl sulfoxide (DMSO) while stirring. The two solutions, containing the host source and metal source, were mixed and stirred for 24 hours in an ice bath at 4°C. A colloid was formed after 30 minutes of stirring in the ice bath, indicating the formation of a complex. Figure 4-3 and Figure A 1 shows photographs of Ni-*p-tert*-Butylcalix[4]arene and Co-*p-tert*-Butylcalix[4]arene as prepared, respectively.

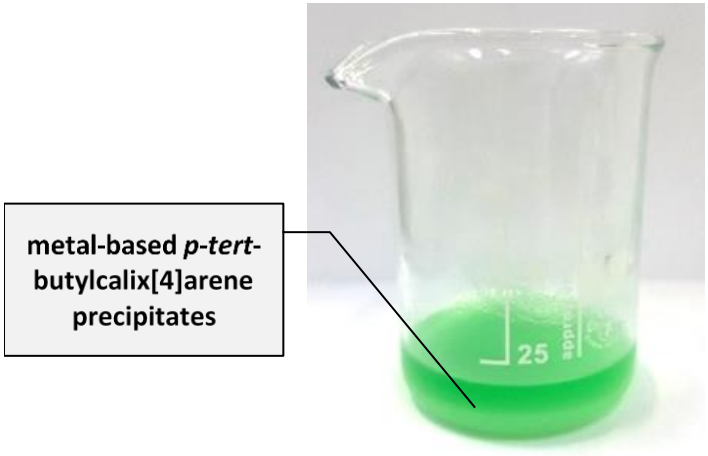

Figure 4-3 Photographs of Ni-*p-tert*-Butylcalix[4]arene as prepared.

The metal-based calixarenes were filtered using a Büchner flask and Millipore vacuum nylon membrane (Isopore Membrane Filters) with a pore size of 0.6 μm. The residue was transferred to a Petri dish and dried at room temperature to form the amorphous precipitates. Figure 4-4 shows a summary of the synthesis procedure of metal-based *p-tert*-butylcalix[4]arene followed in this study.

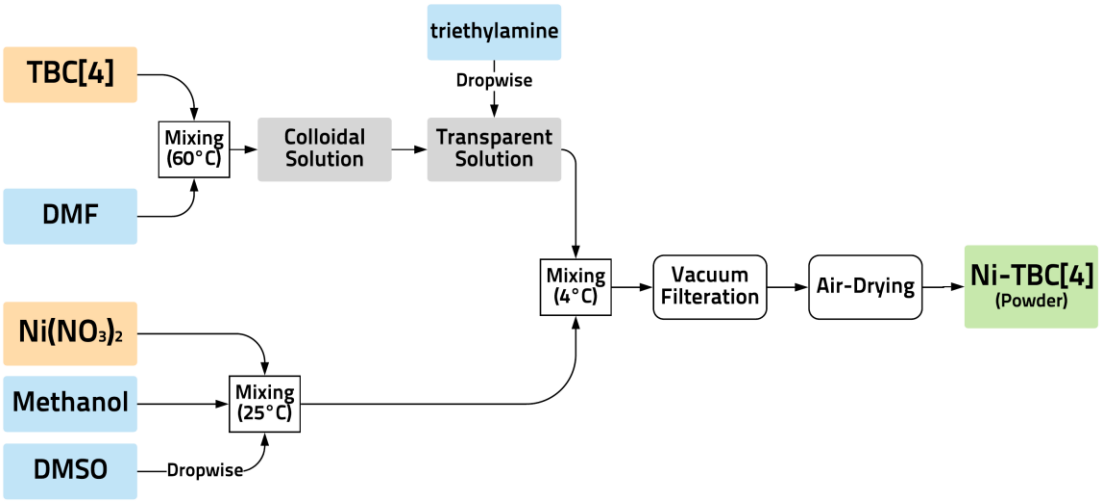

Figure 4-4 Summary of the synthesis procedure of metal-based *p-tert*-butylcalix[4]arene.

4.4.2 Characterization Techniques

To understand the morphology of the synthesized metal-based TBC[4] complexes, scanning electron microscopy (SEM) was conducted using a JEOL JSM-6460LV scanning electron microscope operated at an acceleration voltage of 20 kV; this system was combined with energy dispersive X-ray (EDX) spectroscopy to identify the elemental composition of the samples. Each sample was coated with gold (5 nm thickness) on a sputter coating machine before being placed in the holder to undergo bombardment by electrons. SEM images of the parent calixarene, TBC[4], and of its metal-based derivatives with nickel and cobalt were acquired.

Inductively coupled plasma (ICP) analysis was performed for the metal-based calixarenes to confirm their metal content. The samples were digested in 65% HNO_3. Ten milligrams of each sample was mixed with 5.0 mL of HNO_3 at 60-70°C until the total volume is

reduced to 2.0 mL through evaporation of excess HNO_3. Then, the digested solution is cooled down and its volume raised to 30.0 mL by adding deionized water. The solution is heated to 50 °C for 1.5 h. The solution is filtered using Millipore 0.1 µm filter paper. The filtrate volume is increased to 50.0 mL by adding deionized water. The samples were analyzed using PlasmaQuant® PQ 9000.

XRD analysis was performed using a Rigaku X-ray diffractometer with Cu-K_α radiation and 2θ in a range between 5° and 80° with a scanning rate of 0.02° min^{-1}. The complexation behavior of *p-tert*-butylcalix[4]arene with Ni^{2+} and Co^{2+} was evaluated by UV-vis spectroscopy where the absorbance was measured by JASCO V-670 UV-VIS-NIR Spectrophotometer using standard 1.00-cm quartz cells. The medium used for analysis was ethanol and the analysis was carried out at wavelengths between 200 and 750 nm.

The FT-IR spectra for the free ligand against the formed metal-based complexes helps in understanding the binding locations on the Ni^{2+} and Co^{2+} ions. The metal-based *p-tert*-butylcalix[4]arene complex samples were subjected to ^1H NMR spectroscopy to clarify the properties of calixarene-based ligands and their complexes [58]. The samples were dissolved in deuterated chloroform ($CDCl_3$) solvent and the spectra were recorded using JEOL 500 MHz NMR at room temperature.

To study the thermal behavior of the synthesized complexes, thermogravimetric as well as calorimetric studies were conducted using SDT Q600 Simultaneous DSC/TGA Analyzer that provides simultaneous measurement of weight change and true differential heat flow. The analysis was performed at 50-1200°C with 10±0.01mg samples at 10°C/min heating rate under nitrogen flowing at a rate of 100 mL/min. Figure 4-5 shows

a summary of the characterization techniques conducted to the synthesized metal-based *p-tert*-butylcalix[4]arenes.

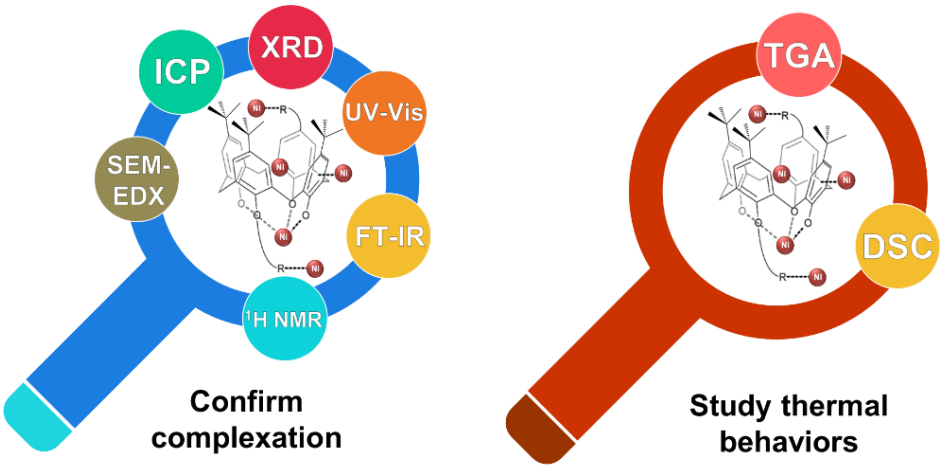

Figure 4-5 Summary of characterization techniques conducted to the synthesized metal-based *p-tert*-butylcalix[4]arenes

4.4.3 Performance Evaluation

The slurry-phase hydrocracking of VGO was accomplished over a standalone dispersed catalyst, a standalone supported catalyst as well as mixed phase catalysts. For each run, the process was conducted isothermally in a 300 mL batch autoclave reactor from Parker Autoclave Engineers, USA. The system was connected to a console to control the speed of agitation and heating and to monitor the actual pressure and temperature of the reactor. Figure 4-6 shows the experiential setup of the reactor system.

The experiments adopting the dispersed catalyst were performed by adding either 100 ppm or 500 ppm metal-based as the metallocalixarene precursor for both Co-TBC[4] and Ni-TBC[4]. For experiment utilizing the solid supported catalyst, a 1:20 catalyst-to-oil ratio was applied. The desired amount of VGO, i.e. 30.0 g, was weighed, mixed with the chosen amount of catalyst (dispersed/supported) and then fed to the batch autoclave reactor. Prior

to conducting each experiment, a leak test using nitrogen was performed to ensure that no leakage would occur. The heater was started to achieve the desired reaction temperature (i.e., 420 and 450°C), and hydrogen was fed into the system at 3.0 MPa to minimize the probability of reactions taking place during the heating period. When the temperature reached the set point, the hydrogen pressure was increased to 8.5 MPa for the hydrocracking reaction. Additionally, the agitator was started at 950 rpm to enhance the mixing of the feed with the catalyst and the hydrogen gas. The relatively high agitation speed would assure uniformity of temperature profile and minimum mass transfer limitation, where the flow inside the reactor would be highly turbulent at impeller Reynolds numbers ≥ 10000 [4, 13, 25]. The maximum pressure observed during the hydrocracking test was ~9 MPa. The reaction continued for one hour before the reactor was cooled to 100°C with the aid of a water-circulating system to suppress further reactions. The amount of gases produced was calculated from the difference in weight of the liquid product (including coke) and the fresh feed. For reproducibility test, the benchmark thermal hydrocracking run was repeated three times. The repeated experiments showed a typical ±2.5% standard deviation of the product yields.

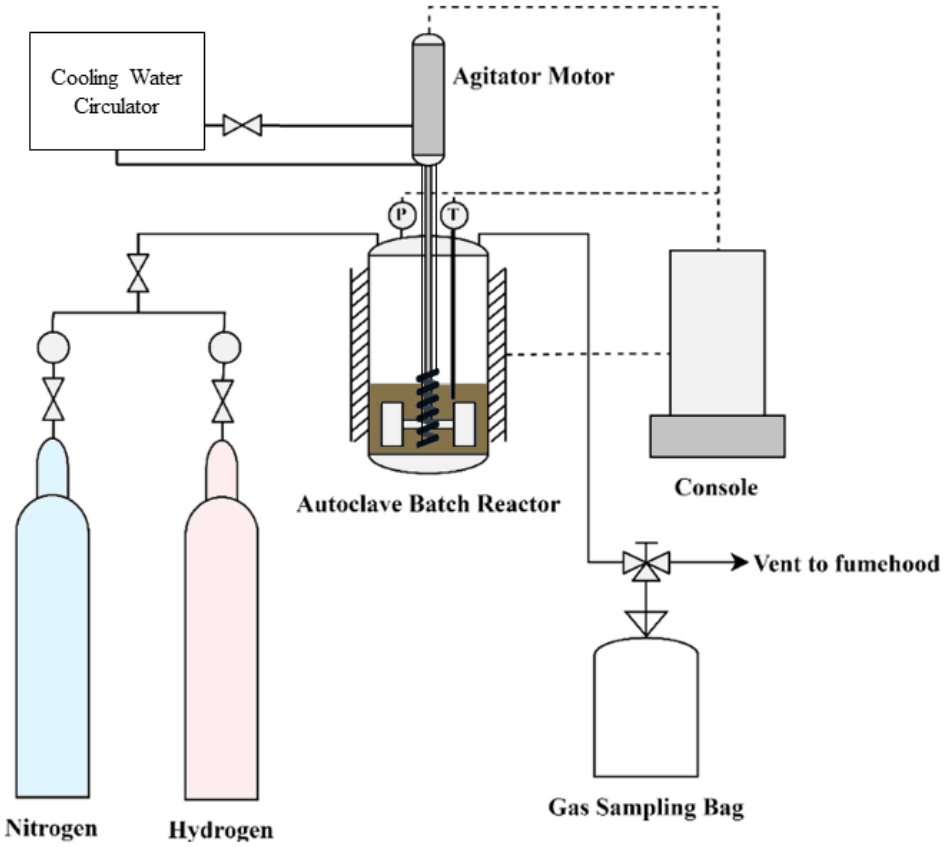

Figure 4-6 Schematic of the autoclave batch reactor setup.

Products Analysis

A thermogravimetric analyzer (TGA) (TA instrument; Model SDT Q600) is used in this work to study the product distribution of the hydrocracking. The amount of each chemical lump based on their boiling point ranges was determined as used by the previous studies reported in the literature [21, 24–26, 137, 145]. Each sample, ~70 mg, was analyzed in the temperature range of 50-600°C with 10°C/min heating rate under nitrogen flowing at 100 mL/min. Five lumps were considered based on distillation boiling ranges: gases, < 90°C; naphtha, 90-221°C; middles distillate, 221-343°C; VGO, 343-565 °C; and coke.

To determine the amount of coke formed during the hydrocracking process, a vacuum filtration unit was employed, as shown in Figure 4-7. Upon completing the filtration, the residue was washed with toluene and centrifuged at 3000 rpm for 20 minutes to ensure that any remaining liquid, including the dispersed metal catalysts, was separated from the coke. Then, the coke was transferred to a Petri dish and dried for two hours to evaporate the remaining liquids and then determine the weight of the dried coke.

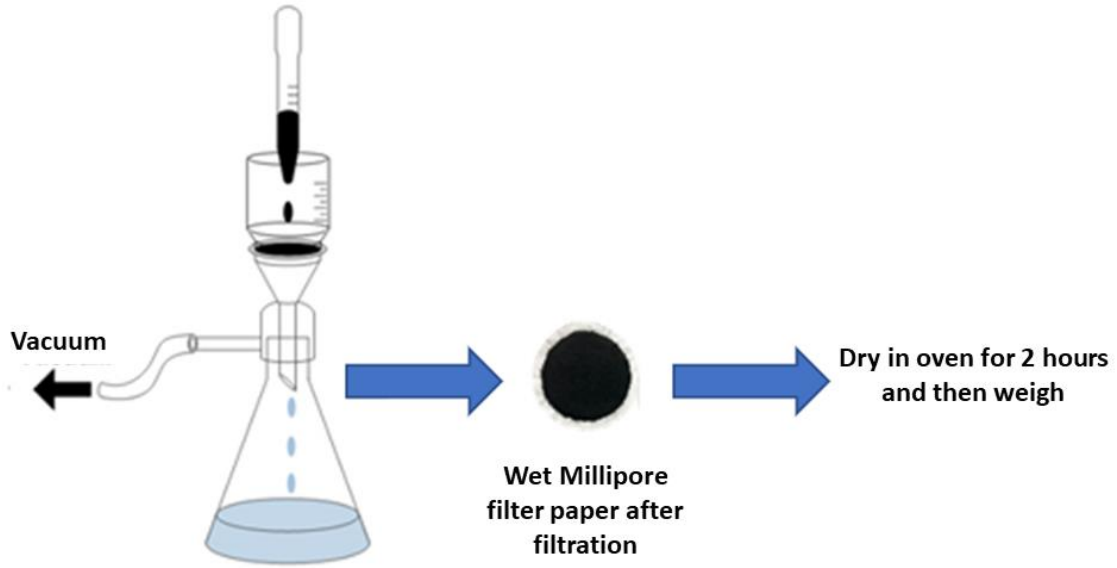

Figure 4-7 Schematic view of the filter unit.

The conversion of VGO is calculated by Equation (4-1) as follows:

$$conversion\ (wt\%) = \frac{W_{VGO_0} - W_{VGO}}{W_{VGO_0}} \times 100 \qquad (4\text{-}1)$$

where W_{VGO_0} and W_{VGO} are the weight of VGO fed initially and remained after the process, respectively. The yield of a product is defined based on its weight percentage from the total effluent as follows in Equation (4-2):

$$Y_i\ (wt\%) = \frac{W_i}{W_p} \times 100 \tag{4-2}$$

where W_i is the weight of the product (i.e. gases, naphtha, distillate, VGO, or coke) and W_p is the weight of the total product. A dimensionless parameter (I) is proposed to comment on the catalytic activity where the higher value implies a better catalytic performance [111]. The dimensionless catalytic activity parameter is calculated as follows:

$$I = \frac{Y_{naph} + Y_{dist}}{Y_{VGO} + Y_{coke} + Y_{gas}} \times 100 \tag{4-3}$$

where Y_{naph}, Y_{dist}, Y_{VGO}, Y_{coke}, and Y_{gas} are the yields of naphtha, distillate, unconverted VGO, coke, and gases, respectively. The turnover frequency was introduced to analyze the hydrotreating property. It is defined as the number of reactions per active site per reaction time [144]. Due to the difficulty of accurately measuring the number of reaction sites, the pseudo turnover frequency (PTOF) considering the total surface area of the catalyst instead. Therefore, the pseudo turnover frequency is defined as [9, 146]:

$$PTOF_i = \frac{number\ of\ i\ atoms\ in\ the\ product}{cat.\ surface\ area \times reaction\ time} \tag{4-4}$$

The instantaneous selectivity in the hydrocracking of VGO to the desired product is defined as [147]:

$$\dot{S}_{i/jk} = \frac{r_i}{r_j + r_k} \tag{4-5}$$

where r_i is the rate of desired pseudo-product formation while r_j and r_k are the rate of formation of other undesired pseudoproducts.

CHAPTER 5

CHARACTERIZATION AND EVALUATION OF (COBALT-, NICKEL)-TBC[4]S

This chapter presents the physicochemical characterization and promotional effects of oil-soluble Co- and Ni- *p-tert*-butylcalix[4]arenes (TBC[4]s) dispersed catalyst precursors for upgrading of heavy vacuum gas oil (HVGO). The Co- and Ni-TBC[4] catalyst precursors were synthesized, and the metal–ligand complexation was confirmed by scanning electron microscopy-energy dispersive X-ray, inductively coupled plasma, X-ray diffraction, UV-vis, Fourier transform infrared, and ^{1}H NMR. The thermogravimetric and calorimetric behaviors of the synthesized complexes, which are key properties of dispersed hydrocracking catalysts, were also studied. The catalytic performance of the synthesized precursors was evaluated using the batch autoclave reactor with varying concentrations of catalyst precursors at 420-450 °C.

5.1 Characterization of Metal-Based *p-tert*-Butylcalix[4]arenes

5.1.1 Scanning Electron Microscopy-Energy Dispersive X-ray (SEM-EDX)

Different magnifications (×1000, ×2500, ×5000, and ×10000) (Figure A 2, Figure A 3 and Figure A 4) were applied to gain greater insight into the surface geometry. Free calixarene (Figure 5-1) has a scattered surface structure; however, the formed complexes—Ni-TBC[4] and Co-TBC[4] (Figure 5-2.a and Figure 5-3.a)—have a smooth homogeneous surface with a crystalline structure. EDX analysis was carried out at a magnification of

×10000 on all samples, and the results showed that nickel is incorporated into the calixarene complex more than cobalt (Figure 5-2.b and Figure 5-3.b). Mapping was also conducted at a magnification of ×10000 for all metal-based calixarenes prepared. Figure 5-2.c shows that the distribution of nickel is showing a high level of homogeneity relative to carbon and oxygen. A similar observation was made for the cobalt complex, as depicted in Figure 5-3.c, which confirms the claim that the cations are linked to TBC[4] with a high level of homogeneity.

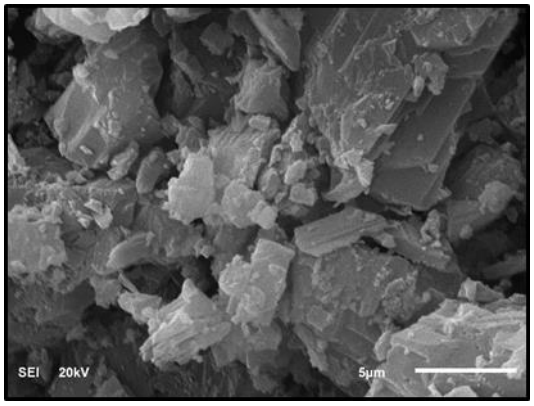

Figure 5-1 SEM images of free TBC[4] at a magnification of ×5000.

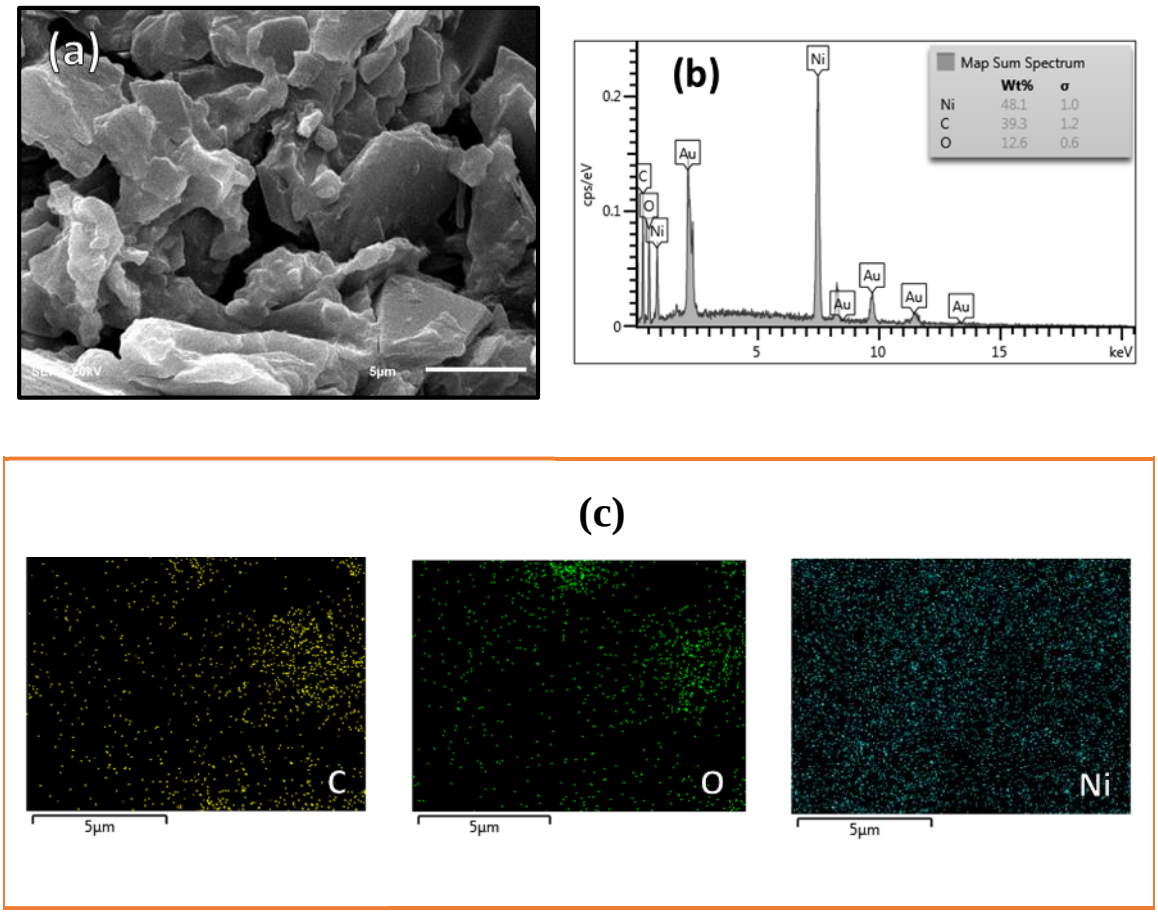

Figure 5-2 (a) SEM images at ×5000, (b) EDX spectrum at ×10000, and (c) mapping of Ni-TBC[4] at ×10000.

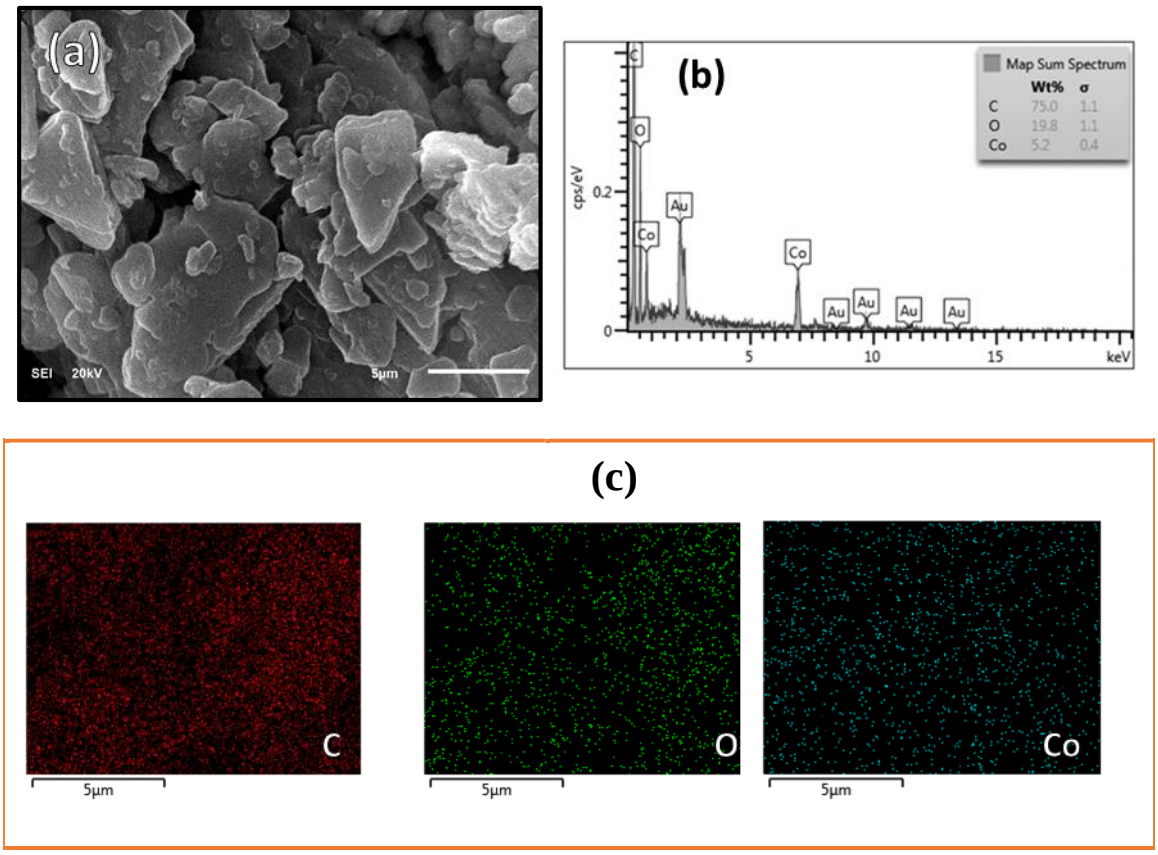

Figure 5-3 (a) SEM images at ×5000, (b) EDX spectrum at ×10000, and (c) mapping of Co-TBC[4] at ×10000.

5.1.2 Inductively Coupled Plasma (ICP)

The results showed that the Ni and Co contents in the Ni-TBC[4] and Co-TBC[4] complexes were 17.2 wt% and 6.2 wt%, respectively. This result is in agreement with the EDX analysis, which showed that nickel forms metallocalixarene complexes to a greater extent than cobalt. ICP analysis is considered to be more accurate since digested samples are analyzed, unlike EDX spectroscopy, which is affected by the degree of homogeneity, which varies as the target analysis area is changed.

5.1.3 X-ray Diffraction Characterization (XRD)

X-ray diffraction is considered as the most convenient experimental method for investigating medium-size organic molecules. Therefore, it could provide information on the nature of conformations of the calixarene derivatives [149]. However, the use of X-ray diffraction for calix[n]arenes with ≥ 6 arene groups is ambiguous due to an increase in the number of atoms. This leads to the appearance of disordered parts of the molecule and decrease in the molecular symmetry which causes poor crystallinity [149]. Since the calixarene used in this study (i.e. *p-tert*-butylcalix[4]arene) contains 4 arene constituents, the XRD results are used to investigate the complexation behavior. Figure 5-4 shows the XRD patterns of the host ligand TBC[4] and its Ni and Co derivatives . The diffractogram of the parent TBC[4] is identical to those reported in literature [150, 151]. The XRD patterns show that calixarene, as well as its derivatives, generally possesses a crystalline structure. However, the reduction in distinguishable peaks after metallocalixarene formation indicates an increase in the crystallinity of the organometallic complexes. Since complex formation does not generally affect the XRD pattern, XRD is considered a suitable approach for identifying the complexes formed based on deviations from the free calixarene XRD pattern [150, 151]. The maximum intensity of pure TBC[4] is at 2θ=20.2°, while that of Ni-TBC[4] and Co-TBC[4] is at 21.44° and 20.8°, respectively. At low values of 2θ (i.e., 10.3° and 11.7°), the patterns of the complexes lack some peaks, while at higher angles, the intensities of the complex peaks are lower than those of the pure calixarene peaks. The intensities of the derivative peaks are dramatically decreased compared to those of pure TBC[4], perhaps due to complexation [150]. Moreover, the peak intensities increase with decreasing cation size, that is, $Co^{2+} > Ni^{2+}$, and the intensities of Co-TBC[4]

peaks are 20.9% lower than those of Ni-TBC[4] peaks. The results obtained from the powder XRD do not efficiently elucidate the nature of cation-ligand complexation, due the relative width of calix structure where the cations are included [150, 152]. Hence, the subsequently presented analyses, i.e. UV-Vis, FT-IR and ^{1}H NMR, were performed to clarify the occurrence of metal coordination.

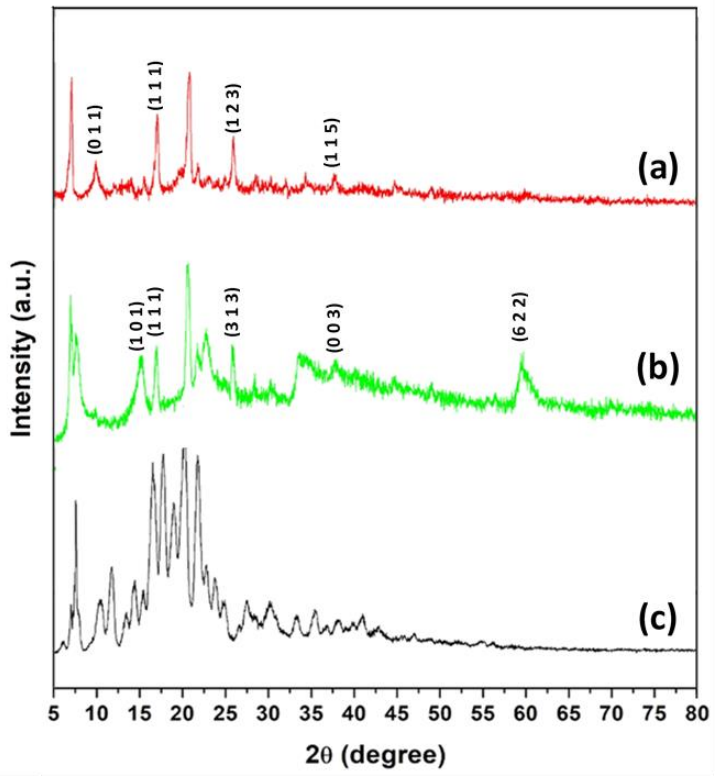

Figure 5-4 XRD patterns of (a) Co-TBC[4], (b) Ni-TBC[4] and (c) free TBC[4].

5.1.4 UV-Visible Spectroscopy

The maximum absorbance (λ_{max}) values for free TBC[4], Co-TBC[4], and Ni-TBC[4] appear to be located at 302, 304, and 308 nm, respectively (Figure 5-5). Maximum absorption in this band is attributed to the π–π* transition that arises either from the π electrons of the carbonyl group or from the electronic transition of benzene residues.

Although the absorbance spectrum of the free ligand consists of a single peak, complexation causes the appearance of other distinguishable humps for Ni^{2+} and Co^{2+} at 398 nm and 520 nm, respectively, due to the enhancement of n–π* electronic transitions of the carbonyl groups as well as the phenoxy oxygen atoms [153, 154]. The complexation of Ni^{2+} and Co^{2+} was found to enhance λ_{max}. Thus, the maximum absorption intensity of Ni-TBC[4] is higher by 95.8% than that of Co-TBC[4]. The spectral differences between the synthesized complexes support the claim that Ni^{2+} and Co^{2+} bind to the TBC[4] skeleton at different locations [153].

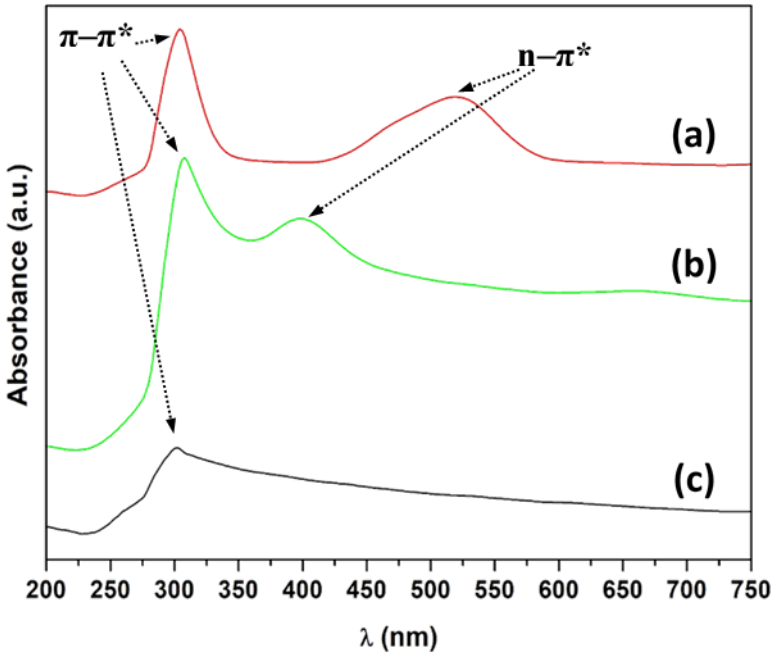

Figure 5-5 UV-Vis spectra of (a) Co-TBC[4], (b) Ni-TBC[4] and (c) free TBC[4].

5.1.5 Fourier Transform Infrared Spectroscopy (FT-IR)

All the observed bands of TBC[4] are in good agreement with the literature [155–157]. The spectrum of free calixarene has a distinctive low-frequency feature at 3123 cm^{-1} due to

stretching of the –OH groups of the cyclic tetramers (Figure 5-6). This stretching arises from the intense intramolecular hydrogen bonding in calixarene that forms an array of circular hydrogen bonding [149, 158]. The broad band at 1428 cm^{-1} corresponds to the bending vibrations of $–CH_2–$ and the vibrations of aromatic –C=C–H [158]. The characteristic absorption at 1479 cm^{-1} in the IR spectrum of the free ligand is attributed to O-H bending vibrations. The absorption bands at 1198, 1122, and 1105 cm^{-1} arise due to the stretching vibrations of C–O. The aromatic ring –C=C– stretching vibrations appear as a broad singlet at 1604 cm^{-1} [159]. Symmetric and asymmetric –CH stretching vibrations of methylene groups are observed at 2865 and 2957 cm^{-1}, respectively.

All the bands for both complexes are shifted to lower frequencies compared with those of the free ligand, which proves the coordination of metal ions. Complexation with Co^{2+} and Ni^{2+} lowers the frequency of –OH stretching to 3154 cm^{-1} and 3147 cm^{-1}, respectively. The alteration of the circular hydrogen bonding caused by imposing transannular bridges between the *para* positions affects the values of ν_{OH}, which decrease with increasing bridge length [149]. Notable changes in the absorption frequencies due to C–O stretching vibrations were also observed upon complexation. The appearance of new peaks at 1651 cm^{-1} for Ni-TBC[4] and at 1677 cm^{-1} for Co-TBC[4] is ascribed to the carbonyl stretching vibrations. DMF impurity molecules create absorption bands corresponding to carbonyl groups at low wavenumbers, i.e., 1677 and 1604 cm^{-1} [105].

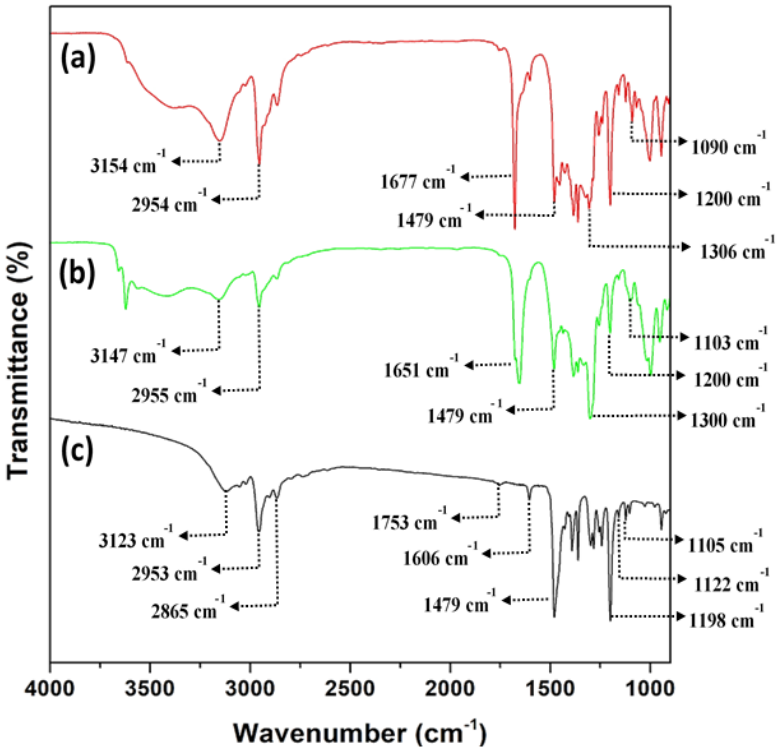

Figure 5-6 FT-IR spectra of (a) Co-TBC[4], (b) Ni-TBC[4] and (c) free TBC[4].

5.1.6 Proton Nuclear Magnetic Resonance (^{1}H NMR) Analysis

The ^{1}H NMR spectrum of free TBC[4] shows a pair of doublets between 3.5 and 4.5 ppm that arises from resonance created by the axial bridging of methylene protons (-CH_2-) due to the presence of equivalent methylene groups with nonequivalent hydrogens (Figure 5-7). Notably, the resonance arising from the bridging methylene groups is an important characteristic of the ^{1}H NMR spectra of calixarenes [149]. Singlet resonances appear within the ^{1}H NMR spectrum due to proton resonances of tert-butyl, Ar-H, and O-H groups [160]. The variation of the O-H singlet position is attributed to the change in ring size of the calixarene skeleton due to complexation [153].

Upon complexation, all proton chemical shifts experience different degrees of variation. The chemical shift of hydroxyl groups moved upfield to 10.3387 ppm and 10.3423 ppm in the spectra of Ni-TBC[4] and Co-TBC[4], respectively, compared with the resonance of the free ligand at 10.3431 ppm. The resonance of aromatic protons, on the other hand, is shifted downfield to 7.2708 ppm and 7.2620 ppm for Ni-TBC[4] and Co-TBC[4], respectively. This result proves the participation of phenoxy oxygen atoms through coordination of the added cation. The two doublets corresponding to Ar-CH_2-Ar experience coalescence upon complexation with Ni^{2+} and Co^{+2}, which indicates stabilization of the minimum energy conformations of calixarene by hindering its conformational freedom and favoring the establishment of a cone conformation [149, 161]. Similar conditions resulted from the complexation of a calix[4]arene derivative with Ag^{+}, as reported by Marcos *et al.* [63]. The ^{1}H NMR spectra of both synthesized derivatives exhibit a singlet at 8.0089 ppm due to presence of an impurity, i.e., DMF [162].

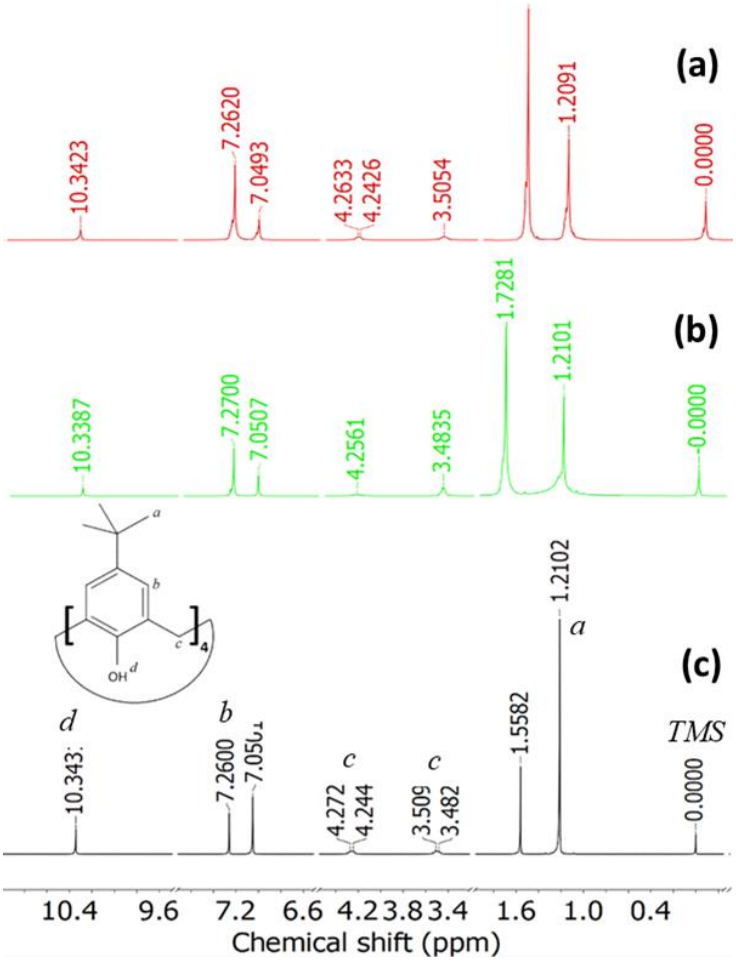

Figure 5-7 ^{1}H NMR spectra of (a) Co-TBC[4], (b) Ni-TBC[4] and (c) free TBC[4].

5.1.7 Thermogravimetric/Calorimetric Analysis

As discussed in the introduction, the low thermal stability of metal-based calixarenes could be positively exploited, and studying their thermal decomposition could provide insight into the mechanism of *in situ* active metal sulfide formation during decomposition. Figure 5-8 shows the TGA curves of TBC[4] and its Co- and Ni-complexes. The thermal decomposition of the parent calixarene occurred between 331-540°C, with a total loss of ~89 wt%. The degradation of TBC[4] occurred in two stages. The first decomposition stage occurred at 331-407°C, with a loss of 46 wt%, while the second took place between 407

and 540°C, with a loss of 36 wt%. It is proposed that the first stage is related to the decomposition of the tert-butyl functional groups of the four arene moieties in TBC[4] while the second stage represents the breakdown of the rest of the calixarene structure [163].

The degradation of the synthesized derivatives, Ni-TBC[4] and Co-TBC[4], started at a lower temperature of ~122°C, with total losses of 63 wt% and 65 wt%, respectively. This observation indicates that the parent calixarene has higher thermal stability than the metal-containing complexes. Both synthesized complexes were found to follow a three-stage decomposition pattern. Ni-TBC[4] formed an anhydrous structure by releasing H_2O and DMF molecules between 157-230°C. The subsequent decomposition stage occurred until 364°C, with a loss of 33 wt%. The last degradation stage ended at 547°C. Co-TBC[4] followed the same decomposition path; however, devolatilization took place earlier at 115-222°C, with a 28 wt% loss. The weight of the residue remaining after thermal pyrolysis of the synthesized complexes was appreciably higher than that yielded by the free ligand because of the formation of metal oxides that remain after the thermal analysis; these oxides are more thermally labile than the ligand itself, which produces an insignificant amount of residue [105]. A previous thermal behavior study by Deligöz *et al.* [164] proved that the atmospheric condition has a strong influence on the exothermal decomposition of calix[4]arene, which could justify the slight differences between some of our results and those of previous thermal behavior studies on calixarene derivatives.

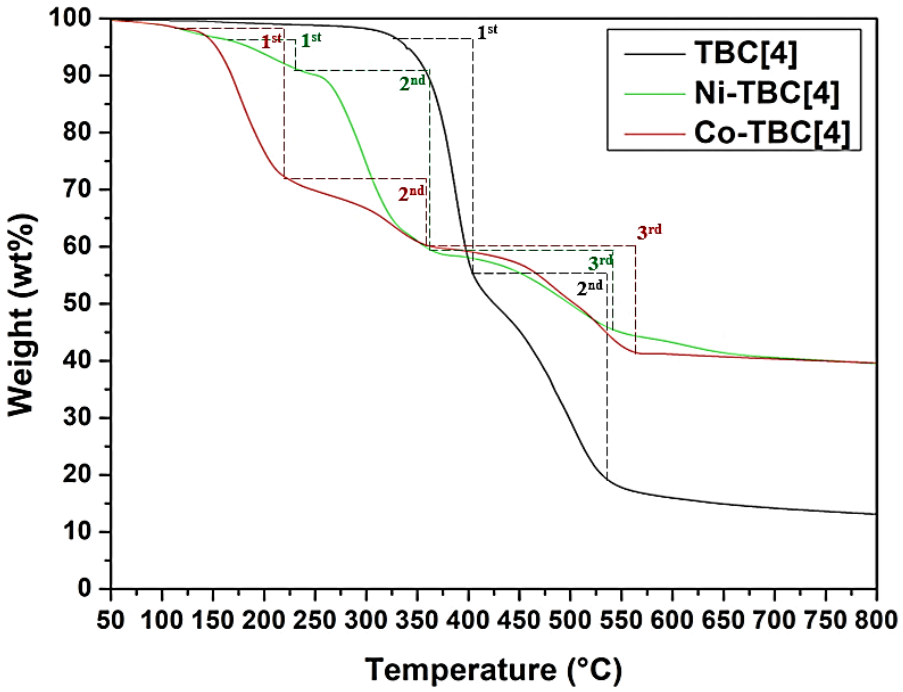

Figure 5-8 TGA profiles of TBC[4], Ni-TBC[4], and Co-TBC[4] (heating rate:10°C/min).

The formation mechanism of the nickel(II) complex with TBC[4] is proposed in Equations (5-1)-(5-3). The pyrolysis of the structure starts with dehydration to form Ni_x(*p-tert*-butylcalix[4]arene)$_y$·n(DMF). Then, further heating results in the formation of the unstable Ni_x(*p-tert*-butylcalix[4]arene)$_y$ intermediate, which undergoes further reaction to form nickel oxide by thermal elimination of TBC[4] since the pyrolysis is studied under atmospheric conditions. The cobalt(II) complex with TBC[4] supposedly undergoes the same degradation mechanism to yield CoO. For our application as a catalytic hydrogenation precursor, metal sulfide will be formed because degradation is taking place *in situ* in the presence of a sulfur-containing VGO feedstock. However, some nickel oxide is also expected to be produced because of the presence of oxygenate species.

$$[Ni_x(p-tert-butylcalix[4]arene)_y \cdot n(DMF)] \cdot mH_2O \xrightarrow[-H_2O]{\Delta} Ni_x(p-tert-butylcalix[4]arene)_y \cdot n(DMF) \quad (5\text{-}1)$$

$$Ni_x(p-tert-butylcalix[4]arene)_y \cdot n(DMF) \xrightarrow[-DMF]{\Delta} Ni_x(p-tert-butylcalix[4]arene)_y \quad (5\text{-}2)$$

$$Ni_x(p-tert-butylcalix[4]arene)_y \xrightarrow[-TBC[4]]{\Delta} NiO \quad (5\text{-}3)$$

To gain more insight into the thermal degradation of TBC[4] and its derivatives, DSC thermograms were examined to study the heat flow changes, either exothermic or endothermic, in the samples with temperature relative to those of an inert reference, i.e., sapphire calibrant. Figure 5-9 shows the DSC thermograms of TBC[4] and its derivatives. The DSC curve of the parent calixarene shows an endothermic peak at approximately 193°C attributed to the melting point. Another broad endothermic peak was observed at 254°C and is ascribed to the cleavage of methylene bridges of phenolic arene groups, which results in failure of the distinctive TBC[4] structure. These observations are in line with previous studies, supporting their validity [154, 164, 165]. According to the DSC profiles of Ni-TBC[4] and Co-TBC[4], the formation of the organometallic structure diminishes the thermal stability of the complexes compared with that of the parent TBC[4]. Upon complexation, the endothermic peak related to the melting point appears at a lower temperature, i.e., 188°C and 189°C for Ni-TBC[4] and Co-TBC[4], respectively. Likewise, the endothermic peak attributed to the methylene bridging scission occurs at 218°C and 220°C for Ni-TBC[4] and Co-TBC[4], respectively. The endothermic peaks appearing below ~125°C for both synthesized derivatives are ascribed to the release of trapped H_2O and DMF molecules remaining in the lattice structure of the complexes after their synthesis [163].

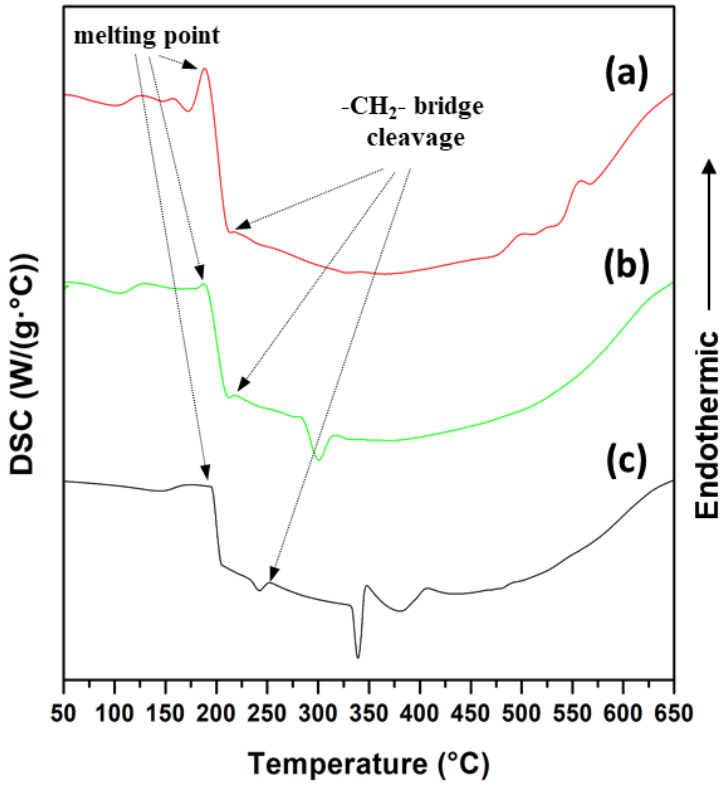

Figure 5-9 DSC of (a) Co-TBC[4], (b) Ni-TBC[4] and (c) free TBC[4] (upward peaks correspond to endothermic peaks).

5.2 Performance Evaluation

The slurry-phase hydrocracking of VGO was accomplished by varying the reaction temperature (420-450°C) and the concentration of the dispersed catalysts. The performance of the synthesized Ni-TBC[4] and Co-TBC[4] complexes as well as their analogues oil-soluble dispersed catalysts, nickel(II) 2-ethylhexanoate and cobalt(II) 2-ethylhexanoate, was evaluated in an autoclave batch reactor at 420°C under a hydrogen pressure of 8.5 MPa for 1 hour. Metal sulfides are active sites for hydrogenation/dehydrogenation reactions. Hence, *in situ* sulfidation took place on the metals leached from the organometallic compounds to form infinitesimally small metal sulfide crystals as proved by Bdwi *et*

al.[24]. Previous studies showed that the *in situ* formation of active metal crystals is independent upon the organic ligand of the dispersed catalyst [37, 166]. The sulfur required for catalytic activation comes from the 2.67 wt.% sulfur content in VGO feedstock, as shown in Table 4-2. Figure 5-10 shows that the product yields of distillate and naphtha were higher after hydrocracking over Co-TBC[4] and Ni-TBC[4] than after hydrocracking over the analogues oil-soluble ligands, but so was the coke deposition. These results reveal that employing either of the synthesized dispersed catalysts improved the product quality by promoting the hydrogenation reactions, which is in agreement with previous studies [6, 46].

The distillate yields increased from 43.58 wt% for the thermal hydrocracking run to 45.71 wt% and 49.66 wt% when Ni-TBC[4] and Co-TBC[4], respectively, were employed. In addition, applying Ni-TBC[4] and Co-TBC[4] increased the naphtha yields to 17.17 wt% and 19.24 wt%, respectively. The coke and gas yields were reduced, which proves the positive effect of metallocalixarene precursors on hydrogenation reactions. Interestingly, the levels of VGO conversion achieved with the analogous catalyst precursors—75% and 89%—were similar to those achieved with the Co- and Ni-calixarene catalyst precursors, respectively. Hence, the synthesized calixarene catalyst precursors are catalytically superior to oil-soluble dispersed cobalt. However, the oil-soluble nickel precursor seemed to exhibit better catalytic performance, with an I-value of 2.52. Although the oil-soluble dispersed nickel catalyst resulted in high conversion, Ni-TBC[4] was more selective and gave the highest yield of distillate, which is the most desired product of VGO hydrocracking. Despite higher coke formation over metal-based calixarenes compared to analogue oil-soluble precursors, the distillate yield increased over Ni-TBC[4] and Co-

TBC[4]. These results can be ascribed to the excessive hydrogenation over the metal calixarenes which reduces the asphaltenes stability [39, 167, 168]. Therefore, coke precursors are activated in the form of destabilized asphaltenes and form coke deposits. Moreover, in the case of Ni-TBC[4], the ICP results showed that metal loadings of Ni-TBC[4] is 17.2 wt%. Therefore, the amount of *p-tert*-butylcalix[4]arene required to attain a specific metal concentration is less compared to analogue commercial oil-soluble precursors, e.g. nickel naphthenate (5-12% Ni) [46] and 2-ethylhexanoate (10-15% Ni) [24, 47].

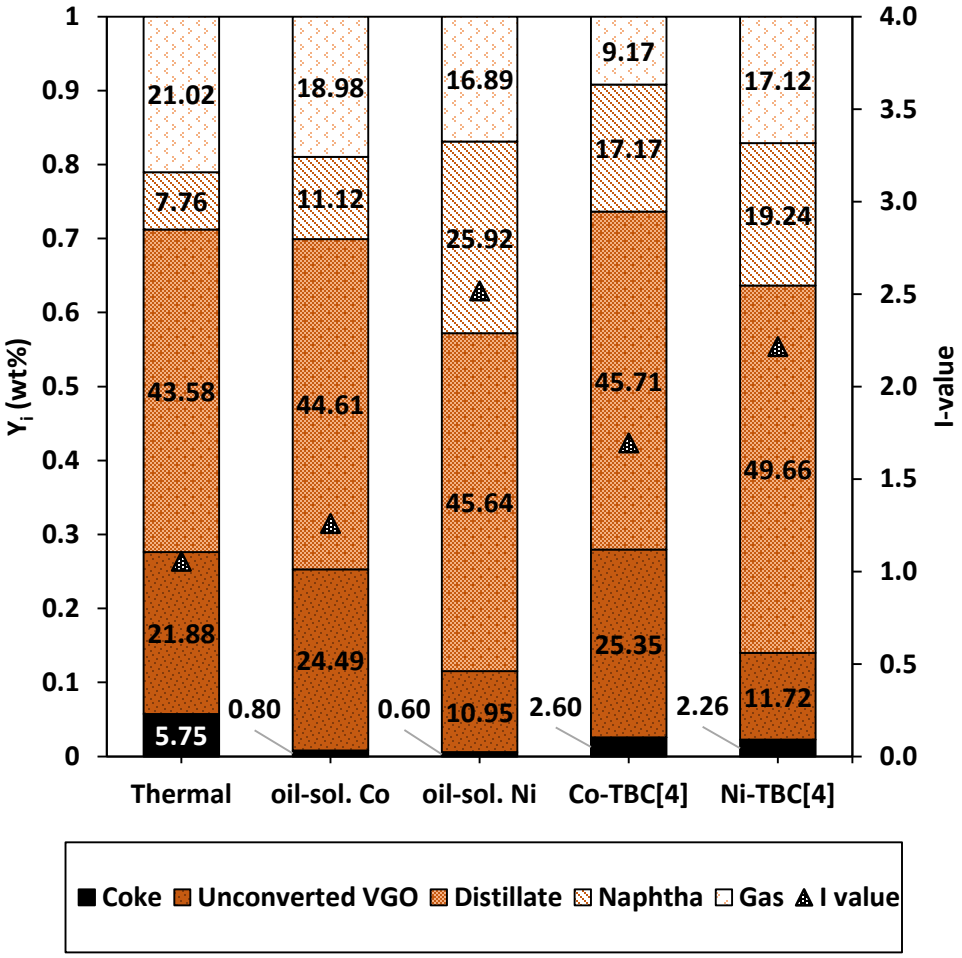

Figure 5-10 Product yield distribution for isothermal VGO hydrocracking at 420°C with a reaction time of one hour, a H_2 pressure of 8.5 MPa and metal-based calixarene organometallic compounds and oil-soluble analogues all containing 500 ppm Co and Ni.

Unlike previously studied metal-based calixarenes for catalytic hydrogenation [169], the catalytic performance in this study was based on their thermal stability since harsh conditions are applied for heavy oil hydrocracking. Metal-based calixarene was effectively soluble in the VGO. As previously stated, when oil-soluble organometallic compounds are used for the hydrocracking of heavy oil [24, 27], the metal will leach from the TBC[4] complex when the process reaches a specific temperature due to the low thermal stability of metal-based calixarenes. Then, the metal will react with the sulfur species present in the feed, resulting in the formation of highly dispersed metal sulfide crystals, which are inherently active sites for catalyzing the hydrogenation reactions. Thus, TBC[4] acts as a carrier for transition metals that promote the dispersion of metal sulfide into VGO, which is reflected in the enhancement of hydrogenation reactions, reducing coke yields and maximizing the yields of lower boiling-point products. Figure A 5 elucidates the *in situ* sulfidation of metals leached from metal-based TBC[4] and oil-soluble 2-ethylhexanoate organometallic compounds.

Thermal cracking of petroleum feedstocks occurs by thermal activation to produce free radicals from C–C homolytic scission, hydrogen rejection during C–H heterolytic or homolytic scission, and C–heteroatom bond scission, where the temperature must be ≥ 350°C [25, 166, 170]. Petroleum feedstocks contain resins that stabilize asphaltenes. To avoid coke precipitation due to destabilized asphaltenes, a maximum dilution proportion in the aliphatic phase and a minimum amount of resins must be achieved [171–173]. The cracking of resins takes place at a higher pace than asphaltene destabilization because of the less aromatic nature of the former, so equilibrium must be maintained between the

resins and asphaltenes throughout the cracking process to avoid asphaltene destabilization and to obtain optimum yields of the valuable liquid products [25, 174].

Although the conversion resulting from thermal hydrocracking is sufficiently high, the lack of active metal sites causes lower yields of low-boiling-point liquid as well as high coke formation. The free radicals formed result in successive β-scission cracking through parallel reaction pathways to produce lighter products in the form of gases as well as the condensation of polynuclear aromatic hydrocarbons (PAHs), which leads to coke deposition. Thus, thermal hydrocracking exhibits much lower selectivity towards valuable products, namely, naphtha and middle distillate. The parallel reactions occurring during thermal cracking cause unavoidable coke formation even though the distribution of products is dependent on the reaction temperature and residence time [166, 170]. Therefore, the equilibrium between different reactions is important and can be controlled by promoting the hydrogen uptake governed by introducing active metal sulfides [46, 175, 176].

Introduction of the dispersed catalyst precursors, which are eventually converted *in situ* to active sites of metal sulfides, will ensure efficient hydrogen uptake by free radicals. Hence, the β-scission reactions and coke formation would be controlled even at low concentrations of dispersed active metal sulfides [166, 177]. The presence of the active metal sulfide crystals lowers the coke formation by sticking on the coke precursors with the aid of the wetting property [12]. This results in stabilizing and inhibiting the coalescing as of the coke precursors as shown by Cyr *et al.* [178]. The dispersed catalyst will also act as a hydrogen donor in the partial hydrogenation of PAHs in the hydrogenation/dehydrogenation cycle [179]. It is worth mentioning that the metallic wall of the reactor vessel is also functioning

in promoting the hydrogen uptake, however, this behavior cannot be generalized since that its contribution to the catalytic hydrogenation effect is considered to be negligible compared to other parameters [180].

While the cracking reactions of PAHs and other macromolecules take place thermally, the active metals transfer hydrogen from the vapor to the liquid reactants [39, 167, 179]. Upon completion of the reaction, the metal sulfide crystals are separated from the liquid product through deposition on coke [24, 111]. The presence of dispersed metal sulfide after this process is complete will ensure the inhibition of coke formation during the cooling period when the temperature and pressure are high enough to enable further cracking reactions that result in the condensation of PAHs. This phenomenon could be extended to continuous hydrocracking processes to minimize fouling in the piping system due to coke deposition; the dispersed metal sulfides would act within the reactor's effluent as anti-fouling agents [181]. Additionally, the presence of the free active metal sulfide crystals would enhance the hydrotreating reactions, such as hydrodenitrogenation, hydrodesulfurization and hydrodeoxygenation [182, 183].

The detailed mechanism of hydrogen transfer has not yet been established due to the complexity of the molecules involved in heavy petroleum feedstocks. Previous studies have proposed that an organic molecule containing an aromatic ring is activated on one active site while hydrogen is activated on another site. Then, the activated hydrogen atoms migrate to the activated aromatic molecules and break the double bonds in a stepwise manner to saturate the bonds [184]. However, there is no experimental proof to support this claim over alternative mechanisms [179].

To overcome the issue of coke deposition, optimization of the metal-based calixarene concentration should be considered to tune the product distribution to the desired levels. Experiments were conducted with different metal concentrations (i.e., 100 ppm and 500 ppm) to study the effects on the hydrocracked product distribution. Figure 5-11 shows the product distributions for Co-TBC[4] and Ni-TBC[4] obtained at different concentrations. For both catalyst precursors, the increasing metal concentration had a directly proportional relationship with the increasing distillate yield. These results show that hydrogen uptake is concentration dependent, as reported by different studies [24, 109, 184]. Although hydrogenation reactions were enhanced by increasing the catalyst concentration to 500 ppm, the coke yields over both Co-TBC[4] and Ni-TBC[4] also slightly increased to 2.60 wt% and 2.26 wt%, respectively. The performance of the dispersed catalyst is delimited by two competing mechanisms. The hydrogen uptake is dependent on the active metal sites concentration and dispersion. On the other hand, the *in situ* formed catalyst particles may cause the clustering of the solid carbonaceous materials by acting as nucleation sites [35]. Additionally, this reverse effect could be attributed to the excessive hydrogenation as a result of increasing metal sulfide concentration by reducing the stability of asphaltenes as claimed by Panariti *et al.* [46].

The VGO conversion over Ni-TBC[4] was 86.17% for 100 ppm Ni and 88.28% for 500 ppm Ni. Additionally, the distillate yield increased from 34.06 wt% to 49.66 wt% while the yield of gases decreased from 26.45 wt% to 17.12 wt% as the Ni concentration increased from 100 ppm to 500 ppm, respectively. Ni-TBC[4] enhances the conversion of VGO to a greater extent than Co-TBC[4].

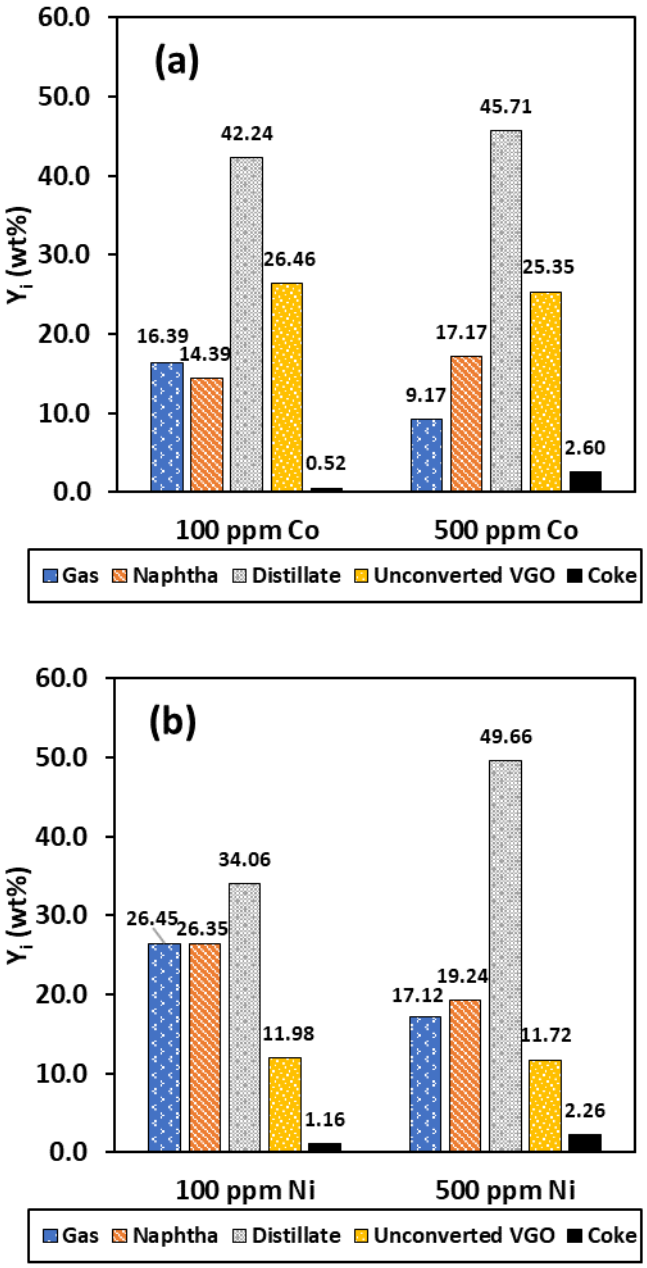

Figure 5-11 Product yield distributions of VGO hydrocracking at 420°C for a reaction time of one hour under an H_2 pressure of 8.5 MPa with (a) Co-TBC[4] and (b) Ni-TBC[4] complexes at different metal concentrations (100 ppm and 500 ppm).

Ni-TBC[4] was also tested at 450°C since it gave the highest yield of distillate. The dimensionless catalytic activity factor decreased from 2.22 to 0.85 as the reaction temperature was increased from 420°C to 450°C, which indicates a decrease in catalytic

performance in terms of the selectivity towards valuable products. Figure 5-12 shows the yields of VGO hydrocracking products when Ni-TBC[4] was used as a dispersed catalyst. The catalytic effect of the dispersed catalyst dropped as the reaction temperature was increased to 450°C, which also resulted in increases in the gas yield from 16.26 wt% to 31.33 wt% and the coke yield from 2.21 wt% to 3.56 wt%. Additionally, the yields of naphtha and distillate dropped by 14.12% and 15.36%, respectively. However, the overall conversion of VGO was 80.69% at 450°C but 72.37% at 420°C. These findings could be interpreted by analyzing the degradation behavior of metallocalixarene in this process. The decomposition of the organometallic structure of Ni-TBC[4] starts at a lower temperature than the process temperature of 218°C, as presented earlier in the DSC thermogram. Therefore, applying a higher temperature of 450°C would cause the formation of *in situ* nickel sulfides, and the probability of deactivation through sintering increases at this temperature. Therefore, the loss of catalytic hydrogenation is ascribed to the shortage of active sites per unit amount [24]. Consequently, conducting the process at a higher temperature resulted in lower yields of naphtha and distillate but higher yields of gases and coke despite higher VGO conversion.

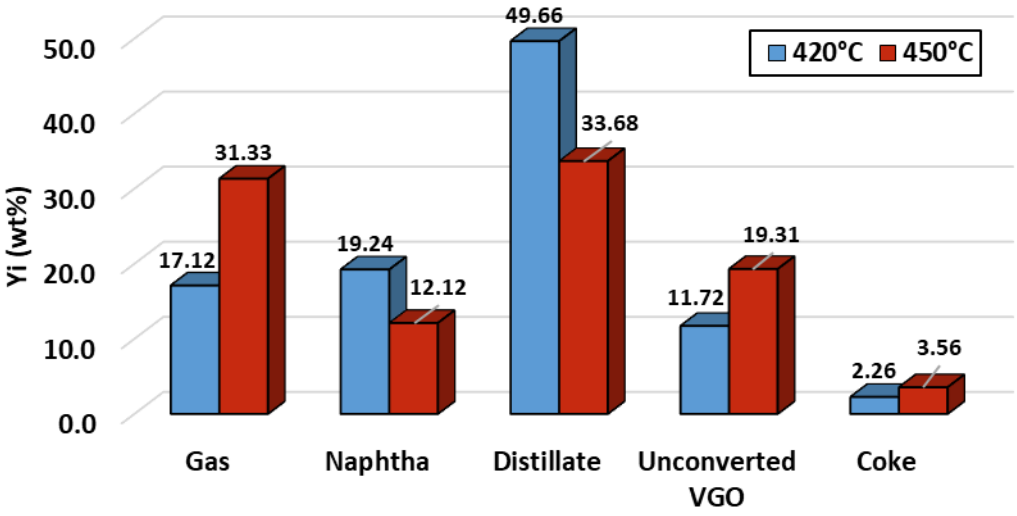

Figure 5-12 Product yield distributions of VGO hydrocracking with Ni-TBC[4] (500 ppm Ni) at 8.5 MPa and at 420°C and 450°C for a reaction time of 1 hour.

5.3 Conclusions

The catalytic performance of the synthesized precursors was evaluated using a batch autoclave reactor with varying concentrations of catalyst precursors at 420–450 °C. The results show that the synthesized metal-based TBC[4] dispersed catalysts evidently enhanced the hydrogenation activity and reduced coke formation. The addition of 500 ppm Co and Ni as standalone dispersed catalysts produced distillate yields of 45.7 and 49.7 wt % and a coke laydown of 2.6 and 2.3 wt %, respectively. Increasing the concentration of catalyst precursors enhanced the conversion of VGO from 86.17% at 100 ppm Ni to 88.28% at 500 ppm Ni. Moreover, as the metal concentration increased from 100 to 500 ppm, the distillate yield increased from 36.87 to 49.66 wt %, while the yield of gases decreased from 20.48 to 17.12 wt % because the hydrogenation reactions were enhanced. In contrast, the yields of distillate and naphtha decreased by 14.12 and 15.36%, respectively, as the temperature increased from 420 to 450 °C.

CHAPTER 6

KINETICS OF THE SYNERGY EFFECTS

This chapter reports the kinetics analysis of slurry phase hydrocracking of HGVO involving Ni-*p-tert*-butylcalix[4]arene (Ni-TBC[4]) as a dispersed co-catalyst along with a commercial first-stage hydrocracking supported catalyst. The synergy between the dispersed and supported commercial catalyst are demonstrated by comparing the product distributions and estimated kinetics parameters during hydrocracking of HVGO using Ni-*p-tert*-butylcalix[4]arene (Ni-TBC[4]) as a standalone catalyst with that of co-catalytic hydrocracking of HVGO using Ni-*p-tert*-butylcalix[4]arene (Ni-TBC[4]) and commercial Ni-W/SiO_2-Al_2O_3-(Y-zeolite) catalyst. The kinetics experiments were conducted different reaction times and temperatures. A five-lump discrete kinetic scheme was developed based on the experimental data governed from both the standalone supported catalyst and the mixed catalysts. The model incorporated the conversion of VGO to distillate, naphtha, and C_1–C_5 gaseous hydrocarbons in addition to coke deposition.

6.1 Synergy Study

The use of a nickel-based *p-tert*-butylcalix[4]arene (Ni-TBC[4]) enhanced the product quality by increasing the distillate and naphtha yield and decreasing the gas yield and coke deposition. A previous paper discussed, in detail, the catalytic enhancement governed by implementing standalone dispersed catalyst precursors for the hydrocracking of VGO [24]. A co-catalytic configuration was applied by introducing the commercial first-stage

hydrocracking catalyst along with the synthesized metal-based calixarene to study the synergic effects governed by using it as an additive. The mixed phase catalysts were studied using the batch autoclave reactor under different reaction conditions and compared against the performance of using the commercial catalyst. The supported solid catalyst-to-oil ratio was fixed at 1:20 for all experiments [24].

In addition to the thermal cracking of hydrocarbons, cracking occurs due to the presence of acidic active sites offered by the supported catalysts. The supported catalyst used in this study has bifunctional active sites in which the cracking reactions occur at the Brønsted and Lewis acid sites present in Y-zeolite and Al_2O_3-SiO_2, while the hydrogenation of the carbenium ions resulting from cracking occurs with the aid of the supported metal sulfides. The presence of dispersed metal sulfides helps boost the hydrogenation of the carbenium ions obtained by the catalytic cracking reactions. Additionally, the free metal sulfide crystals promote the hydrotreating reactions that include hydrodesulfurization, hydrodenitrogenation, and hydrodeoxygenation [182, 183]. During the hydrocracking reaction, some of the *in situ* formed metal sulfide will be separated from liquid product through deposition on the solid supported surface as proved by Bdwi *et al.* [24].

The results presented in Figure 6-1 reveal that the hydrocracking of VGO with the Ni-TBC[4] complex (500 ppm Ni) resulted in reduction in coke formation from 5.75 wt% to 2.09 wt% and increase in distillate yield from 43.58 wt% to 45.98 wt% compared to the thermal hydrocracking run. These results prove the positive effect of implementing the metallocalixarene precursors on hydrogenation reactions. Employing the presulfided supported catalyst alone for VGO hydrocracking enhanced its conversion from 78.12 % to 83.2 % compared with thermal hydrocracking. Interestingly, introducing the Ni-TBC[4]

(500 ppm Ni) along with the supported catalyst shows higher catalytic hydrogenation activity, which resulted in increased yields of naphtha from 15.27 wt% to 16.36 wt% and distillate from 52.17 wt% to 53.57 wt% compared with the use of the supported catalyst individually in a comparable VGO conversion of about 83 %. In addition, the yields of coke and gases decreased by 35.86 wt% and 13.90 wt%, respectively, which also confirms the enhancement in catalytic hydrogenation in the presence of Ni-TBC[4]. The actual yields of hydrocracking over mixed catalysts were compared with those obtained by the algebraic average of the product yields obtained after hydrocracking over the supported catalyst alone and the Ni-TBC[4] alone. The value of the dimensionless catalytic activity parameter proves the existence of synergy between the two catalysts since it is much higher than that acquired through the algebraically calculated yields.

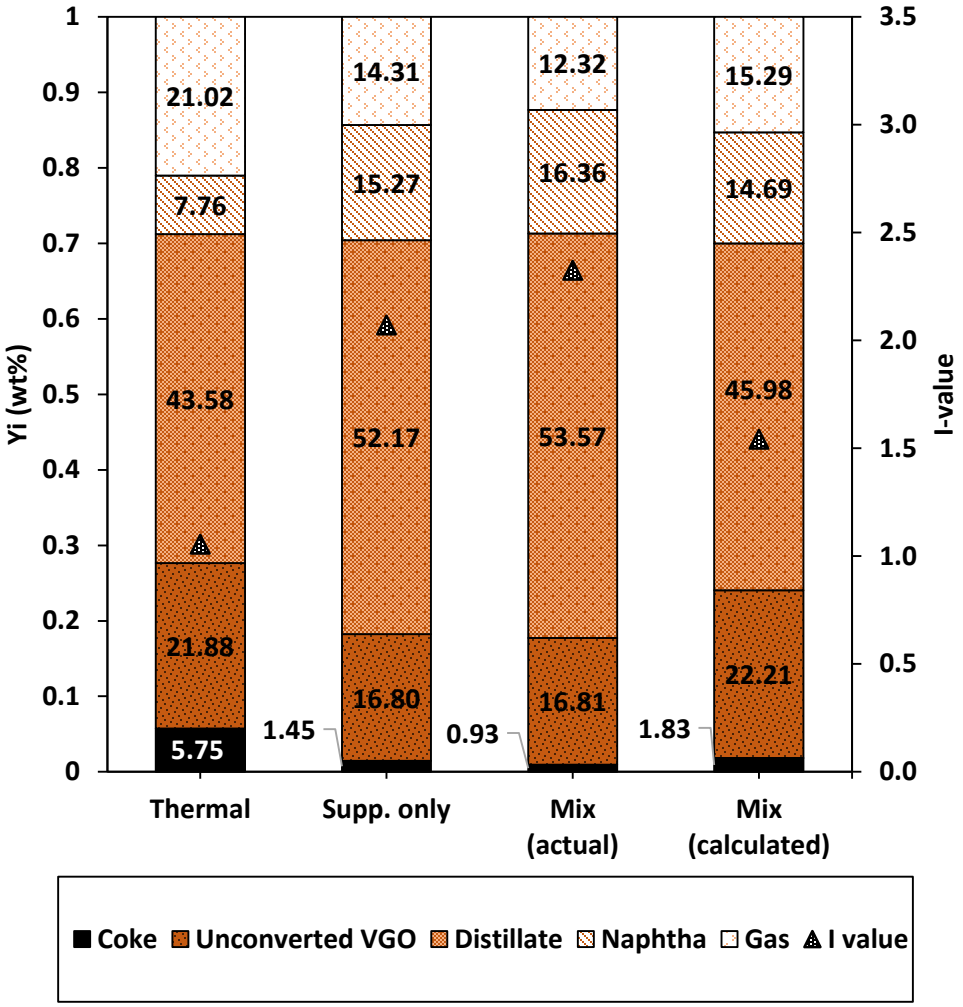

Figure 6-1 Product yield distribution of VGO hydrocracking at 420°C for a reaction time of one hour under a H_2 pressure of 8.5 MPa isothermally with the standalone supported catalyst (1:20 catalyst-to-oil ratio) and mixed catalysts.

Elemental analysis of the liquid effluent from hydrocracking through the different catalytic configurations revealed that the introduction of the dispersed catalyst as an additive in addition to the supported commercial catalyst enhanced the product quality by boosting the H/C ratio and reducing the sulfur content that is present in the form of heteroatom-containing organic compounds, such as thiophenol and 4,6-DMBT, through hydrotreating reactions, which results in the formation of the gaseous product hydrogen sulfide (H_2S).

The analysis of C, H, N, and S was conducted by an elemental analyzer (EA) (PerkinElmer CHNS 2400 Analyzer). The thermal hydrocracking run showed unfavorable results in which the product H/C ratio was less than 21.74% less than that in VGO feedstock (Figure 6-2). The reduction in H/C ratio during thermal cracking indicates that the hydrogenation reactions of the unstable intermediates could not keep pace with the excessive cracking due to the lack of hydrogenation sites. Therefore, polymerization of free radicals occurs instead, causing hydrogen release followed by condensation of the low H/C molecules, such as polycyclic aromatic hydrocarbons (PAHs), although the sulfur and nitrogen contents have shown notable reductions. The use of standalone supported catalyst clearly improved the H/C ratio, which increased slightly by 16.67 % compared with the thermal hydrocracking run. Furthermore, conducting the process over the mixed phase catalysts provided a liquid product with the best H/C ratio of 0.26. This observation is justified by the fact that the use of the Ni-TBC[4] in addition to the supported solid catalyst offers more catalytic hydrogenation sites, as reflected in high quality liquid product. Additionally, the sulfur and nitrogen contents experienced a notable reduction to 0.56 wt% and 0.29 wt%, respectively.

The pseudo turnover frequency of sulfur atoms removal from heteroatom-containing organic compounds shows a boosting effect in the presence of the dispersed catalyst in addition to the solid catalyst. The number of sulfur atoms removed by both catalytic configurations was deducted from those removed by thermal hydrocracking to eliminate the contribution of hydrodesulfurization occurring thermally. The PTOF value was increased from 3.53E+3 to 5.73E+3 S atoms removed/($\mu m^2 \cdot h$) upon introducing 500 ppm Ni to the catalytic system. The increase in the PTOF demonstrates the enhancement of the

hydrotreating reactions, even though additional surface area was provided by the active dispersed nickel sulfides that were formed *in situ*.

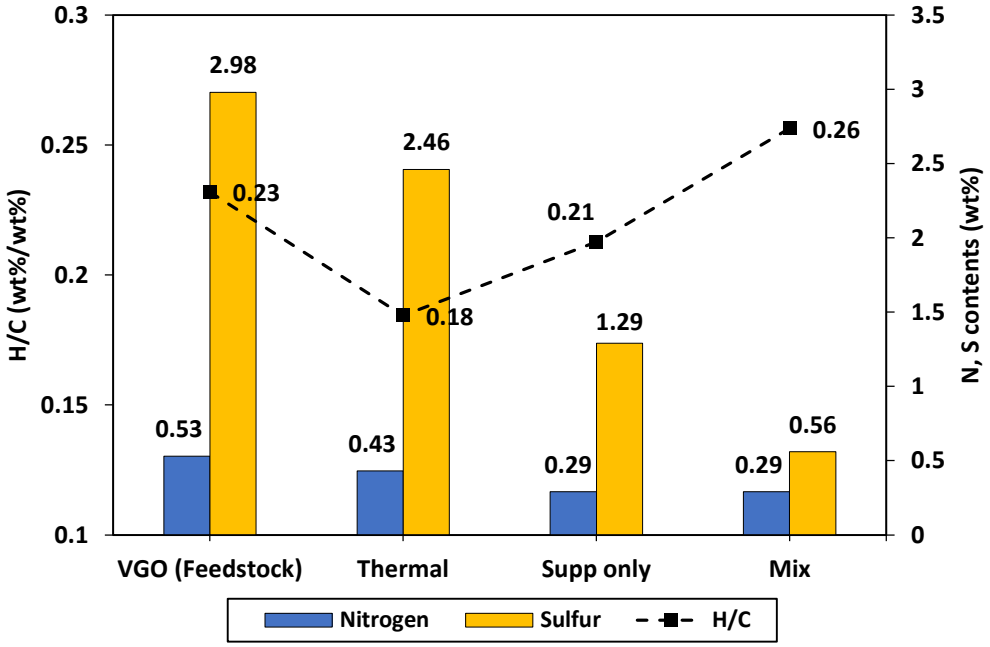

Figure 6-2 H/C ratio and nitrogen and sulfur contents of VGO feedstock and liquid products after conducting hydrocracking experiments at 420°C for a reaction time of one hour under a H_2 pressure of 8.5 MPa isothermally with the standalone supported catalyst and the mixed catalysts.

The effects of varying the reaction temperature on the catalytic performance were investigated for the co-catalyst system at 390, 420, and 450°C, where the supported catalyst was loaded along with the Ni-TBC[4] dispersed catalyst at a concentration of 500 ppm Ni. The dimensionless catalytic activity factor increased from 1.50 at 390°C, reached an optimum value of 2.33 at 420°C and then decreased to 2.17 upon increasing the reaction temperature to 450°C. The conversion of VGO showed a steady and sharp increase from 68.12% to 96.07% by intensifying the reaction severity.

Figure 6-3 shows that the yield of distillate reached an optimum value of 53.57 wt% when the process was operated at 420°C. This observation is in accordance with the expectation that at a low reaction temperature (390°C), a lower amount of metal is leached from the TBC[4]; however, increasing the reaction temperature to 420°C allows the maximum amount of metal to be leached. Thermogravimetric analysis (TGA) (TA SDT Q600) of the nickel-based calixarene show that its distinctive structure begins degrading at 364°C to release the cations. Therefore, operating the process at 420°C would assure the leaching and *in situ* formation of the much higher amount of active nickel sulfide crystals. Consequently, highly dispersed metal sulfides are formed within the reactant, which is also reflected in reductions in the coke and gas yields. Nevertheless, the catalytic hydrogenation performance decreased when the process was conducted at an even higher temperature, i.e., 450°C. This behavior is explained by the agglomeration of the dispersed metal sulfides that led to the formation of large crystals with less surface-area-to-volume [24].

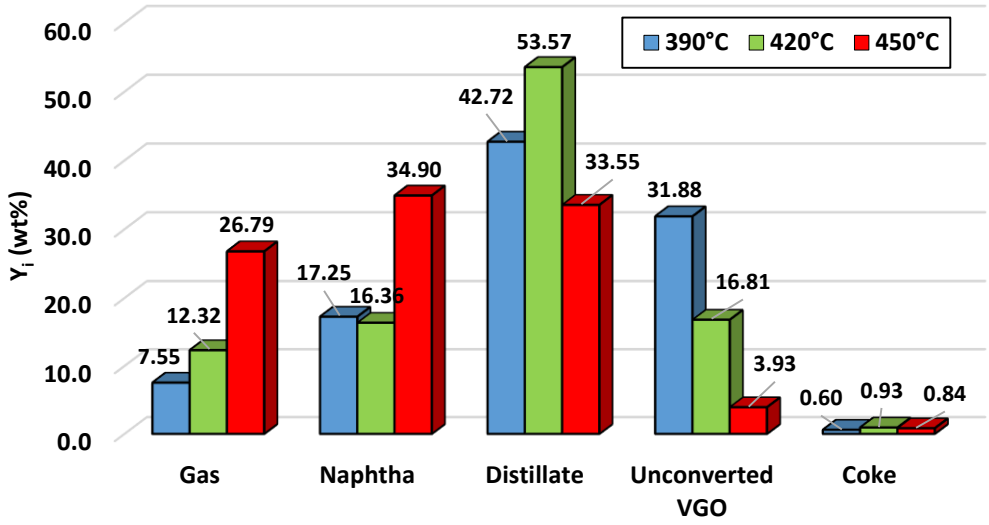

Figure 6-3 Product yield distribution of VGO hydrocracking over the mixed catalysts (the supported catalyst and the Ni-TBC[4] complex) at 8.5 MPa at 390°C, 420°C, and 450°C for 1 h.

Hydrocracking of VGO was conducted over supported as well as mixed (supported and dispersed) catalysts for different reaction periods (i.e., 0.5, 1, and 1.5 h), while the reaction temperature was maintained at 420°C. As anticipated, the catalytic performance had a directly proportional relationship with the reaction time, which was reflected in promoting the VGO conversion as well as the desired liquid products, i.e., the distillate and naphtha. The fractional conversion of VGO (Figure 6-4.a) increased the reaction time for both catalytic setups. Extending the reaction time to 1.5 h favored the conversion of VGO with an increase of 5.24 % compared with the use of the standalone supported catalyst. Although the yield of gases and coke experienced a slight increase over the course of the reaction times, this increase does not match the remarkable boost of the naphtha and distillate yields. This finding was validated by analyzing the dimensionless catalytic activity parameter, the *I*-value, which began at 1.85 for 0.5 h and attained its highest value at 2.69 for a reaction time of 1.5 h.

The yield of gases produced when mixed catalysts were used is slightly higher than that for standalone supported catalysts at short reaction times, as shown in Figure S 2.d. Nevertheless, when the reaction time was extended to 1 h and 1.5 h, the yield of gases dropped to 12.32 wt% and 17.48 wt% compared with 14.31 wt% and 18.39 wt%, respectively, for the supported catalysts only. This observation is due to the hydrogenation capability of the nickel sulfide crystals, which was enhanced by the heightened dispersion capability provided by the Ni-TBC[4]. The coke depositions upon hydrocracking over the standalone supported catalyst ranged between 1.18 wt% and 1.57 wt%. However, this value was dramatically reduced to 0.77 wt% and 0.99 wt% for the reaction times of 0.5 h and 1.5 h, respectively. This result is because of the consistent hydrogenation capability enabled

by the presence of the dispersed catalyst that works on inhibiting the coke precursor activity by preventing its evolution to form coke deposits [24].

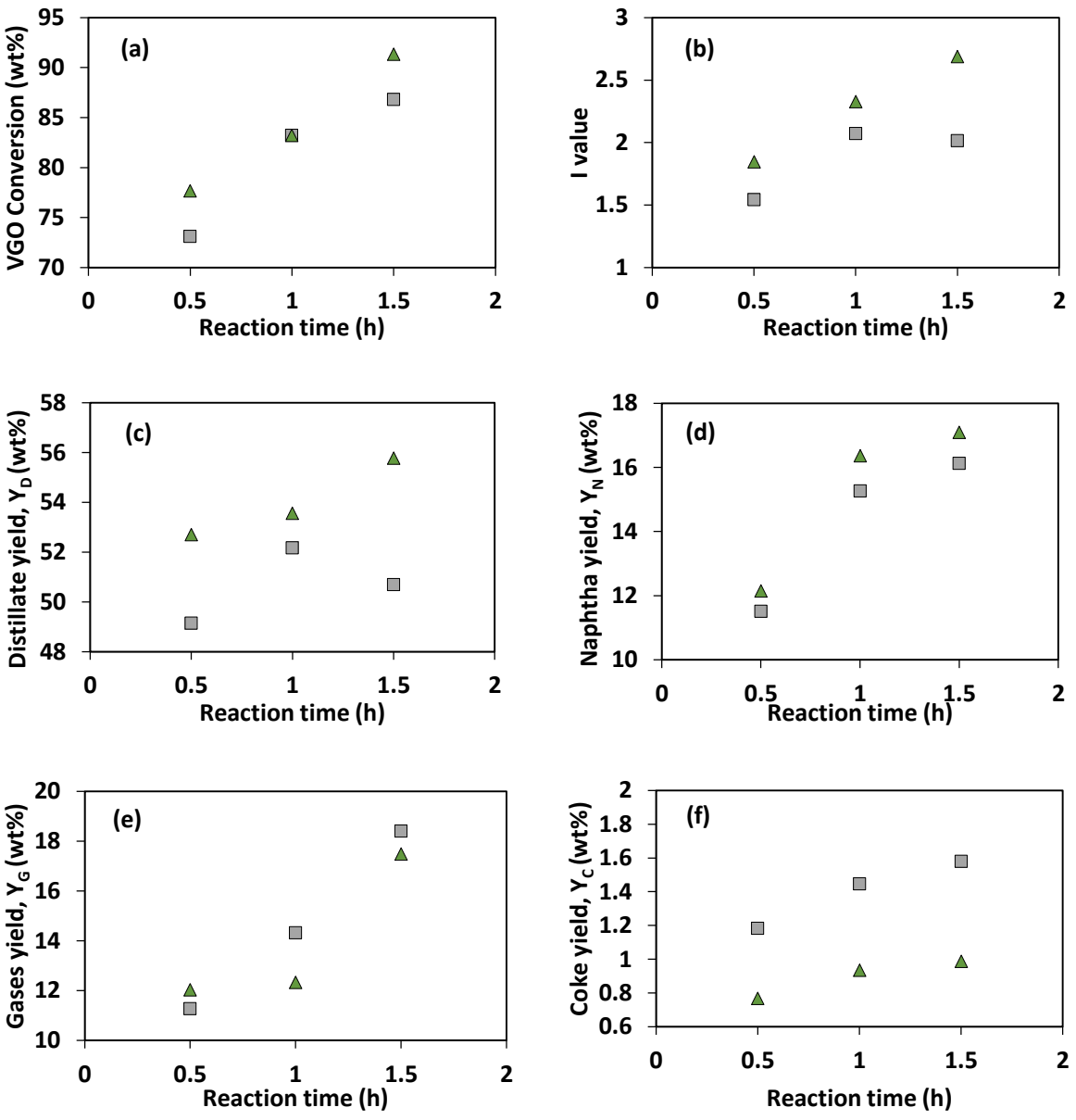

Figure 6-4 (a) VGO conversion; (b) I value; the yield of (c) distillate, (d) naphtha, (e) gases, and (f) coke for hydrocracking using supported catalyst (■) and mixed catalysts (▲) at 420°C under hydrogen pressure of 8.5 MPa.

6.2 Kinetic Study

6.2.1 Reaction Pathways and Model Development

The heavy oil contains wide ranges of different hydrocarbon components that make it very complex in terms of characterization. Modeling this type of feed that results in producing an enormous network of interconnected reactions requires sophisticated analytical and numerical techniques. Fortunately, alternative methods of kinetic modeling have been proposed in the literature to solve this issue by simplifying the reactions through different techniques to obtain predictable results of the wide range of product distribution. Due to their practicality, discrete or traditional lumping techniques are considered one of the most commonly used techniques applied where the products are segregated into pseudo-components depending on specific characteristics, such as distillation cuts or chemical groups, to simplify the task of estimating kinetic parameters [128]. In the discrete lumped approach, the chemical components involved in the process are distributed in lumps in which they are assigned as pseudo-components. In this study, discrete lumping was performed based on distillation boiling ranges to create five lumps: gases, C_1–C_5 hydrocarbons; naphtha (90-221°C); middle distillates (221-343°C); VGO (343-565°C) and coke. The 5-lump model is used for kinetic modeling of the hydrocracking process with both dispersed and supported catalysts to evaluate their synergic effect. The VGO feed was processed in batch mode, and the experiments were conducted at different reaction times of 0.5, 1.0, and 1.5 h to obtain the relation between time and product yield.

It is worth mentioning that although hydrogen is involved as a reactant in the process, it has been eliminated from the reaction scheme due to its presence during the process as an

excess reactant. Therefore, it is considered that the hydrogen stoichiometric share does not affect the other stoichiometric values of the reactants and products, so the rate of the reaction does not depend explicitly on the partial pressure of hydrogen by assuming that it is approaching unity. The reactor was assumed to run under isothermal reactor conditions since negligible temperature changes were observed during the process. Rigorous mixing during the hydrocracking process was taken into account to eliminate the possibility of an external mass transfer limitation, although an internal mass transfer limitation might exist [24]. Thus, the activation energies estimated in this study are considered as apparent activation energies.

The reaction scheme is formulated by considering the cracking of VGO into four major groups of products, namely, distillate, naphtha, gases, and coke. The distillate pseudo-component cracks further to produce naphtha that is further cracked to produce gaseous products. The probability of coke formation from light products (i.e., distillate, naphtha, and gases) is negligible according to previous studies, so the coke is assumed to be formed only from VGO [24]. Figure 6-5 presents the proposed reaction scheme for the competing reactions involved in the catalytic hydrocracking of VGO investigated. Based on the proposed mechanism, the governing equations representing hydrocracking of VGO after implementing the model in the design equation for a batch reactor would result in the following expression:

Rate of VGO consumption:

$$\frac{dY_V}{dt} = -(k_{VD} + k_{VN} + k_{VG} + k_{VC}){Y_V}^2 \tag{6-1}$$

The reaction rates of formation of the pseudoproducts, i.e. distillate, naphtha, coke, and gases, are as follows:

$$r_D = \frac{dY_D}{dt} = k_{VD}{Y_V}^2 - k_{DN}Y_D \tag{6-2}$$

$$r_N = \frac{dY_N}{dt} = k_{VN}{Y_V}^2 + k_{DN}Y_D - k_{NG}Y_N \tag{6-3}$$

$$r_G = \frac{dY_G}{dt} = k_{VG}{Y_V}^2 + k_{NG}Y_N + k_{DG}Y_D \tag{6-4}$$

$$r_C = \frac{dY_C}{dt} = k_{VC}{Y_V}^2 \tag{6-5}$$

where Y_i represents the yield of pseudo-component i, i.e., V: VGO, D: distillate, N: naphtha, G: gases, and C: coke. Although most of the kinetic models developed in the literature for the hydrocracking of heavy oil suggest that all reaction steps follow the first-order reaction [12], the rate of disappearance of VGO is assumed to be second order. Sanchez and Ancheyta [139] were the first to suggest that after performing an experimental study on the hydrocracking reaction of heavy oil under moderate conditions, the hydrocracking reaction step is better represented by an apparent second-order kinetic reaction. This suggestion was attributed to the assumption that the most reactive compound in the hydrocracking of the vacuum residue (VR) disappears quickly. Thus, the hydrocracking step is represented with a second-order equation, while the following reaction is represented with a first-order equation. The temperature-dependent rate constants (k_{ij}) are represented by the Arrhenius formula, as follows:

$$k_{ij} = k_{ij_0}\, exp\left[-\frac{E_{ij}}{R}\left(\frac{1}{T} - \frac{1}{T_m}\right)\right] \tag{6-6}$$

where k_{ij_0} is the pre-exponential factor for the j formation reaction from i, E_{ij} is the apparent activation energy for the j formation reaction from i, R is the universal gas constant, T is the reaction temperature, and T_m is the centering temperature [148], which resides around the mean range of the reaction temperature applied. The centering temperature is implemented to simplify the search for kinetic parameters by reducing the statistical correlation between the pre-exponential factor and the apparent activation energy.

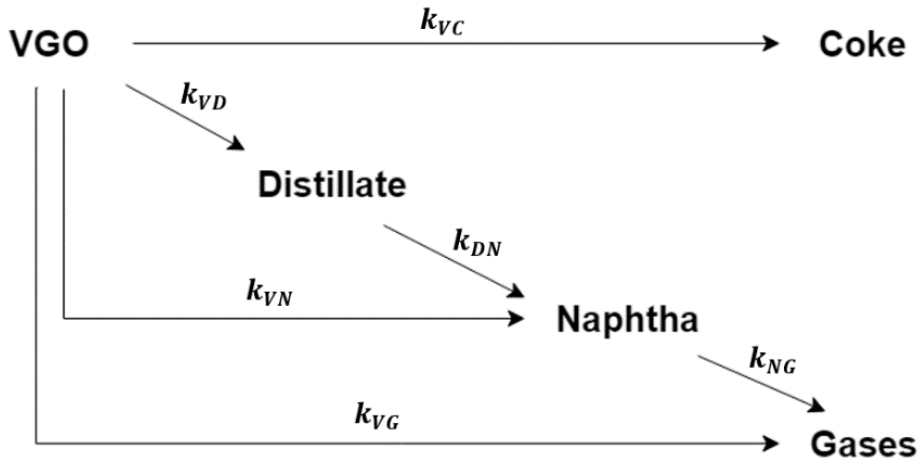

Figure 6-5 Proposed reaction scheme for VGO hydrocracking.

Parameters Estimation Strategy

The experiments were conducted over a range of temperatures (390, 420, and 450°C) as well as a range of times (0.5, 1, and 1.5 h), which resulted in 45 data points. The estimation of kinetic parameters is conducted at a degree of freedom of 33 (degree of freedom = No. of experimental data points – No. of parameters to be estimated) since 12 kinetic parameters of pre-exponential factors and activation energies are presented in the rate of reactions that are derived from the reaction rate constants as mentioned in Equation (6-6).

The kinetic parameters were estimated first by simultaneously solving the differential equations and then fitting the data points, which was performed by encoding and solving Equations (6-1)-(6-5) in the MATLAB programming interface (MATLAB and Statistics Toolbox Release 2014a, The MathWorks, Inc., Natick, Massachusetts, United States.). The *ode45* subroutine (the Rung-Kutta-Gill method) and *lsqcurvefit* subroutine (the modified Marquad method) were used for solving the differential equations and fitting the points, respectively. The parameters were estimated by minimizing the sum of squares of the residual (SSR) (Equation (6-7)).

$$SSR = \sum_{j=1}^{N}\sum_{i=1}^{M}\left(Y_{ij}^{exp} - Y_{ij}^{cal}\right)^2 \tag{6-7}$$

where Y_{ij}^{exp}, Y_{ij}^{cal}, and N are experimental yields, the yield calculated by the model and the number of runs, respectively. The model was assessed by determining the coefficient of determination (R^2), ensuring that the lowest SSR, the lowest cross-correlation coefficient (γ) and the individual 95 % confidence intervals for the estimated parameters are attained. Finally, the model accuracy was evaluated by computing the mean average deviation (MAD%) for each lump of pseudo-component yield.

$$MAD\% = \frac{\sum_{i=1}^{N}\left[\left|Y_i^{exp} - Y_i^{cal}\right|/Y_i^{exp}\right]}{N} \times 100 \tag{6-8}$$

6.2.2 Results of Kinetics of the Synergy Effects

Table 6-1 shows the kinetic parameters based on the reaction scheme proposed in Figure 6-5 of the hydrocracking of VGO over supported catalyst versus hydrocracking over mixed-phase catalysts. The highest activation energy within the reaction series VGO →

distillate → naphtha → gases was 80.918 kcal/mol for the cracking reaction of distillate to produce naphtha, while the lowest value (64.448 kcal/mol) was found for the cracking of naphtha to gases for hydrocracking over the standalone supported catalyst.

The introduction of the Ni-TBC[4] catalyst precursor together with the solid catalyst greatly affected all apparent kinetic parameters, thus verifying the claim that the dispersed catalyst enhances the hydrogenation reactions. The apparent activation energy of the distillate formation (VGO→distillate) experienced a marked reduction from 65.39 kcal/mol to 57.32 kcal/mol after the addition of 500 ppm of Ni in the form of the Ni-TBC[4] catalyst precursor. Although the activation energy of the distillate formation reaction is still considered to be relatively high, its frequency factor delivers the highest value among all reactions involved at 3.06 h^{-1}. This observation indicates that the distillate formation reaction possesses the highest kinetic energy towards the reaction; however, more severe process conditions are required due to the relatively high activation energy.

The estimated apparent parameters of reactions involved in VGO hydrocracking under standalone supported catalysts are in line with similar previously studied systems that support their validity [24, 140, 185]. Table A 1 shows previously reported estimated apparent kinetic parameters of hydrocracking of VGO. Despite the fact that the referenced studies have reported the kinetic parameters that govern catalytic hydrocracking of VGO using the discrete lumping method, each study estimated its own kinetic parameters based on different lumping approaches, reaction pathways and technical operations, such as reactor modes (i.e., batch and continuous) and catalyst type. Therefore, caution must be taken when comparing the predicted apparent kinetic parameters.

It is worth mentioning that a preliminary reaction scheme (Figure A 6) was proposed in the first place by assuming all the occurrence of all possible reaction pathways, including the formation of gases from the distillate. The estimated apparent activation energy of gases formation from distillate showed a relatively high value at 212.7 kcal/mol which indicates that the reaction has an extremely low probability to take place (Table A 2). Therefore, it has been excluded while the modified reaction scheme presented earlier in Figure 4.5 has been adopted in this study.

Table 6-1 Estimated kinetic parameters for hydrocracking of VGO feed over the standalone supported catalyst and mixed (supported+dispersed) catalysts for reaction scheme presented in (Figure 6-5).

Parameter	Standalone supported catalysts		Mixed catalysts	
	E_{ij} (kcal/mol)	k_{ij} (h^{-1})	E_{ij} (kcal/mol)	k_{ij} (h^{-1})
k_{VD}	65.39	2.496	57.32	3.057
k_{VN}	1.71e-3	0.976	19.67	1.474
k_{VG}	0.16	1.258	45.88	1.199
k_{VC}	35.91	0.138	17.85	0.086
k_{DN}	80.92	0.127	72.54	0.100
k_{NG}	64.45	0.231	24.80	0.301

Note: The subscripts V, D, N, G, and C stand for VGO, distillate, naphtha, gases, and coke, respectively.

6.2.3 Model Validation

The parity plots in Figure 6-6 compare the experimental and calculated yields for VGO hydrocracking over both standalone supported solid catalysts and mixed phase catalysts, where the x-axis represents experimental data and the y-axis represents calculated yields. All points fall in the close range of variations around the diagonal line, thus proving a high degree of accuracy and precision of fitting the experimental data.

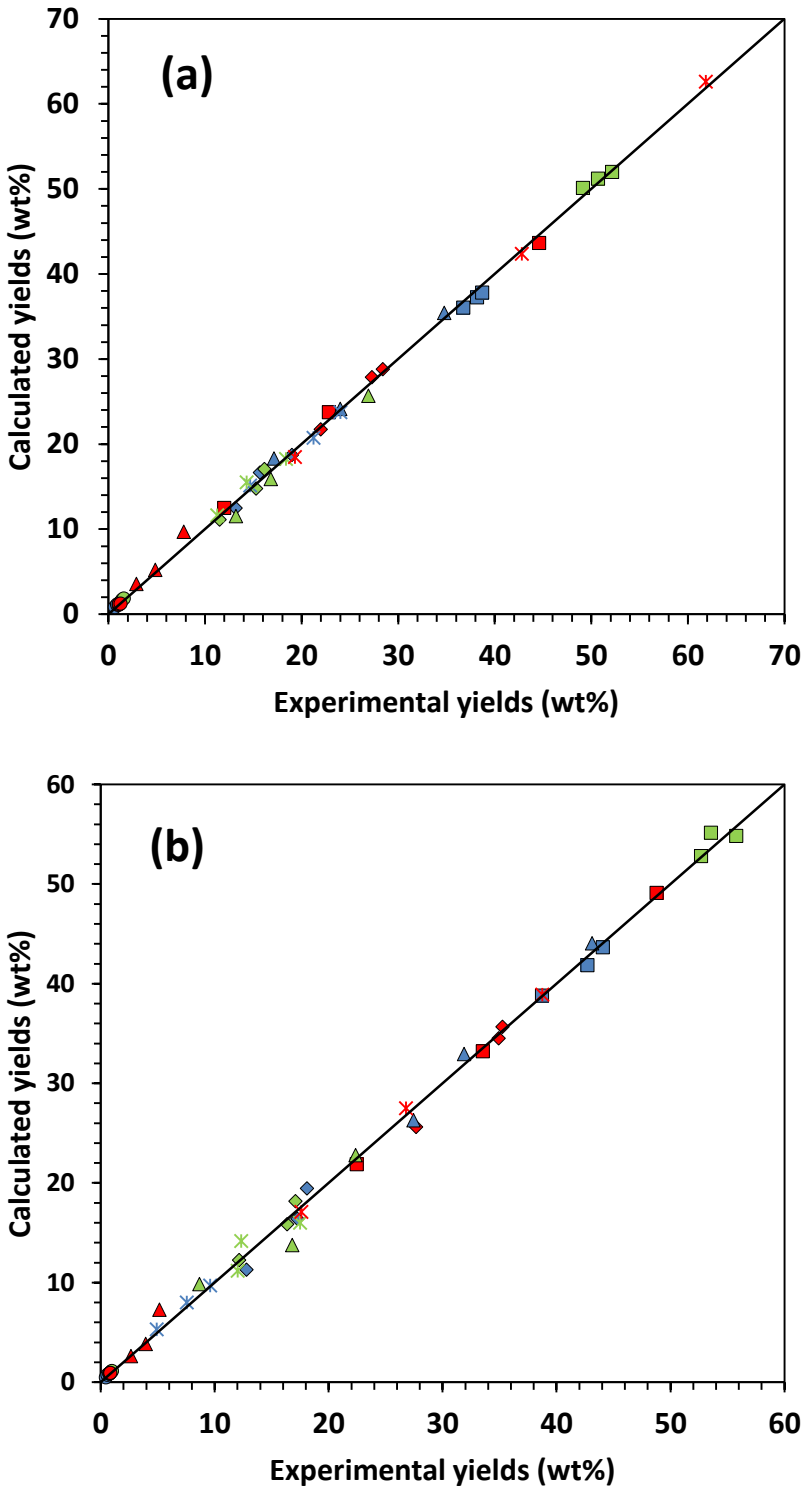

Figure 6-6 Parity plots of the yields of (▲) VGO; (■) distillate; (◆) naphtha; (*) gases; and (●) coke upon hydrocracking over (a) supported solid catalysts and (b) over mixed catalysts at different reaction temperatures. (markers' colors indicate reaction temperatures, i.e. blue=390°C, green=420°C, and red=450°C).

Figure 6-7 and Figure 6-8 show the experimental and model predicted product yields versus VGO conversion at 390, 420, and 450°C for hydrocracking over the solid supported catalyst and mixed supported and dispersed catalysts, respectively. Also, Figure A 7 and Figure A 8 show the experimental and model predicted product yields versus reaction time at 390, 420, and 450°C for hydrocracking over the solid supported catalyst and mixed supported and dispersed catalysts, respectively. The experimental data points and the curve fitted by the model show appreciable comparability for all cases.

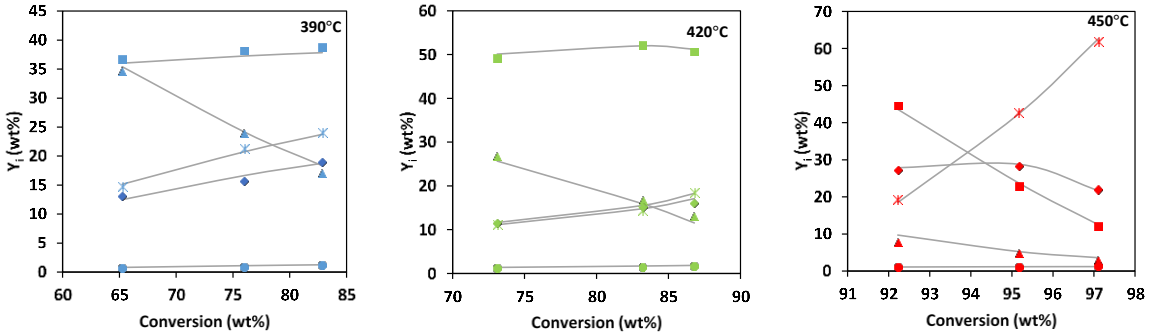

Figure 6-7 Predicted (lines) and experimental (symbols) yields of (▲) VGO; (■) distillate; (◆) naphtha; (*) gases; and (●) coke versus conversion for hydrocracking of vacuum gas oil over the solid supported catalyst.

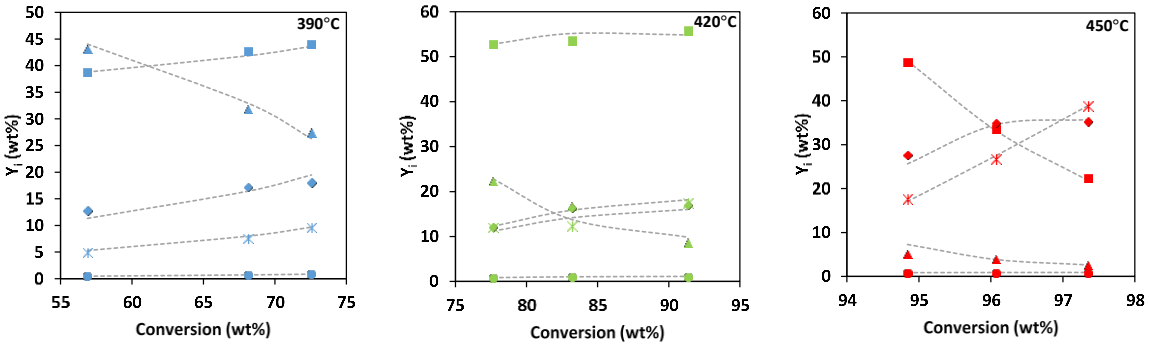

Figure 6-8 Predicted (dashed lines) and experimental (symbols) yields of (▲) VGO; (■) distillate; (◆) naphtha; (*) gases; and (●) coke versus conversion for hydrocracking of vacuum gas oil over mixed catalysts.

The accuracy of the estimated apparent parameters was also assessed by evaluating the mean absolute deviation (MAD) of the yields for each lump of pseudo-components calculated for all reaction temperatures applied. The results show that the $MAD\%$ values for naphtha, distillate, unconverted VGO, gases, and coke yields for hydrocracking over the solid supported catalyst were 3.3, 2.2, 9.9, 2.8, and 13 %, respectively. The yields obtained by applying mixed phase catalysts showed generally improved validation of the model, where the mean absolute deviations were 4.1, 0.99, 9.5, 4.5, and 3.2 % for naphtha, distillate, unconverted VGO, gases, and coke yields, respectively.

6.2.4 Rate Analysis

Figure 6-9 shows the Arrhenius plots for the specific reaction rate constants for supported and mixed catalyst systems. For both catalytic configurations applied, the Arrhenius plots show the expected trends of negative slopes. From this observation, it is deduced that the developed model and the estimated parameters imply a good thermodynamic consistency. Therefore, applying the 5-lump discrete model is considered a suitable approach for modeling these VGO hydrocracking systems over either supported solid catalysts only or both solid and dispersed catalysts in slurry-phase [24]. The Arrhenius plots support the claim that VGO cracks more easily to produce light liquid products upon introducing the dispersed catalyst where the k-value is favored for all reaction temperatures under consideration.

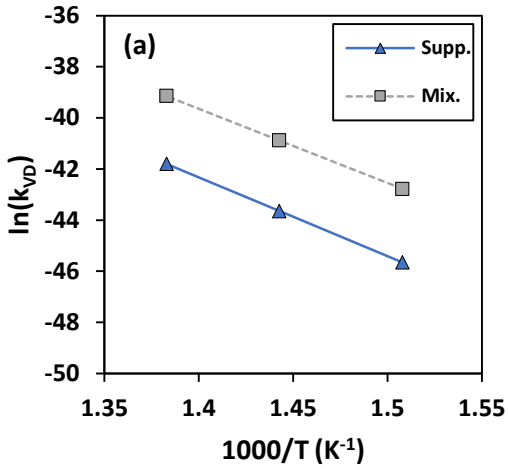
(a)
Supp.
Mix.
ln(k_VD)
1000/T (K^-1)

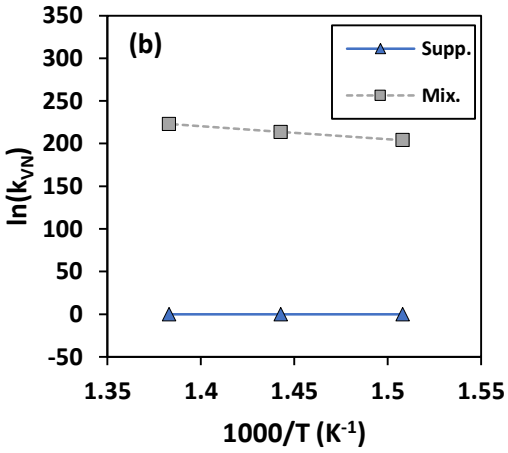
(b)
Supp.
Mix.
ln(k_VN)
1000/T (K^-1)

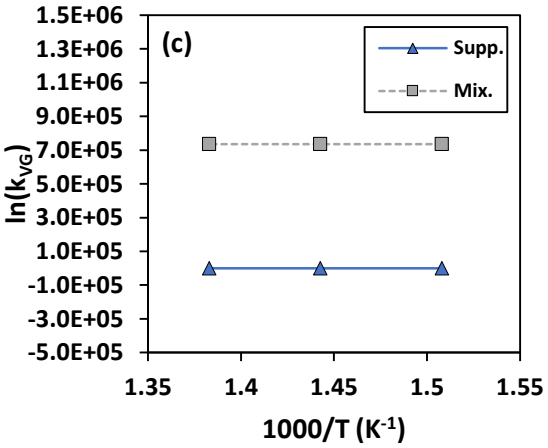
(c)
Supp.
Mix.
ln(k_VG)
1000/T (K^-1)

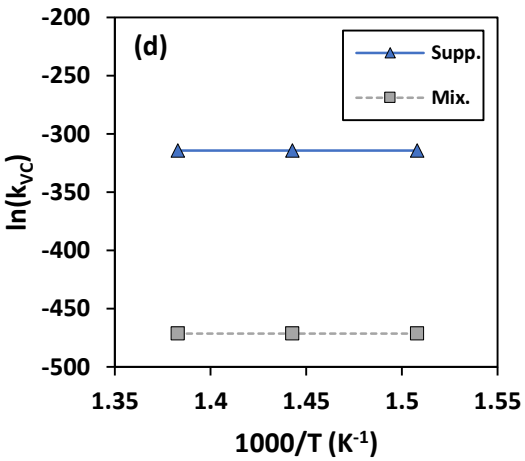
(d)
Supp.
Mix.
ln(k_VC)
1000/T (K^-1)

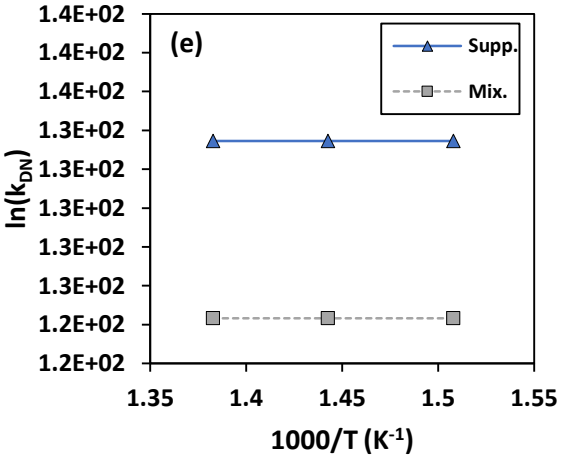
(e)
Supp.
Mix.
ln(k_DN)
1000/T (K^-1)

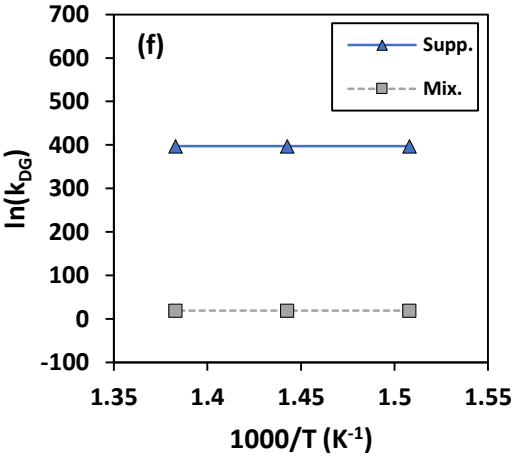
(f)
Supp.
Mix.
ln(k_DG)
1000/T (K^-1)

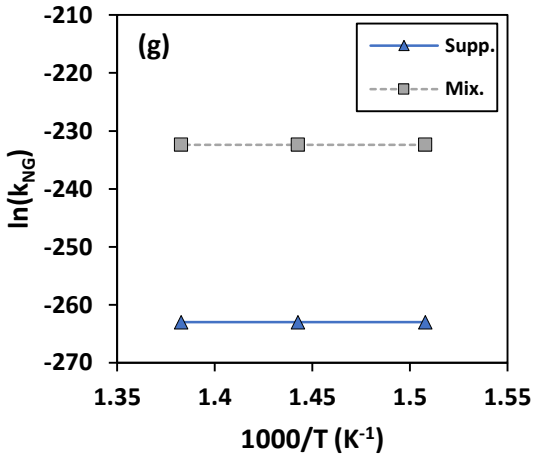

Figure 6-9 Arrhenius plots for the different specific reaction rate constant for supported and mixed catalysts systems.

A closer observation of Figure 6-9 clearly shows the positive effects of using mixed catalysts over the standalone supported catalysts. The VGO→distillate conversion rate (Figure 6-9.a) over mixed catalyst is higher than standalone supported catalyst and in both cases it is highly temperature dependent. The VGO→naphtha conversion rate (Figure 6-9.b) over mixed catalyst is significantly higher than standalone supported catalyst and more temperature dependent in the case of mixed catalysts. The rates of secondary reactions distillate→naphtha and distillate→gases are higher over standalone supported catalysts which indicate that the mixed catalysts enhance the primary reactions involving VGO conversion. The formation of gases from naphtha is also enhanced by mixed catalysts. However, the mixed catalysts significantly reduced the carbon formation rates as shown in Figure 6-9.d.

The reaction rate constants were evaluated with the aid of the previously estimated parameters of pre-exponential factors and the apparent activation energies to understand its effects on the rates of reactions involved in the hydrocracking process. The rate

constants were estimated at different temperatures between the lowest and highest temperatures applied experimentally, which were 390°C and 450°C, respectively. The rate constant of the middle distillate formation reaction shows an exponential increase for the hydrocracking process with mixed catalysts compared to the standalone supported catalyst, as presented in Figure 6-10.a. However, Figure 6-10.b shows that the rate constant of the gas formation reaction, which was ~1.28 $wt\%^{-1} \cdot h^{-1}$ for the supported catalyst only, was drastically reduced by introducing the metal-based calixarene to 2.12E-14 $wt\%^{-1} \cdot h^{-1}$ to 2.98E-13 $wt\%^{-1} \cdot h^{-1}$ for reaction temperatures of 390°C and 450°C, respectively.

Figure 6-11.a shows the VGO conversion rates versus the reaction time of the four reactions at 420°C of hydrocracking over supported as well as mixed phase catalysts. The profiles clarify that the VGO was converted to form the products with appreciable differences for both catalytic configurations. The overall rate of VGO conversion decreased sharply from -2.152E+4 wt%/h until it reached -6.114E+3 wt%/h after half an hour of the reaction period. The disappearance rate experienced slower reduction thereafter upon extending the reaction time, and a value of -1.635E+3 wt%/h was exhibited after 1.5 h. This result is attributed to the continuous disappearance of VGO, which is then countered by the extremely low conversion rates of the subsequent pseudo-components within the batch system.

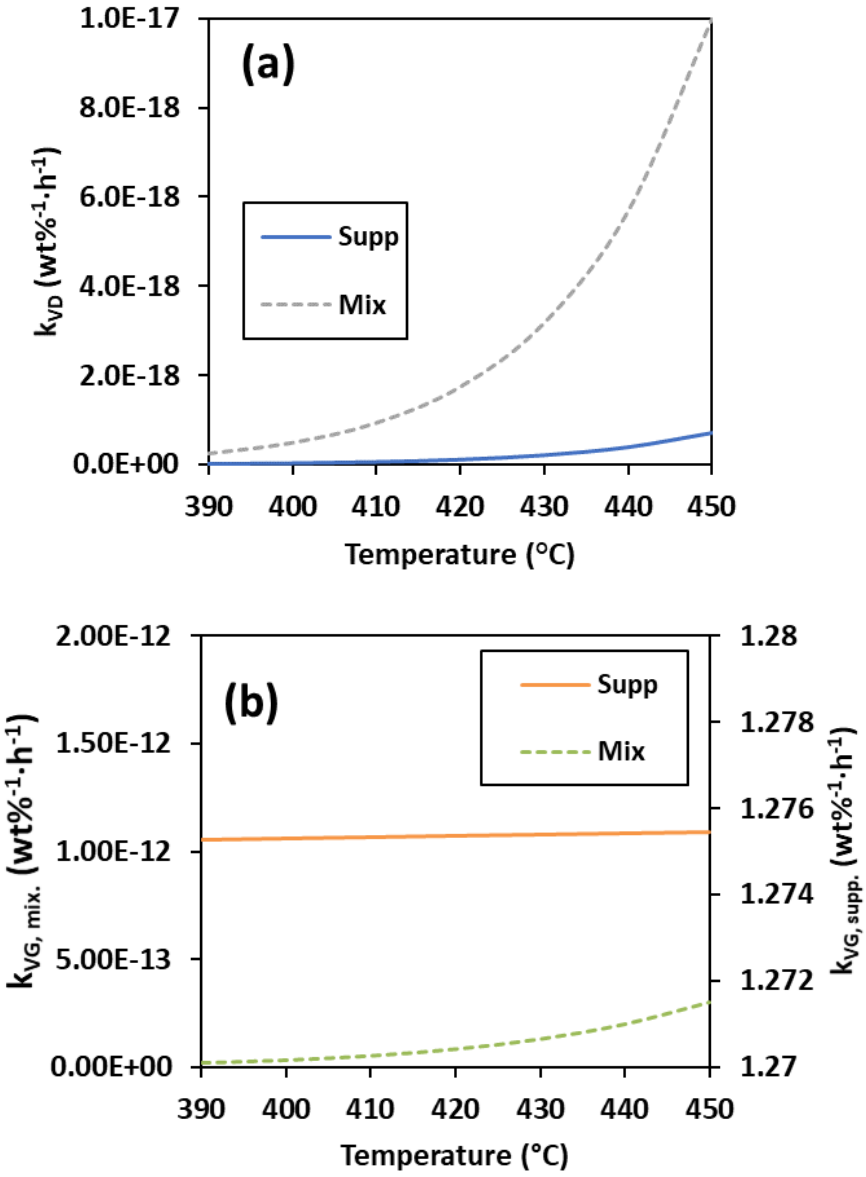

Figure 6-10 Effect of the reaction temperature on the rate constant for supported and mixed phase catalytic systems of (a) the distillate formation reaction and (b) the gas formation reaction.

The addition of the Ni-TBC[4] dispersed catalyst precursor seems to affect the VGO conversion rates to various degrees. The conversion rate started at -2.571E+4 wt%/h and showed an exponential increase with a continuous divergence from the standalone supported catalyst system over the course of the reaction period until reaching a value of -

4.026E+3 wt%/h at 1.5 h with an increasing percentage of ~146%. The rate of distillate formation from VGO over the standalone supported catalyst reaction, R_{VD}, was faster than the naphtha and gas formation rates from VGO, R_{VN} and R_{VG}, respectively, while the coke deposition rate, R_{VC}, was the slowest ($R_{VD} > R_{VG} > R_{VN} > R_{VC}$). In effect, the main conversion pathway of VGO was in favor of producing distillate, followed by the production of naphtha and gases to lesser extents, whereas the coke deposition rate was further diminished. Unlike the rate with the standalone supported catalyst, the rate of naphtha production from VGO, R'_{VN}, surpassed the rate of gases evolving R'_{VG} upon addition of the Ni-TBC[4]. Consequently, the arrangement of reaction rates altered to be $R'_{VD} > R'_{VN} > R'_{VG} > R'_{VC}$.

The distillate and naphtha were mainly produced from VGO over the course of the reaction period, which explains the observation that the rates of formation for both catalytic configurations are controlled by the conversion rate of VGO, which is much faster than the other reaction rates. Figure 6-11.b proves that the effect of the other rates has a minor effect on the overall formation rates of distillate and that they almost coincide with rate of distillate formation from VGO for catalytic configurations. Similar results were observed on the rate of naphtha formation as presented in Figure A 9.

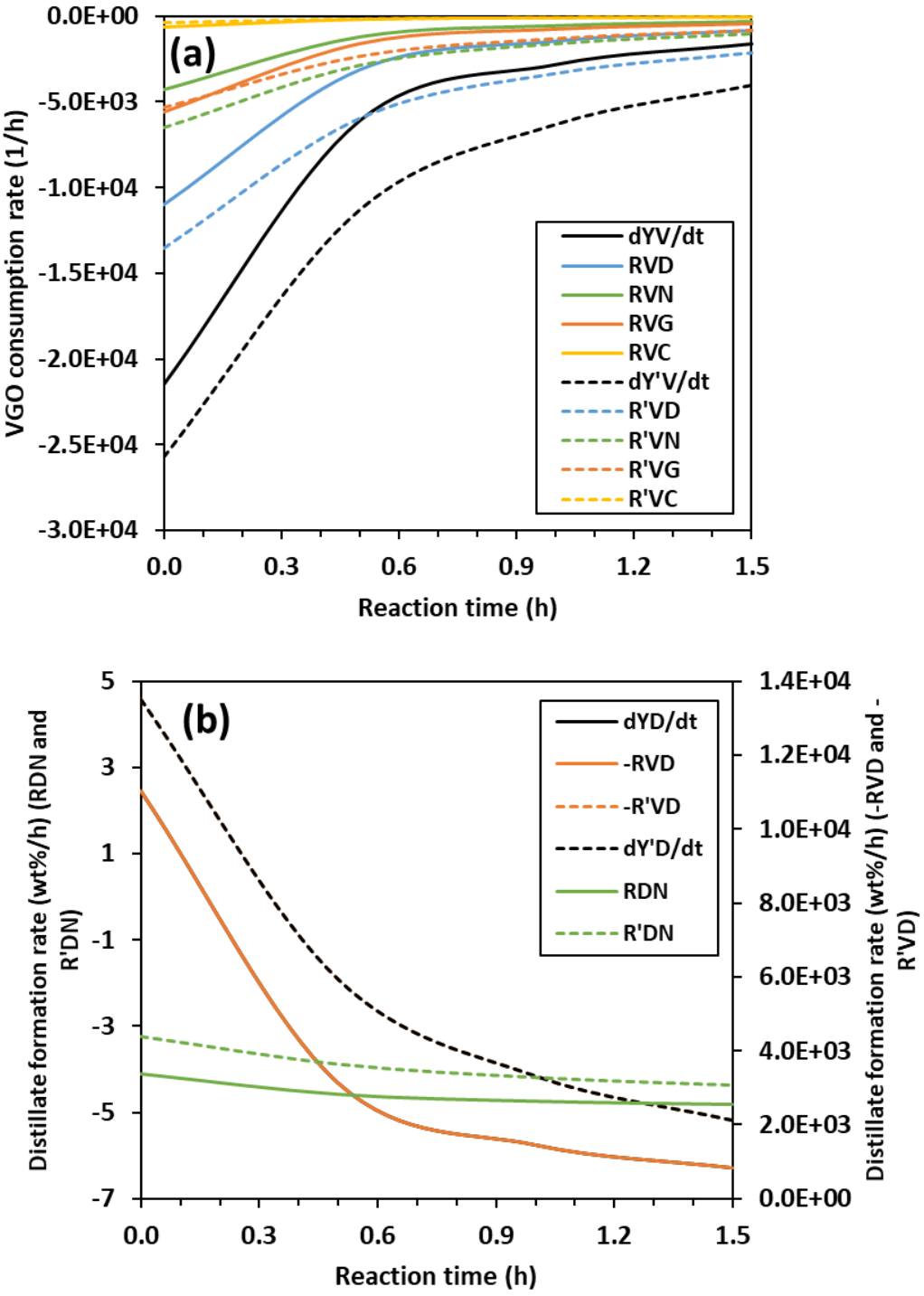

Figure 6-11 (a) VGO conversion rate and (b) distillate formation rate versus reaction time of hydrocracking over supported as well as mixed catalysts at 420°C (where Rji and R'ji refer to the rate of i formation from j for supported and mixed-catalyst systems, respectively).

The contour plots shown in Figure 6-12 present the instantaneous selective hydrocracking of VGO to distillate ($\dot{S}_{D/NGC}$). The figures were plotted on a linear basis using OriginPro 8.5 (OriginLab, Northampton, MA). As anticipated, the distillate instantaneous selectivity of VGO hydrocracking over the standalone supported catalyst reached its maximum at higher reaction temperatures. Conducting the hydrocracking over the supported catalyst in addition to the Ni-TBC[4] complex results in a generally enhanced selectivity of distillate even under mild conditions (Figure 6-12.b). However, under severe conditions beyond 420°C, the selectivity to produce distillate in the mixed catalytic system is lower than that achieved by the hydrocracking over the standalone supported catalyst because of the favorable naphtha yield and the loss of some of the catalytic activity offered by the Ni-TBC[4] catalyst precursor, which has limited thermal stability. Therefore, conducting the hydrocracking over the standalone supported catalyst requires severe conditions to reach appreciable instantaneous selectivity to the distillate in the absence of additional hydrogenation active sites offered via the dispersed catalyst.

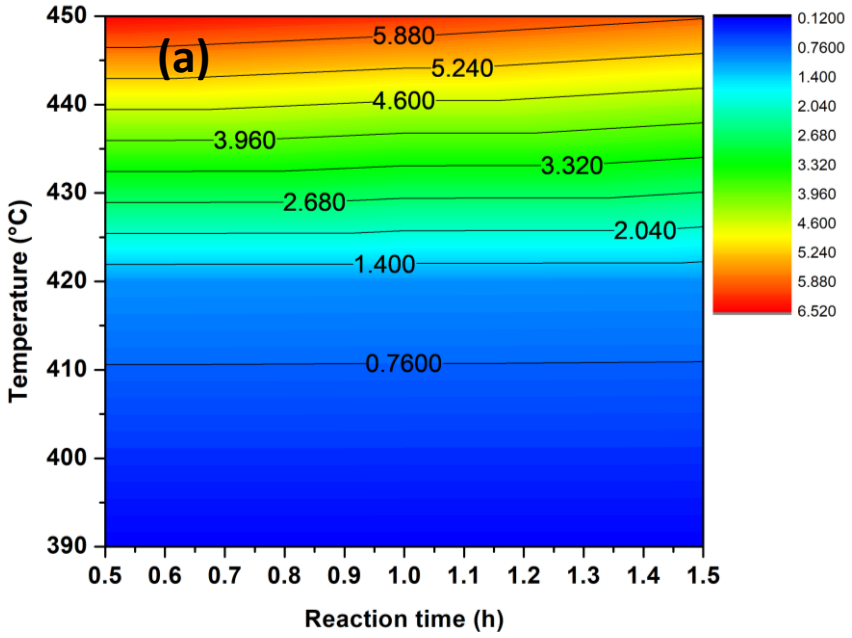

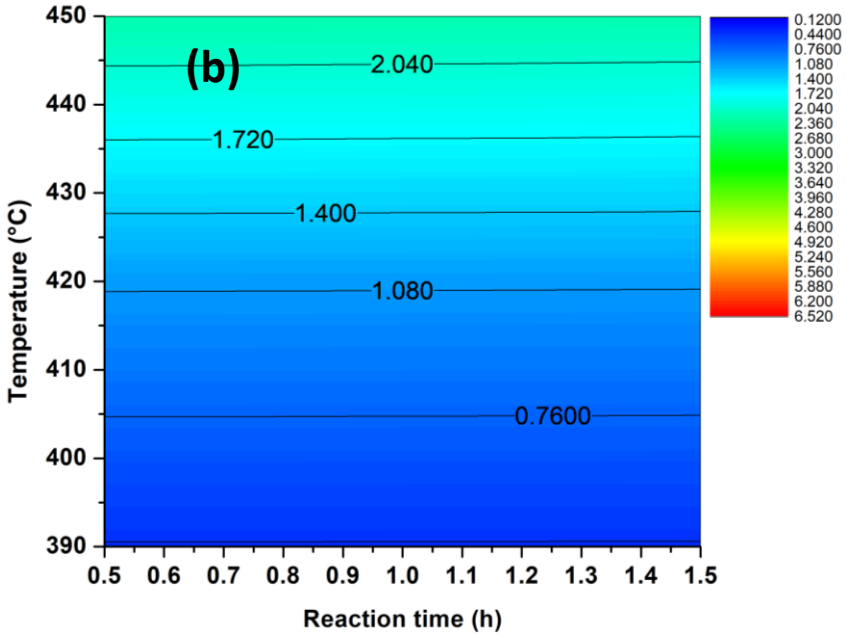

Figure 6-12 Instantaneous selectivity in VGO hydrocracking to distillate ($\dot{S}_{D/NGC}$) over (a) the standalone supported and (b) the mixed catalysts.

6.3 Conclusions

The yields of coke and gases decreased upon introducing the dispersed catalyst along with the supported solid catalyst by 35.86 % and 13.90 %, respectively. The yield of naphtha increased from 15.27 wt% to 16.36 wt%, and that of distillate increased from 52.17 wt% to 53.57 wt% compared with the use of the supported catalyst, while the conversion of VGO was unchanged at about 83.20 %. The value of the dimensionless catalytic activity parameter proved the existence of the synergy between the two catalysts since it is much higher than that acquired through the algebraically calculated yields. The hydrogenation capability of the dispersed catalyst was confirmed by performing an elemental analysis, which revealed that introducing the dispersed catalyst in addition to the supported commercial catalyst enhanced the product quality by boosting the H/C ratio and reducing the sulfur content that is present in the form of heteroatom-containing organic compounds.

The pseudo turnover frequency of sulfur atom removal from heteroatom-containing organic compounds shows a boosting effect in the presence of the dispersed catalyst in addition to the solid catalyst. The PTOF increased from 3.53E+3 to 5.73E+3 S atoms removed/($\mu m^2 \cdot h$) upon introducing 500 ppm Ni to the catalytic system. The activation energy of the distillate formation experienced a notable reduction from 65.39 kcal/mol to 57.32 kcal/mol by introducing the Ni-TBC[4] catalyst precursor together with the supported catalyst. Parity plots and the MAD% of each lump proved a high degree of accuracy and precision of fitting the experimental data for both catalytic systems. The results show that the pseudocomponents were produced mainly from the sequential cracking of VGO.

CHAPTER 7

CONCLUSIONS & RECOMMENDATIONS

7.1 Conclusions

The following statements are the main conclusions of the experimental and kinetic studies:

i. Co- and Ni-based TBC[4] were successfully synthesized and characterized using different techniques, i.e., SEM-EDX, ICP, XRD, UV-Vis, FT-IR, and ^{1}H NMR. The results confirm the coordination of the cations with the TBC[4] ligand to form organometallic compounds.

ii. The DSC profile of Ni-TBC[4] and Co-TBC[4] shows that the organometallic structure has reduced thermal stability compared with that of the parent TBC[4] which is depicted by lowering their melting points and methylene bridging temperature occurrences. The low thermal stability can be positively exploited by employing calixarenes as a carrier of the metal, where the active sites are formed by the destruction of the organometallic complex upon reaching the desired reaction conditions.

iii. The batch autoclave tests show that the yields of distillate and naphtha were higher after hydrocracking over Co-TBC[4] and Ni-TBC[4]. The addition of 500 ppm Co and Ni as standalone dispersed catalysts increased the yield of distillate to 45.71

wt% and 49.66 wt%, while the amount of coke deposition decreased to 2.60 wt% and 2.26 wt%.

iv. The introduction of the dispersed catalyst precursors, which are eventually converted *in situ* to active sites of metal sulfides, will ensure efficient hydrogen uptake by free radicals. Hence, the β-scission reactions and coke formation would be controlled even at low concentrations of dispersed active metal sulfides. The presence of the active metal sulfide crystals lowers the coke formation by sticking on the coke precursors with the aid of the wetting property. This results in stabilizing and inhibiting the coalescing as of the coke precursors. The dispersed catalyst will also act as a hydrogen donor in the partial hydrogenation of PAHs in the hydrogenation/dehydrogenation cycle.

v. High concentrations of the dispersed catalyst show catalytic enhancement in terms of enhancing the distillate yield and suppressing the gases formation since that the hydrogen uptake is concentration dependent. However, the coke deposition found to experience a slight increase that is attributed to the excessive hydrogenation as a result of increasing metal sulfide concentration, which also reduces the stability of asphaltenes. Therefore, coke precursors are activated in the form of destabilized asphaltenes to form coke deposits.

vi. Applying higher reaction temperature leads to decreasing the yields of distillate and naphtha due to the deactivation of the *in situ* nickel sulfides through sintering. Therefore, the loss of catalytic hydrogenation is ascribed to the shortage of active sites per unit amount.

vii. The yields of coke and gases decreased upon introducing the dispersed catalyst along with the presulfided, commercial, first-stage hydrocracking supported catalyst by 35.86 % and 13.90 %, respectively. In contrast, the yields of naphtha increased from 15.27 wt% to 16.36 wt% and distillate from 52.17 wt% to 53.57 wt% compared with the use of the standalone supported catalyst, where the conversion of VGO is comparable at ~83.20 %.

viii. The synergy between the catalysts was proved by comparing the actual yield of mixed-phase catalysts with those obtained by the algebraic average of the product yields. The value of the dimensionless catalytic activity parameter proves the existence of synergy between the two catalysts since it is much higher than that acquired through the algebraically calculated yields.

ix. The hydrogenation capability of the dispersed catalyst was confirmed by performing an elemental analysis, which revealed that introducing the dispersed catalyst in addition to the supported commercial catalyst enhanced the product quality by boosting the H/C ratio and reducing the sulfur content that is present in the form of heteroatom-containing organic compounds. The pseudo turnover frequency of sulfur atom removal from heteroatom-containing organic compounds shows a boosting effect in the presence of the dispersed catalyst in addition to the solid catalyst. The PTOF increased from 3.53E+3 to 5.73E+3 S atoms removed/($\mu m^2 \cdot h$) upon introducing 500 ppm Ni to the catalytic system. This result was because of the enhancement of the hydrotreating reactions even though additional surface area was supplied by the active dispersed nickel sulfides themselves that were formed *in situ*.

x. A five lump discrete kinetic model was developed based on the experimental data by incorporating the conversion of VGO to distillate, naphtha, and C_1-C_5 gaseous hydrocarbons in addition to coke deposition. The activation energy of the distillate experienced a notable reduction from 65.393 kcal/mol to 57.322 kcal/mol by introducing the Ni-TBC[4] catalyst precursor together with the supported catalyst.

7.2 Recommendations

The following are the recommendations suggested to be addressed for forthcoming researches in this topic:

i. Metallocalixarene should be formed from derivatized parent molecules, such as hexaacetate *p*-methylcalix[6]arene, since they might improve the solubility in heavy oil during hydrocracking, which would increase the hydrogen uptake as a result of enhanced dispersion of the active metal sites formed subsequently.

ii. The method adopted for characterizing the liquid product in this research was based on the discrete lumping approach, which is one of the commonly used in catalytic models of complex petroleum feedstocks. Nevertheless, it suggested to further analyze these lumps in order to have an idea of their contents of paraffins, aromatics, etc., and therefore establish more clear differences in the behavior of each catalyst studied.

APPENDICES

Figure A 1 Photographs of (b) Co-*p-tert*-Butylcalix[4]arene as prepared.

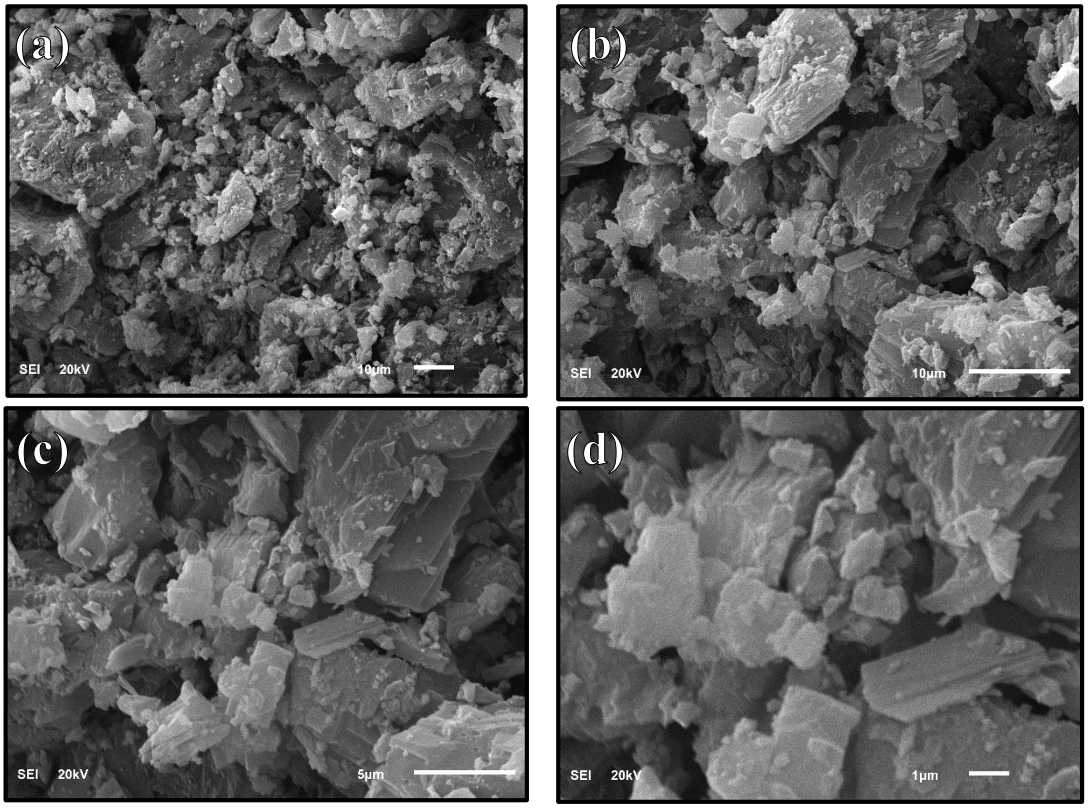

Figure A 2 SEM images for free *p-tert*-Butylcalix[4]arene at a magnification of (a) ×1000, (b) ×2500, (c) ×5000, and (d) ×10000.

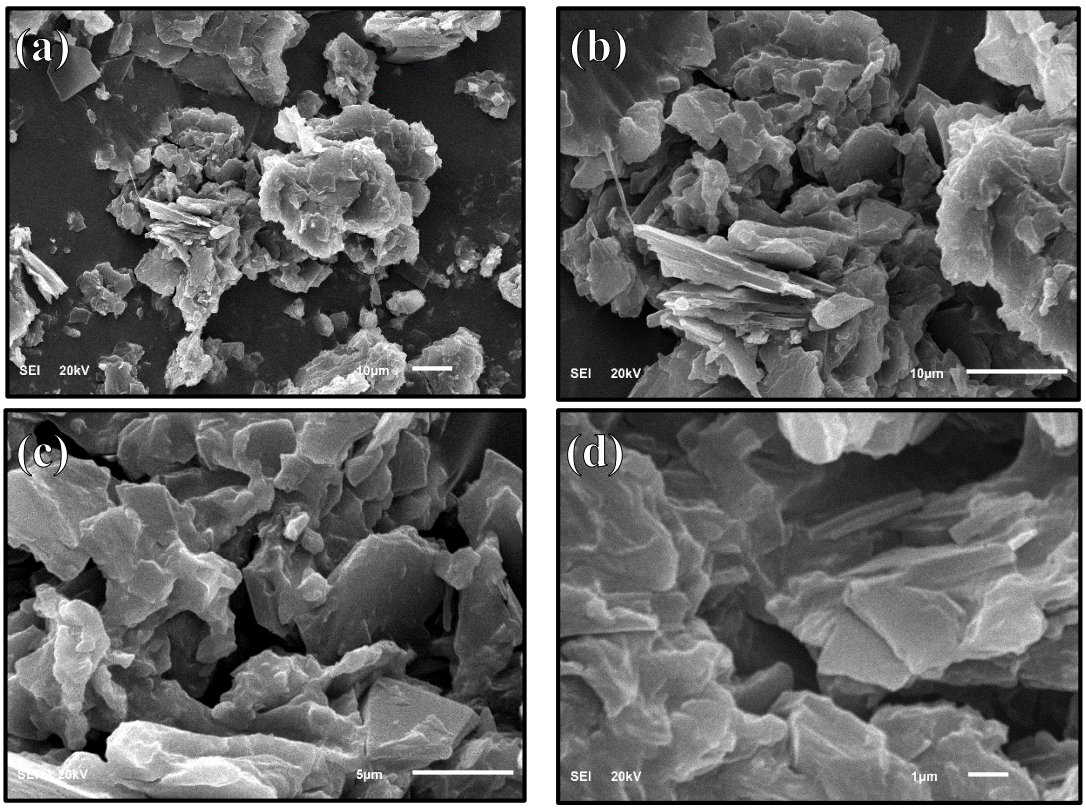

Figure A 3 SEM images for Ni-*p-tert*-Butylcalix[4]arene at magnification of (a) ×1000, (b) ×2500, (c) ×5000, and (d) ×10000.

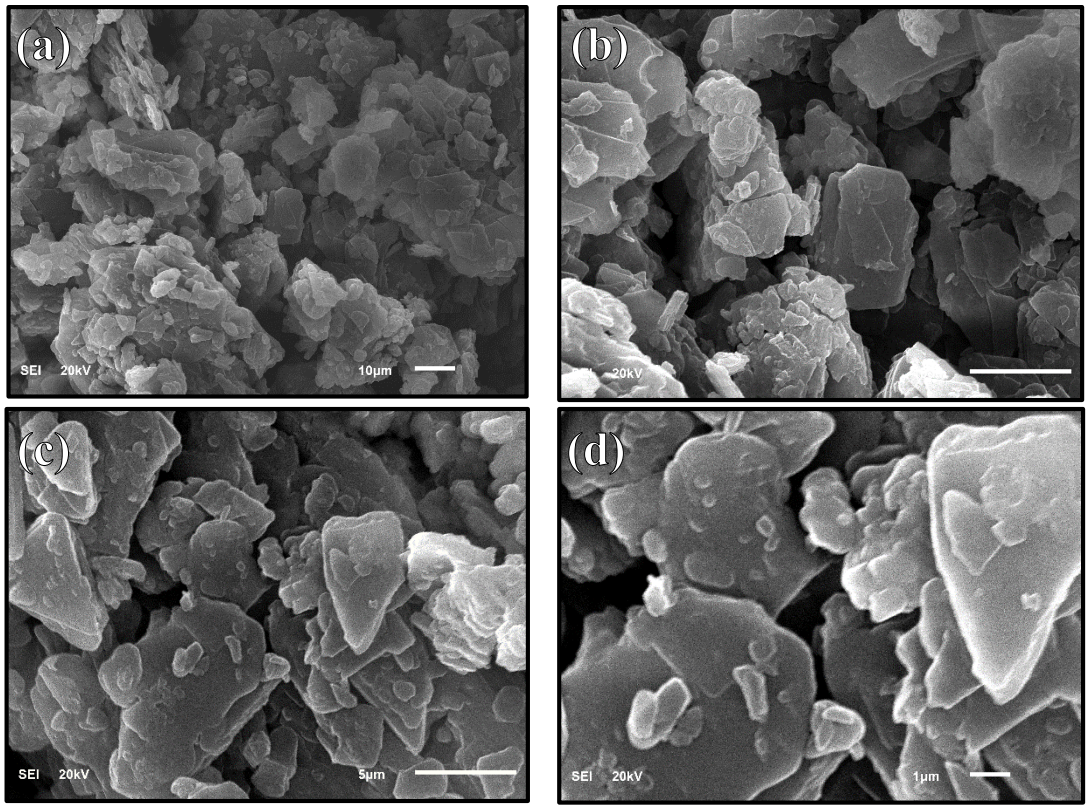

Figure A 4 SEM images for Co-*p*-*tert*-Butylcalix[4]arene at magnification of (a) ×1000, (b) ×2500, (c) ×5000, and (d) ×10000.

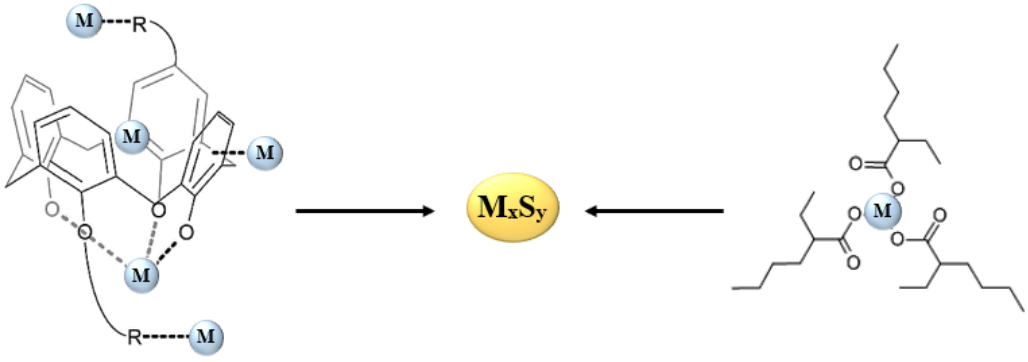

Figure A 5 Scheme of the proposed sulfidation of metal derived from TBC[4] and 2-ethylhexanoate organic ligands (M: metal, S: sulfur, R: alkyl group).

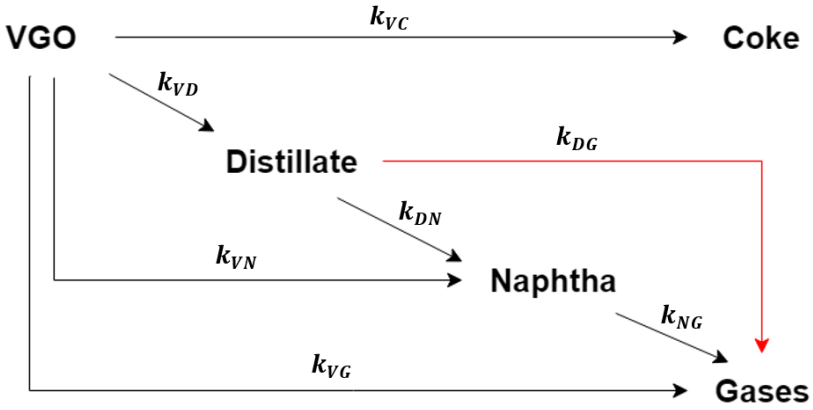

Figure A 6 Preliminary reaction scheme proposed for hydrocracking of vacuum gas oil (VGO) in this study.

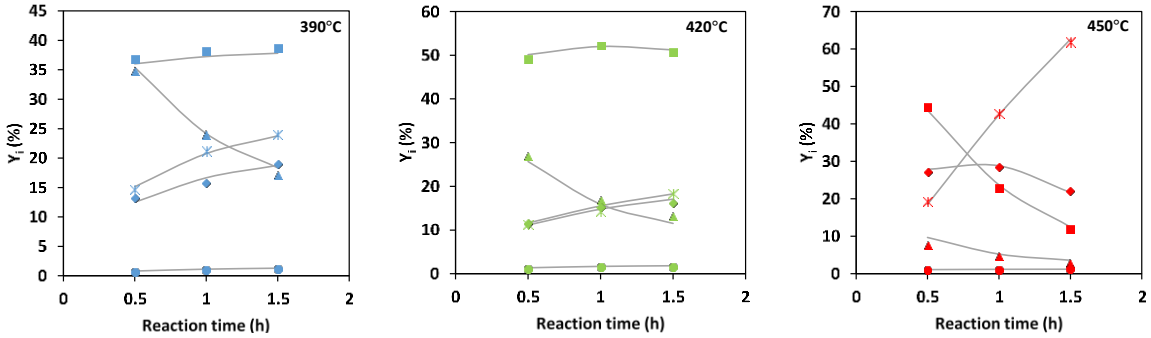

Figure A 7 Predicted (lines) and experimental (symbols) yields of (▲) VGO; (■) distillate; (◆) naphtha; (*) gases; and (●) coke versus reaction time for hydrocracking of vacuum gas oil over the solid supported catalyst.

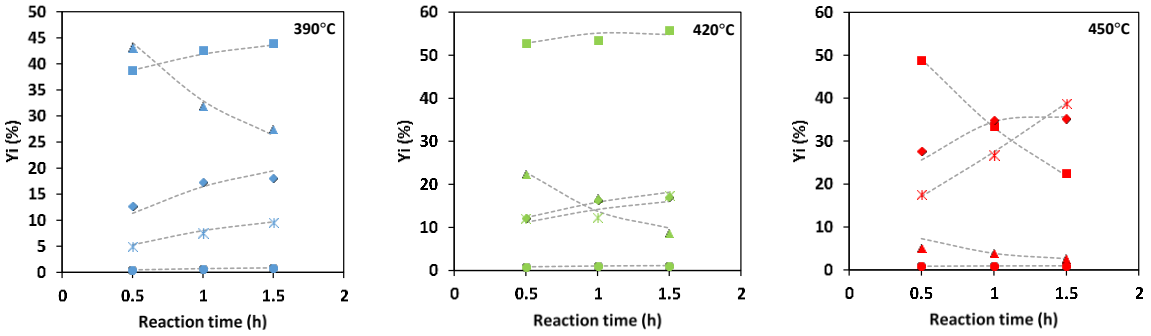

Figure A 8 Predicted (dashed lines) and experimental (symbols) yields of (▲) VGO; (■) distillate; (◆) naphtha; (*) gases; and (●) coke versus reaction time for hydrocracking of vacuum gas oil over mixed catalysts.

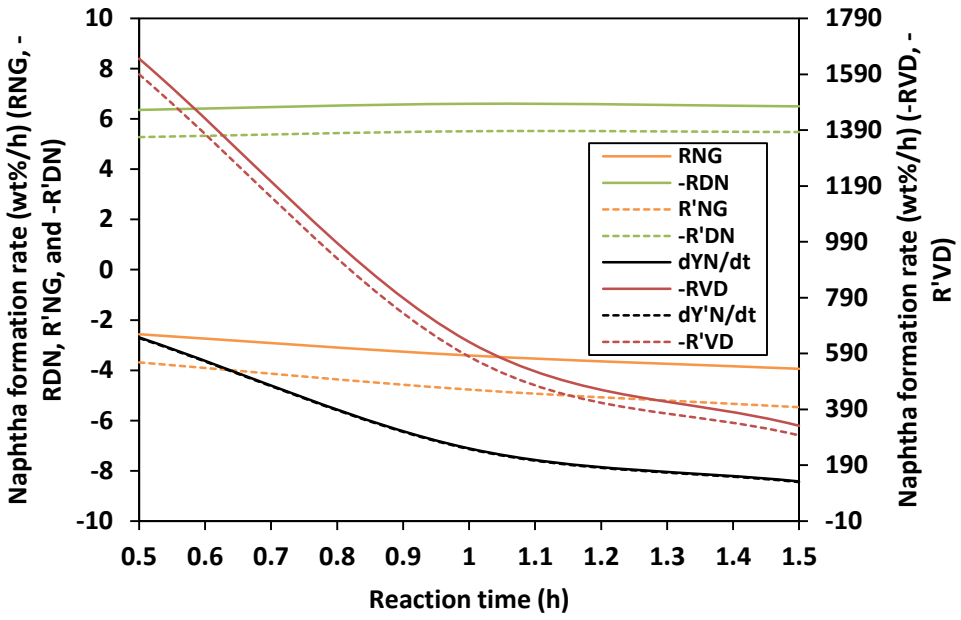

Figure A 9 Naphtha formation rate versus reaction time of hydrocracking over standalone supported as well as mixed-phase catalysts at 420°C. (where Rji and R'ji refers to the rate of i formation from j for supported and mixed-catalysts systems, respectively).

Table A 1 Comparison of reported kinetic studies in the literature of hydrocracking of VGO.

n-Lump	Mode/Catalyst	Reactions involved	Activation energy (kJ/mol)	Pre-exponential factor (h^{-1} or $m^3\ hr^{-1}\ m^3\ cat^{-1}$)	Reference
four	continuous/RK-MNi (commercial zeolite-based catalyst)	VGO → distillate	46.78	6.82E+3	Faraji *et al.* 2017 [185]
		VGO → naphtha	108.4	2.44E+07	
		VGO → gases	70.33	7.36E+02	
		distillate → naphtha	92.17	1.52E+03	
		distillate → gases	107.4	2.48E+07	
		naphtha→gases	174.6	7.43E+02	
five	batch/supported catalyst (W-Ni/Al_2O_3-SiO_2) + Co 2-ethyl-hexanoate	VGO → distillate	6.180	0.657	Bdwi *et al.* 2017 [24]
		VGO → naphtha	440.7	2.167	
		VGO → gases	59.16	2.400	
		VGO → coke	10.41	0.165	
		distillate → naphtha	253.6	0.005	
		naphtha→gases	375.1	0.002	
five	batch/supported catalyst (W-Ni/Al_2O_3-SiO_2) + Ni-*p*-*tert*-butylcalix[4]arene	VGO → distillate	239.8	3.057	Present study
		VGO → naphtha	82.32	1.474	
		VGO → gases	192.0	1.199	
		VGO → coke	74.67	0.086	
		distillate → naphtha	303.5	0.100	
		naphtha → gases	103.8	0.301	

Table A 2 Estimated kinetic parameters for hydrocracking of VGO feed over the supported catalyst and mixed (supported+dispersed) catalysts after modifying the reaction scheme (Figure A 6).

Parameter	Standalone supported catalyst		Mixed catalysts	
	E_{ij} (kcal/mol)	k_{ij} (h^{-1})	E_{ij} (kcal/mol)	k_{ij} (h^{-1})
k_{VD}	61.298	2.371	57.798	2.947
k_{VN}	4.44e-14	0.972	18.491	1.283
k_{VG}	2.31e-3	1.278	41.947	1.419
k_{VC}	25.286	0.159	37.986	0.114
k_{DN}	84.016	0.115	78.514	0.084
k_{DG}	212.711	5.47E-05	13.575	0.001
k_{NG}	68.785	0.196	60.558	0.101

where subscripts V, D, N, G, and C stand for VGO, distillate, naphtha, gases, and coke, respectively.

NOMENCLATURE

E_{ij}	the apparent activation energy for the j formation reaction from i, kcal/mol
R_{ij}	the rate of the i formation reaction from j, wt%/h^{-1}
T_m	centering temperature, K
W_i	the weight of pseudo-component i, g
W_p	the weight of the total product, g
Y_i	the yield of pseudo-component i, $Y_i\ (wt\%) = \frac{W_i}{W_p} \times 100$, wt%
k_{ij_0}	pre-exponential factor for j formation reaction from i, h^{-1}
k_{ij}	the specific rate of j formation reaction from i, wt%$^{-n}$·h^{-1} where n depends on the reaction order
I	dimensionless catalytic activity parameter, $I = \frac{Y_N Y_D}{Y_V Y_C Y_G} \times 100$
t	reaction time, h
$\dot{S}_{i/jk}$	instantaneous selectivity to the i product, $\dot{S}_{i/jk} = \frac{r_i}{r_j + r_k}$
r_i	the overall reaction rate of i formation, wt%/h

Subscripts

V	VGO
D	distillate
N	naphtha
G	gases
C	coke

Superscripts

apostrophe (')	mixed catalysts
dot accent ($\dot{}$)	instantaneous parameter

REFERENCES

1. U.S. Energy Information Administration: Annual Energy Outlook 2018 with projections to 2050. , Washington, D.C. (2018)

2. Gary, J.H., Handwerk, G.E., Kaiser, M.J.: Petroleum Refining: Technology and Economics. CRC Press (2007)

3. Kandiyoti, R.: Hydroprocessing of heavy oils and residua. J. Energy Inst. 81, 184–184 (2008)

4. Angeles, M.J., Leyva, C., Ancheyta, J., Ramírez, S.: A review of experimental procedures for heavy oil hydrocracking with dispersed catalyst. Catal. Today. 220–222, 274–294 (2014)

5. Sahu, R., Song, B.J., Im, J.S., Jeon, Y.P., Lee, C.W.: A review of recent advances in catalytic hydrocracking of heavy residues. J. Ind. Eng. Chem. 27, 12–24 (2015)

6. Zhang, S., Liu, D., Deng, W., Que, G.: A review of slurry-phase hydrocracking heavy oil technology. Energy and Fuels. 21, 3057–3062 (2007)

7. Rana, M.S., Sámano, V., Ancheyta, J., Diaz, J.A.I.: A review of recent advances on process technologies for upgrading of heavy oils and residua. Fuel. 86, 1216–1231 (2007)

8. Ancheyta, J.: Modeling of Processes and Reactors for Upgrading of Heavy Petroleum. (2013)

9. Furimsky, E.: Catalysts for Upgrading Heavy Petroleum Feeds. (2007)

10. Bellussi, G., Rispoli, G., Landoni, A., Millini, R., Molinari, D., Montanari, E., Moscotti, D., Pollesel, P.: Hydroconversion of heavy residues in slurry reactors: Developments and perspectives. J. Catal. 308, 189–200 (2013)

11. Todić, B., Ordomsky, V. V., Nikačević, N.M., Khodakov, A.Y., Bukur, D.B.: Opportunities for intensification of Fischer-Tropsch synthesis through reduced formation of methane over cobalt catalysts in microreactors. Catal. Sci. Technol. 5, 1400–1411 (2015)

12. Nguyen, M.T., Nguyen, N.T., Cho, J., Park, C., Park, S., Jung, J., Lee, C.W.: A review on the oil-soluble dispersed catalyst for slurry-phase hydrocracking of heavy oil. J. Ind. Eng. Chem. 43, 1–12 (2016)

13. Quitian, A., Ancheyta, J.: Experimental Methods for Developing Kinetic Models for Hydrocracking Reactions with Slurry-Phase Catalyst Using Batch Reactors. Energy and Fuels. 30, 4419–4437 (2016)

14. Al-Marshed, A., Hart, A., Leeke, G., Greaves, M., Wood, J.: Effectiveness of

Different Transition Metal Dispersed Catalysts for In Situ Heavy Oil Upgrading. Ind. Eng. Chem. Res. 54, 10645–10655 (2015)

15. Bhattacharyya, A., Bricker, M.L., Mezza, B.J., Bauer, L.J.: Process for using iron oxide and alumina catalyst with large particle diameter for slurry hydrocracking, (2011)

16. Sharypov, V.I., Kuznetsov, B.N., Beregovtsova, N.G., Reshetnikov, O.L., Baryshnikov, S. V: Modification of iron ore catalysts for lignite hydrogenation and hydrocracking of coal-derived liquids. Fuel. 75, 39–42 (1996)

17. Nguyen-Huy, C., Kweon, H., Kim, H., Kim, D.K., Kim, D.W., Oh, S.H., Shin, E.W.: Slurry-phase hydrocracking of vacuum residue with a disposable red mud catalyst. Appl. Catal. A Gen. 447–448, 186–192 (2012)

18. Matsumura, A., Kondo, T., Sato, S., Saito, I., De Souza, W.F.: Hydrocracking Brazilian Marlim vacuum residue with natural limonite. Part 1 : Catalytic activity of natural limonite. Fuel. 84, 411–416 (2005)

19. Krasuk Julio H., Silva Fernando J., Galiasso Roberto E., S.A.: Process for hydroconversion and upgrading of heavy crudes of high metal and asphaltene content, (1989)

20. Du, H., Li, M., Liu, D., Ren, Y., Duan, Y.: Slurry-phase hydrocracking of heavy oil and model reactant: effect of dispersed Mo catalyst. Appl. Petrochemical Res. 5, 89–98 (2015)

21. Ortiz-Moreno, H., Ramírez, J., Cuevas, R., Marroquín, G., Ancheyta, J.: Heavy oil upgrading at moderate pressure using dispersed catalysts: Effects of temperature, pressure and catalytic precursor. Fuel. 100, 186–192 (2012)

22. Liu, D., Li, M., Deng, W., Que, G.: Reactivity and composition of dispersed NI catalyst for slurry-phase residue hydrocracking. Energy and Fuels. 24, 1958–1962 (2010)

23. Luo, H., Deng, W., Gao, J., Fan, W., Que, G.: Dispersion of water-soluble catalyst and its influence on the slurry-phase hydrocracking of residue. Energy and Fuels. 25, 1161–1167 (2011)

24. Bdwi, E.A.S., Ali, S.A., Quddus, M.R., Al-Bogami, S.A., Razzak, S.A., Hossain, M.M.: Kinetics of Promotional Effects of Oil-Soluble Dispersed Metal (Mo, Co, and Fe) Catalysts on Slurry Phase Hydrocracking of Vacuum Gas Oil. Energy & Fuels. 31, 3132–3142 (2017)

25. Ortiz-Moreno, H., Ramírez, J., Sanchez-Minero, F., Cuevas, R., Ancheyta, J.: Hydrocracking of Maya crude oil in a slurry-phase batch reactor. II. Effect of catalyst load. Fuel. 130, 263–272 (2014)

26. Martinez-Grimaldo, H., Ortiz-Moreno, H., Sanchez-Minero, F., Ramírez, J., Cuevas-Garcia, R., Ancheyta-Juarez, J.: Hydrocracking of Maya crude oil in a

slurry-phase reactor. I. Effect of reaction temperature. Catal. Today. 220–222, 295–300 (2014)

27. Liu, C., Zhou, J., Que, G., Liang, W., Zhu, Y.: Hydrocracking of Gudao residue with dispersed-phase Mo catalyst. Fuel. 73, 1544–1550 (1994)

28. Petrukhina, N.N., Sizova, I.A., Maksimov, A.L.: Nickel–molybdenum and cobalt–molybdenum sulfide hydrogenation and hydrodesulphurization catalysts synthesized in situ from bimetallic precursors. Catal. Ind. 9, 247–256 (2017)

29. Tian, K.P., Mohamed, A.R., Bhatia, S.: Catalytic upgrading of petroleum residual oil by hydrotreating catalysts: a comparison between dispersed and supported catalysts. Fuel. 77, 1221–1227 (1998)

30. Jian, C., Yihong, L., Yunhua, L., Guohe, Q.: Hydrocracking of Gudao Residual Oil with Dispersed Catalysts Using Supercritical Water-Syngas as a Hydrogen Source. Pet. Sci. Technol. 23, 1453–1462 (2005)

31. Afanasiev, P.: The influence of reducing and sulfiding conditions on the properties of unsupported MoS2-based catalysts. J. Catal. 269, 269–280 (2010)

32. Al-Rashidy, A.H.: Hydrocracking of Vacuum Gas Oil Using Fe, Ni and Mo Based Dispersed Catalyst, (2015)

33. Bagheri, S.R., Gray, M.R., Shaw, J.M., McCaffrey, W.C.: In situ observation of mesophase formation and coalescence in catalytic hydroconversion of vacuum residue using a stirred hot-stage reactor. Energy and Fuels. 26, 3167–3178 (2012)

34. Zhang, S., Deng, W., Luo, H., Lui, D., Que, G.: Slurry-phase residue hydrocracking with dispersed nickel catalyst. Energy and Fuels. 22, 3583–3586 (2008)

35. Furimsky, E.: Catalysts for Upgrading Heavy Petroleum Feeds. Elsevier (2007)

36. Shen, R., Liu, C., Que, G.: Hydrocracking of Liaohe vacuum residue with bimetallic oil-soluble catalysts. ACS Div. Fuel Chem. Prepr. 43, 481–483 (1998)

37. Watanabe, I., Otake, M., Yoshimoto, M., Sakanishi, K., Korai, Y., Mochida, I.: Behaviors of oil-soluble molybdenum complexes to form very fine MoS2 particles in vacuum residue. Fuel. 81, 1515–1520 (2002)

38. Du, H., Liu, D., Li, M., Wu, P., Yang, Y.: Effects of the temperature and initial hydrogen pressure on the isomerization reaction in heavy oil slurry-phase hydrocracking. Energy and Fuels. 29, 626–633 (2015)

39. Rezaei, H., Ardakani, S.J., Smith, K.J.: Comparison of MoS2 catalysts prepared from mo-micelle and mo-octoate precursors for hydroconversion of cold lake vacuum residue: Catalyst activity, coke properties and catalyst recycle. Energy and Fuels. 26, 2768–2778 (2012)

40. Rezaei, H., Ardakani, S.J., Smith, K.J.: Study of MoS2 catalyst recycle in slurry-

phase residue hydroconversion. In: Energy and Fuels. pp. 6540–6550. American Chemical Society (2012)

41. Rezaei, H., Liu, X., Ardakani, S.J., Smith, K.J., Bricker, M.: A study of Cold Lake Vacuum Residue hydroconversion in batch and semi-batch reactors using unsupported MoS2 catalysts. Catal. Today. 150, 244–254 (2010)

42. Kim, Sung Ho; Kim, Ki Duk; Lee, Y.K.: Effects of dispersed MoS2 catalysts and reaction conditions on slurry phase hydrocracking of vacuum residue. J. Catal. 347, 127–137 (2017)

43. Bearden, R., Aldridge, C.L.: Hydroconversion of Heavy Hydrocarbons, (1979)

44. Dabkowski, M.J., Shih, S.S., Albinson, K.R.: Upgrading of petroleum residue with dispersed additives. Presented at the (1991)

45. Panariti, N., Del Bianco, A., Del Piero, G., Marchionna, M.: Petroleum residue upgrading with dispersed catalysts. Part 1. Catalysts activity and selectivity. Appl. Catal. A Gen. 204, 203–213 (2000)

46. Panariti, N., Del Bianco, A., Del Piero, G., Marchionna, M., Carniti, P.: Petroleum residue upgrading with dispersed catalysts. Part 2. Effect of operating conditions. Appl. Catal. A Gen. 204, 215–222 (2000)

47. Nguyen, T.S., Tayakout-Fayolle, M., Lacroix, M., Gotteland, D., Aouine, M., Bacaud, R., Afanasiev, P., Geantet, C.: Promotion effects with dispersed catalysts for residue slurry hydroconversion. Fuel. 160, 50–56 (2015)

48. Shi, B., Que, G.: Hydrocracking of LiaoHe Vacuum Residue with Oil-Soluble Co-Ni Bimetallic Catalysts and Hydrogen Donor. ACS Div. Fuel Chem. Prepr. 48, 722–724 (2003)

49. Jeon, S.G., Na, J.G., Ko, C.H., Lee, K.B., Rho, N.S., Park, S. Bin: A new approach for preparation of oil-soluble bimetallic dispersed catalyst from layered ammonium nickel molybdate. Mater. Sci. Eng. B Solid-State Mater. Adv. Technol. 176, 606–610 (2011)

50. Jeon, S.G., Na, J.G., Ko, C.H., Yi, K.B., Rho, N.S., Park, S. Bin: Preparation and application of an oil-soluble CoMo bimetallic catalyst for the hydrocracking of oil sands bitumen. Energy and Fuels. 25, 4256–4260 (2011)

51. Harris, S.: The relation between electronic trends and the promoter effect on catalytic activity of hydrodesulfurization catalysts. Polyhedron. 5, 151–155 (1986)

52. Zhou Bing, Zhou Zhenhua, W.Z.: Hydrocarbon-Soluble, Bimetallic Catalyst Precursors and Methods for Making Same, (2010)

53. Oguzie, E.E., Onuoha, G.N., Onuchukwu, A.I.: Inhibitory mechanism of mild steel corrosion in 2 M sulphuric acid solution by methylene blue dye. Mater. Chem. Phys. 89, 305–311 (2005)

54. Gutsche, C.D., Iqbal, M., Stewart, D.: Calixarenes. 18. Synthesis Procedures for p -tert -Butylcalix[4]arene. J. Org. Chem. 51, 742–745 (1986)

55. Gutsche, C.D.: Calixarenes : an introduction. RSC Pub (2008)

56. Homden, D.M., Redshaw, C.: The use of calixarenes in metal-based catalysis. Chem. Rev. 108, 5086–5130 (2008)

57. Vinet, L., Zhedanov, A.: Calixarenes 50th Anniversary: Commemorative Issue. Springer (1994)

58. Casnati, A., De Mendoza, J., Reinhoudt, D.N., Ungaro, R.: Determination of Calixarene Conformations by Means of NMR Techniques. Springer Netherlands, Dordrecht (1999)

59. Gutsche, C.D., Dhawan, B., No, K.H., Muthukrishnan, R.: Calixarenes. 4. The Synthesis, Characterization, and Properties of the Calixarenes from p-tert-Butylphenol. J. Am. Chem. Soc. 103, 3782–3792 (1981)

60. Kelloff, G., Huebner, R.J., Lee, Y.K., Toni, R., Gilden, R.: Hamster-tropic sarcomagenic and nonsarcomagenic viruses derived from hamster tumors induced by the Gross pseudotype of Moloney sarcoma virus. Proc. Natl. Acad. Sci. U. S. A. 65, 310–317 (1970)

61. Lenthall, J.T., Steed, J.W.: Organometallic cavitands: Cation-π interactions and anion binding via π-metallation, (2007)

62. Floriani, C., Floriani-Moro, R.: The M-C bond functionalities bonded to an oxo-surface modeled by Calix[4]arenes, (2001)

63. Marcos, P.M., Ascenso, J.R., Segurado, M.A.P., Pereira, J.L.C.: p-tert-butyldihomooxacalix[4]arene/p-tert-butylcalix[4]arene: Transition and heavy metal cation extraction and transport studies by ketone and ester derivatives. J. Incl. Phenom. 42, 281–288 (2002)

64. Śliwa, W.: Calixarene complexes with transition metal ions, (2005)

65. Jose, P., Menon, S.: Lower-rim substituted calixarenes and their applications, (2007)

66. Dumazet-Bonnamour, I., Halouani, H., Oueslati, F., Lamartine, R.: Calixarenes for metal cations extraction. Comptes Rendus Chim. 8, 881–891 (2005)

67. Yordanov, A.T., Max Roundhill, D., Mague, J.T.: Extraction selectivities of lower rim substituted calix[4]arene hosts induced by variations in the upper rim substituents. Inorganica Chim. Acta. 250, 295–302 (1996)

68. Yordanov, A.T., Mague, J.T., Max Roundhill, D.: Solvent extraction of divalent palladium and platinum from aqueous solutions of their chloro complexes using an N,N-dimethyldithiocarbamoylethoxy substituted calix[4]arene. Inorganica Chim. Acta. 240, 441–446 (1995)

69. Malone, J.F., Marrs, D.J., McKervey, M.A., O'Hagan, P., Thompson, N., Walker, A., Arnaud-Neu, F., Mauprivez, O., Schwing-Weill, M.J., Dozol, J.F., Rouquette, H., Simon, N.: Calix[n]arene phosphine oxides. A new series of cation receptors for extraction of europium, thorium, plutonium and americium in nuclear waste treatment. J. Chem. Soc. Chem. Commun. 0, 2151–2153 (1995)

70. Arnaud-Neu, F., Böhmer, V., Dozol, J.F., Grüttner, C., Jakobi, R.A., Kraft, D., Mauprivez, O., Rouquette, H., Schwing-Weill, M.J., Simon, N., Vogt, W.: Calixarenes with diphenylphosphoryl acetamide functions at the upper rim. A new class of highly efficient extractants for lanthanides and actinides. J. Chem. Soc. Perkin Trans. 2. 6, 1175–1182 (1996)

71. Akdoğan, A., Deniz, M., Cebecioğlu, S., Şen, A., Deligöz, H.: Liquid-liquid extraction of transition metal cations by nine new azo derivatives calix[n]arene. Sep. Sci. Technol. 37, 973–980 (2002)

72. Enright, G.D., Udachin, K.A., Moudrakovski, I.L., Ripmeester, J.A.: Thermally programmable gas storage and release in single crystals of an organic van der Waals host. J. Am. Chem. Soc. 125, 9896–9897 (2003)

73. Arduini, A., Cantoni, M., Graviani, E., Pochini, A., Secchi, A., Sicuri, A.R., Ungaro, R., Vincenti, M.: Gas-phase complexation of neutral molecules by upper rim bridged calix[4]arenes. Tetrahedron. 51, 599–606 (1995)

74. Atwood, J.L., Barbour, L.J., Jerga, A., Schottel, B.L.: Guest transport in a nonporous organic solid via dynamic van der Waals cooperativity. Science (80-.). 298, 1000–1002 (2002)

75. Liu, D., Cui, W., Zhang, S., Que, G.: Role of dispersed Ni catalyst sulfurization in hydrocracking of residue from Karamay. Energy and Fuels. 22, 4165–4169 (2008)

76. Hontama, N., Inokuchi, Y., Ebata, T., Dedonder-Lardeux, C., Jouvet, C., Xantheas, S.S.: Structure of the calix[4]arene-(H2O) Cluster: The world's smallest cup of water. J. Phys. Chem. A. 114, 2967–2972 (2010)

77. Ozmen, M., Ozbek, Z., Buyukcelebi, S., Bayrakci, M., Ertul, S., Ersoz, M., Capan, R.: Fabrication of Langmuir-Blodgett thin films of calix[4]arenes and their gas sensing properties: Investigation of upper rim para substituent effect. Sensors Actuators, B Chem. 190, 502–511 (2014)

78. Kaneko, S., Inokuchi, Y., Ebata, T., Aprà, E., Xantheas, S.S.: Laser spectroscopic and theoretical studies of encapsulation complexes of calix[4]arene. J. Phys. Chem. A. 115, 10846–10853 (2011)

79. Horvat, G., Stilinović, V., Hrenar, T., Kaitner, B., Frkanec, L., Tomišić, V.: An integrated approach (thermodynamic, structural, and computational) to the study of complexation of alkali-metal cations by a lower-rim calix[4]arene amide derivative in acetonitrile. Inorg. Chem. 51, 6264–6278 (2012)

80. Özbek, C., Okur, S., Mermer, Ö., Kurt, M., Sayin, S., Yilmaz, M.: Effect of Fe doping on the CO gas sensing of functional calixarene molecules measured with quartz crystal microbalance technique. Sensors Actuators, B Chem. 215, 464–470 (2015)

81. Udachin, K.A., Moudrakovski, I.L., Enright, G.D., Ratcliffe, C.I., Ripmeester, J.A.: Loading-dependent structures of CO2in the flexible molecular van der Waals host p-tert-butylcalix[4]arene with 1 : 1 and 2 : 1 guest-host stoichiometries. Phys. Chem. Chem. Phys. 10, 4636–4643 (2008)

82. Thallapally, P.K., Wirsig, T.B., Barbour, L.J., Atwood, J.L.: Crystal engineering of nonporous organic solids for methane sorption. Chem. Commun. 0, 4420–4422 (2005)

83. Atwood, J.L., Barbour, L.J., Jerga, A.: A new type of material for the recovery of hydrogen from gas mixtures. Angew. Chemie - Int. Ed. 43, 2948–2950 (2004)

84. Hontama, N., Inokuchi, Y., Ebata, T., Dedonder-Lardeux, C., Jouvet, C., Xantheas, S.S.: Structure of the calix[4]arene-(H2O) Cluster: The world's smallest cup of water. J. Phys. Chem. A. 114, 2967–2972 (2010)

85. Sanz, S., Ferreira, K., McIntosh, R.D., Dalgarno, S.J., Brechin, E.K.: Calix[4]arene-supported FeIII2LnIII2 clusters. Chem. Commun. 47, 9042–9044 (2011)

86. Karotsis, G., Kennedy, S., Dalgarno, S.J., Brechin, E.K.: Calixarene supported enneanuclear Cu(ii) clusters. Chem. Commun. 46, 3884–3886 (2010)

87. Redshaw, C., Rowan, M.A., Warford, L., Homden, D.M., Arbaoui, A., Elsegood, M.R.J., Dale, S.H., Yamato, T., Casas, C.P., Matsui, S., Matsuura, S.: Oxo- and imidovanadium complexes incorporating methylene- and dimethyleneoxa-bridged calix[3]- and -[4]arenes: Synthesis, structures and ethylene polymerisation catalysis. Chem. - A Eur. J. 13, 1090–1107 (2007)

88. Zanotti-Gerosa, A., Solari, E., Giannini, L., Floriani, C., Re, N., Chiesi-Villa, A., Rizzoli, C.: Titanium-carbon functionalities on an oxo surface defined by a calix [4] arene moiety and its redox chemistry. Inorganica Chim. Acta. 270, 298–311 (1998)

89. Chen, Y., Zhang, Y., Shen, Z., Kou, R., Chen, L.: Ethylene polymerization catalyzed by rare earth calixarene catalytic system. Eur. Polym. J. 37, 1181–1184 (2001)

90. Dieleman, C., Steyer, S., Jeunesse, C., Matt, D.: Diphosphines based on an inherently chiral calix[4]arene scaffold: synthesis and use in enantioselective catalysis. J. Chem. Soc. Dalt. Trans. 0, 2508–2517 (2001)

91. Quintard, A., Darbost, U., Vocanson, F., Pellet-Rostaing, S., Lemaire, M.: Synthesis of new calix[4]arene based chiral ligands bearing β-amino alcohol groups and their application in asymmetric transfer hydrogenation. Tetrahedron: Asymmetry. 18, 1926–1933 (2007)

92. Marson, A., Freixa, Z., Kamer, P.C.J., Van Leeuwen, P.W.N.M.: Chiral

calix[4]arene-based diphosphites as ligands in the asymmetric hydrogenation of prochiral olefins. Eur. J. Inorg. Chem. 18, 4587–4591 (2007)

93. Hoppe, E., Limberg, C.: Oxovanadium(V) tetrathiacalix[4]arene complexes and their activity as oxidation catalysts. Chem. - A Eur. J. 13, 7006–7016 (2007)

94. Hoppe, E., Limberg, C., Ziemer, B.: Mono- and dinuclear oxovanadium(V)calixarene complexes and their activity as oxidation catalysts. Inorg. Chem. 45, 8308–8317 (2006)

95. Limberg, C.: Calixarene-based oxovanadium complexes as molecular models for catalytically active surface species and homogeneous catalysts, (2007)

96. Parlevliet, F.J., Kiener, C., Fraanje, J., Goubitz, K., Lutz, M., Spek, A.L., Kamer, P.C.J., van Leeuwen, P.W.N.M.: Calix[4]arene based monophosphites, identification of three conformations and their use in the rhodium-catalysed hydroformylation of 1-octene. J. Chem. Soc. Dalt. Trans. 0, 1113–1122 (2000)

97. Steyer, S., Jeunesse, C., Matt, D., Welter, R., Wesolek, M.: Heterofunctionalised phosphites built on a calix[4]arene scaffold and their use in 1-octene hydroformylation. Formation of 12-membered P,O-chelate rings. J. Chem. Soc. Dalt. Trans. 0, 4264–4274 (2002)

98. Shimizu, S., Suzuki, T., Shirakawa, S., Sasaki, Y., Hirai, C.: Water-Soluble Calixarenes as New Inverse Phase-Transfer Catalysts. Their Scope in Aqueous Biphasic Alkylations and Mechanistic Implications. Adv. Synth. Catal. 344, 370–378 (2002)

99. Sémeril, D., Matt, D., Toupet, L.: Highly regioselective hydroformylation with hemispherical chelators. Chem. - A Eur. J. 14, 7144–7155 (2008)

100. Sémeril, D., Jeunesse, C., Matt, D., Toupet, L.: Regioselectivity with hemispherical chelators: Increasing the catalytic efficiency of complexes of diphosphanes with large bite angles. Angew. Chemie - Int. Ed. 45, 5810–5814 (2006)

101. Bühl, M., Terstegen, F., Löffler, F., Meynhardt, B., Kierse, S., Müller, M., Näther, C., Lüning, U.: On the Mechanism and Stereoselectivity of the Copper(I)-Catalyzed Cyclopropanation of Olefins − A Combined Experimental and Density Functional Study. European J. Org. Chem. 2001, 2151–2160 (2001)

102. Palermo, A., Solovyov, A., Ertler, D., Okrut, A., Gates, B.C., Katz, A.: Dialing in single-site reactivity of a supported calixarene-protected tetrairidium cluster catalyst. Chem. Sci. 8, 4951–4960 (2017)

103. Fujita, J., Ohnishi, Y., Ochiai, Y., Matsui, S.: Ultrahigh resolution of calixarene negative resist in electron beam lithography. Appl. Phys. Lett. 68, 1297 (1995)

104. Novembre, A., Liu, S.: Chemistry and processing of resists for nanolithography. Woodhead Publishing Limited (2013)

105. Deligöz, H., Karakuş, Ö.Ö., Çilgi, G.K.: A brief review on the thermal behaviors of calixarene-azocalixarene derivatives and their complexes. J. Macromol. Sci. Part A Pure Appl. Chem. 49, 259–274 (2012)

106. Kůtek, F.: Contributions to the chemistry of the rarer elements XXXIX. Addition compounds of N, N-dimethylformamide and N, N-dimethylacetamide with scandium perchlorate (translation). Collect. Czechoslov. Chem. Commun. 32, 3767–3770 (1967)

107. Krishnamurthy, S.S., Soundararajan, S.: Dimethyl and Diphenyl Formamide Complexes of Lanthanide Perchlorates. Can. J. Chem. 47, 995 (1969)

108. Bünzli, J.C.G., Froidevaux, P., Harrowfield, J.M.: Photophysical Properties of Lanthanide Dinuclear Complexes with p-tert-Butylcalix[8]arene. Inorg. Chem. 32, 3306–3311 (1993)

109. Kennepohl, D., Sanford, E.: Conversion of Athabasca Bitumen with Dispersed and Supported Mo-Based Catalysts as a Function of Dispersed Catalyst Concentration. Energy & Fuels. 10, 229–234 (1996)

110. Nguyen, T.S., Tayakout-Fayolle, M., Ropars, M., Geantet, C.: Hydroconversion of an atmospheric residue with a dispersed catalyst in a batch reactor: Kinetic modeling including vapor-liquid equilibrium. Chem. Eng. Sci. 94, 214–223 (2013)

111. Li, C., Meng, H., Yang, T., Li, J., Qin, Y., Huang, Y., Deng, W.: Study on catalytic performance of oil-soluble iron-nickel bimetallic catalyst in coal/oil co-processing. Fuel. 219, 30–36 (2018)

112. Li, C., Yang, T., Deng, W., Zhang, H., Cui, M.: Effects of Iron(III) Dodecylbenzenesulfonate on the Slurry-Phase Hydrocracking of Venezuela Fuel Oil with an Oil-Soluble Mo Catalyst. Energy & Fuels. 30, 4710–4716 (2016)

113. Inukai, Y.: Hydroliquefaction of Illinois No. 6 coal with petroleum atmospheric residue using oil-soluble molybdenum catalyst. Fuel Process. Technol. 43, 157–167 (1995)

114. Rankel, L.A.: Hydrocracking vacuum resid with NiW bifunctional slurry catalysts. Fuel Process. Technol. 37, 185–202 (1994)

115. Jeong, H., Lee, Y.: Comparison of Unsupported WS2 and MoS2 Catalysts for Slurry Phase Hydrocracking of Vacuum Residue. Appl. Catal. A Gen. 572, 90–96 (2019)

116. Cyr, T., Lewkowicz, L., Ozum, B., Lott, R.K., Lee, L.-K.: Hydrocracking process involving colloidal catalyst formed in situ, (1996)

117. Chianelli, R.R., Siadati, M.H., De la Rosa, M.P., Berhault, G., Wilcoxon, J.P., Bearden, R., Abrams, B.L.: Catalytic Properties of Single Layers of Transition Metal Sulfide Catalytic Materials. Catal. Rev. 48, 1–41 (2006)

118. Silvy, R.P., Grange, P., Delannay, F., Delmon, B.: Influence of the nature of the

activating molecules on the catalytic activity of cobalt-molybdenum/alumina catalysts. Appl. Catal. 46, 113–129 (1989)

119. Stanislaus, A.: Handbook of Spent Hydroprocessing Catalysts. Elsevier (2016)

120. Petit, C., Mauge, F., Lavalley, J.C.: Acidity induced by H2S adsorption on unpromoted and promoted sulfided catalysts. Stud. Surf. Sci. Catal. 106, 157–166 (1997)

121. Besenbacher, F., Brorson, M., Clausen, B.S., Helveg, S., Hinnemann, B., Kibsgaard, J., Lauritsen, J. V., Moses, P.G., Nørskov, J.K., Topsøe, H.: Recent STM, DFT and HAADF-STEM studies of sulfide-based hydrotreating catalysts: Insight into mechanistic, structural and particle size effects. Catal. Today. 130, 86–96 (2008)

122. Topsøe, H.: The role of Co-Mo-S type structures in hydrotreating catalysts. Appl. Catal. A Gen. 322, 3–8 (2007)

123. Brorson, M., Carlsson, A., Topsøe, H.: The morphology of MoS2, WS2, Co-Mo-S, Ni-Mo-S and Ni-W-S nanoclusters in hydrodesulfurization catalysts revealed by HAADF-STEM. Catal. Today. 123, 31–36 (2007)

124. Lauritsen, J. V., Helveg, S., Lægsgaard, E., Stensgaard, I., Topsøe, H., Besenbacher, F.: Atomic-Scale Structure of Co–Mo–S Nanoclusters in Hydrotreating Catalysts. J. Catal. 197, 1–5 (2001)

125. Daage, M., Chianelli, R.R.: Structure-function relations in molybdenum sulfide catalysts: The “Rim-Edge” model. J. Catal. 149, 414–427 (1994)

126. Ghosh, U., Kulkarni, K., A.D.Kulkarni, P.L.Chaudhari: Review – Hydrocracking using Different Catalysts. Chem. Process Eng. Res. 34, 51–56 (2015)

127. Majka, M., Tomaszewicz, G., Mianowski, A.: Experimental study on the coal tar hydrocracking process over different catalysts. J. Energy Inst. 91, 1164–1176 (2018)

128. Elizalde, I., Mederos, F.S., Mena-Cervantes, V.Y., Hernández-Altamirano, R., Muñoz, J.A.D.: Dynamic modeling of adiabatic reactor for hydrocracking of VGO by using of the continuous lumping approach. Fuel Process. Technol. 152, 200–206 (2016)

129. Yui, S.M., Sanford, E.C.: Mild Hydrocracking of Bitumen-Derived Coker and Hydrocracker Heavy Gas Oils: Kinetics, Product Yields, and Product Properties. Ind. Eng. Chem. Res. 28, 1278–1284 (1989)

130. Valavarasu, G., Bhaskar, M., Sairam, B., Balaraman, K.S., Balu, K.: A four lump kinetic model for the simulation of the hydrocracking process. Pet. Sci. Technol. 23, 1323–1332 (2005)

131. Elkilani, A., Fahim, M.: Six-Lump Hydrocracking Model for Maximizing Aviation Turbine Kerosene. Pet. Sci. Technol. 33, 237–244 (2015)

132. Sadighi, S., Ahmad, A., Masoudian, S.K.: Effect of lump partitioning on the accuracy of a commercivaalcuu m gas oil hydrocracking model. Int. J. Chem. React. Eng. 10, (2012)

133. Sadighi, S., Ahmad, A.: An optimisation approach for increasing the profit of a commercial VGO hydrocracking process. Can. J. Chem. Eng. 91, 1077–1091 (2013)

134. Callejas, M.A., Martínez, M.T.: Hydrocracking of a Maya residue. Kinetics and product yield distributions. Ind. Eng. Chem. Res. 38, 3285–3289 (1999)

135. Ali, M.A., Tatsumi, T., Masuda, T.: Development of heavy oil hydrocracking catalysts using amorphous silica-alumina and zeolites as catalyst supports. Appl. Catal. A Gen. 233, 77–90 (2002)

136. Sadighi, S., Ahmad, A., Rashidzadeh, M.: 4-Lump kinetic model for vacuum gas oil hydrocracker involving hydrogen consumption. Korean J. Chem. Eng. 27, 1099–1108 (2010)

137. Puron, H., Arcelus-Arrillaga, P., Chin, K.K., Pinilla, J.L., Fidalgo, B., Millan, M.: Kinetic analysis of vacuum residue hydrocracking in early reaction stages. Fuel. 117, 408–414 (2014)

138. De Almeida, R.M., Guirardello, R.: Hydroconversion kinetics of Marlim vacuum residue. Catal. Today. 109, 104–111 (2005)

139. Sánchez, S., Ancheyta, J.: Effect of pressure on the kinetics of moderate hydrocracking of Maya crude oil. Energy and Fuels. 21, 653–661 (2007)

140. Sadighi, S.: Modeling a vacuum gas oil hydrocracking reactor using axialdispersion lumped Kinetics. Pet. Coal. 55, 156–168 (2013)

141. Hassanzadeh, H., Abedi, J.: Modelling and parameter estimation of ultra-dispersed in situ catalytic upgrading experiments in a batch reactor. Fuel. 89, 2822–2828 (2010)

142. Asaee, S.D.S., Vafajoo, L., Khorasheh, F.: A new approach to estimate parameters of a lumped kinetic model for hydroconversion of heavy residue. Fuel. 134, 343–353 (2014)

143. Cui, G., Wang, J., Fan, H., Sun, X., Jiang, Y., Wang, S., Liu, D., Gui, J.: Towards understanding the microstructures and hydrocracking performance of sulfided Ni-W catalysts: Effect of metal loading. Fuel Process. Technol. 92, 2320–2327 (2011)

144. Chorkendorff, I., Niemantsverdriet, J.W.: Concepts of Modern Catalysis and Kinetics. (2003)

145. Purón, H., Pinilla, J.L., Berrueco, C., Montoya De La Fuente, J.A., Millán, M.: Hydrocracking of maya vacuum residue with NiMo catalysts supported on mesoporous alumina and silica-alumina. Energy and Fuels. 27, 3952–3960 (2013)

146. Altajam, M.A., Ternan, M.: Hydrocracking of Athabasca bitumen using Co-Mo catalysts supported on wide pore carbon extrudates. Fuel. 68, 955–960 (1989)

147. Varde, N., Fogler, H.S.: Asynchronous learning of chemical reaction engineering. Chem. Eng. Educ. 35, 290–295 (2001)

148. Hossain, M.M., de Lasa, H.I.: Reduction and oxidation kinetics of Co-Ni/Al2O3 oxygen carrier involved in a chemical-looping combustion cycles. Chem. Eng. Sci. 65, 98–106 (2010)

149. Vicens, J., Böhmer, V.: Calixarenes: a versatile class of macrocyclic compounds. Kluwer Academic Publishers, Dordrecht/Boston/London (1991)

150. Benevelli, F., Kolodziejski, W., Wozniak, K., Klinowski, J.: Solid-state NMR studies of alkali metal ion complexes of p-tertbutyl-calixarenes. Chem. Phys. Lett. 308, 65–70 (1999)

151. Chaabane, R. Ben, Gamoudi, M., Guillaud, G., Jouve, C., Lamartine, R., Bouazizi, A., Maaref, H.: Study of the membrane morphology and investigation of sensitivity to ions for sensors based on calixarenes. Sensors Actuators, B Chem. 31, 41–44 (1996)

152. Graham, B.F., Harrowfield, J.M., Tengrove, R.D.: Evidence of a Host : Guest Complex between p-t-Butylcalix [4] arene and Carbon Dioxide ∗. J. Incl. Phenom. Macrocycl. Chem. 43, 179–182 (2002)

153. Adhikari, B.B., Gurung, M., Chetry, A.B., Kawakita, H., Ohto, K.: Highly selective and efficient extraction of two Pb2+ ions with a p-tert-butylcalix[6]arene hexacarboxylic acid ligand: An allosteric effect in extraction. RSC Adv. 3, 25950–25959 (2013)

154. Zahir, H.: Synthesis and Characterization of Trivalent Cerium Complexes of p-tert-Butylcalix [4,6,8]Arenes: Effect of Organic Solvents. J. Chem. 2013, 1–6 (2013)

155. Amiri, A., Babaeiez, F., Monajjemi, M.: Vibrational Analysis of P-Tert-Butyl-Calix[4]Arene Conformers by Ab Initio Calculations. Phys. Chem. Liq. 46, 397–398 (2008)

156. Opaprakasit, P., Scaroni, A., Painter, P.: Intramolecular hydrogen bonding and calixarene-like structures in p-cresol/formaldehyde resins. J. Mol. Struct. 570, 25–35 (2001)

157. Furer, V.L., Borisoglebskaya, E.I., Kovalenko, V.I.: Band intensity in the IR spectra and conformations of calix[4]arene and thiacalix[4]arene. Spectrochim. Acta - Part A Mol. Biomol. Spectrosc. 61, 355–359 (2005)

158. Chennakesavulu, K., Basariya, M.R., Sreedevi, P., Bhaskar Raju, G., Prabhakar, S., Rao, S.S.: Study on thermal decomposition of calix[4]arene and its application in thermal stability of polypropylene. Thermochim. Acta. 515, 24–31 (2011)

159. Brodskii, A.I., Kotorlenko, L.A., Samoilenko, S.A., Pokhodenko, V.D.: IR spectra of screened phénols, phenol radicals, quinone and cyclohexanedione. J. Appl. Spectrosc. 14, 633–638 (1971)

160. Guzzo, R.N., Jakeline Cunha Rezende, M., Kartnaller, V., Walkimar de Carneiro, J.M., Stoyanov, S.R., Moreira da Costa, L.: Experimental and DFT evaluation of the 1 H and 13 C NMR chemical shifts for calix[4]arenes. J. Mol. Struct. J. 1157, 97–105 (2018)

161. Adhikari, B.B., Gurung, M., Kawakita, H., Ohto, K.: Cation complexation with p-tert-butylcalix[5]arene pentacarboxylic acid derivative: An allosteric regulation of the first metal ion for stepwise extraction of the second ion. Analyst. 136, 3758–3769 (2011)

162. Fulmer, G.R., Miller, A.J.M., Sherden, N.H., Gottlieb, H.E., Nudelman, A., Stoltz, B.M., Bercaw, J.E., Goldberg, K.I.: NMR chemical shifts of trace impurities: Common laboratory solvents, organics, and gases in deuterated solvents relevant to the organometallic chemist. Organometallics. 29, 2176–2179 (2010)

163. Deligöz, H., Özen, Ö., Çilgi, G.K.: Structural analysis of calix[n]arene-iron(III) complexes (n=4,6,8) and thermal decomposition of the parent calix[n]arenes. J. Coord. Chem. 60, 73–83 (2007)

164. Deligöz, H., Özen, Ö., Çilgi, G.K., Çetişli, H.: A study on the thermal behaviours of parent calix[4]arenes and some azocalix[4]arene derivatives. Thermochim. Acta. 426, 33–38 (2005)

165. Chennakesavulu, K., Raviathul Basariya, M., Bhaskar Raju, G., Prabhakar, S.: Study on thermal decomposition of calix[6]arene and calix[8]arene. J. Therm. Anal. Calorim. 103, 853–862 (2011)

166. Quitian, A., Leyva, C., Ramírez, S., Ancheyta, J.: Exploratory study for the upgrading of transport properties of heavy oil by slurry-phase hydrocracking. Energy and Fuels. 29, 9–15 (2015)

167. Wiehe, I.A.: A phase separation kinetic model for coke formation. Prepr. - Am. Chem. Soc. Div. Pet. Chem. 38, 428–433 (1993)

168. Sheu, E.Y., Mullins, O.C.: Asphaltenes. Springer US, Boston, MA (1995)

169. Marson, A., Freixa, Z., Kamer, P.C.J., Van Leeuwen, P.W.N.M.: Chiral calix[4]arene-based diphosphites as ligands in the asymmetric hydrogenation of prochiral olefins. Eur. J. Inorg. Chem. 2007, 4587–4591 (2007)

170. Kim, S.H., Kim, K.D., Lee, H., Lee, Y.K.: Beneficial roles of H-donors as diluent and H-shuttle for asphaltenes in catalytic upgrading of vacuum residue. Chem. Eng. J. 314, 1–10 (2017)

171. Mousavi-Dehghani, S.A., Riazi, M.R., Vafaie-Sefti, M., Mansoori, G.A.: An analysis of methods for determination of onsets of asphaltene phase separations. J.

Pet. Sci. Eng. 42, 145–156 (2004)

172. Speight, J.G.: Petroleum asphaltenes - Part 1: Asphaltenes, resins and the structure of petroleum. Oil Gas Sci. Technol. 59, 467–477 (2004)

173. Speight, J.G.: The chemical and physical structure of petroleum: Effects on recovery operations. J. Pet. Sci. Eng. 22, 3–15 (1999)

174. Nguyen, T.M., Jung, J., Lee, C.W., Cho, J.: Effect of asphaltene dispersion on slurry-phase hydrocracking of heavy residual hydrocarbons. Fuel. 214, 174–186 (2018)

175. Yang, M.G., Nakamura, I., Fujimoto, K.: Hydro-thermal cracking of heavy oils and its model compound. Catal. Today. 43, 273–280 (1998)

176. Ancheyta, J., Rana, M.S., Furimsky, E.: Hydroprocessing of heavy petroleum feeds: Tutorial, (2005)

177. LaMarca, C., Libanati, C., Klein, M.T., Cronauer, D.C.: Enhancing Chain Transfer during Coal Liquefaction: A Model System Analysis. Energy and Fuels. 7, 473–478 (1993)

178. Cyr, T., Lewkowicz, L., Ozum, B., Lott, R.K., Lee, L.-K.: Hydrocracking process involving colloidal catalyst formed in situ, (1996)

179. Gray, M.R., McCaffrey, W.C.: Role of chain reactions and olefin formation in cracking, hydroconversion, and coking of petroleum and bitumen fractions. Energy and Fuels. 16, 756–766 (2002)

180. Schmidt, E., Song, C., Schobert, H.H.: Hydrotreatment of 4-(1-Naphthylmethyl) bibenzyl in the Presence of Iron Catalysts and Sulfur. Energy & fuels. 10, 597–602 (1996)

181. Rueda, N., Bacaud, R., Vrinat, M.: Highly dispersed, nonsupported molybdenum sulfides. J. Catal. 169, 404–406 (1997)

182. Yang, T., Jie, Y., Li, B., Kai, X., Yan, Z., Li, R.: Catalytic hydrodeoxygenation of crude bio-oil over an unsupported bimetallic dispersed catalyst in supercritical ethanol. Fuel Process. Technol. 148, 19–27 (2016)

183. Manek, E., Haydary, J.: Hydrocracking of vacuum residue with solid and dispersed phase catalyst: Modeling of sediment formation and hydrodesulfurization. Fuel Process. Technol. 159, 320–327 (2017)

184. Sanford, E.C., Steer, J.G., Muehlenbachs, K., Gray, M.R.: Residuum Hydrocracking with Supported and Dispersed Catalysts: Stable Hydrogen and Carbon Isotope Studies on Hydrogenation and Catalyst Deactivation. Energy and Fuels. 9, 928–935 (1995)

185. Faraji, D., Sadighi, S., Mazaheri, H.: Modeling and Evaluating Zeolite and

Amorphous Based Catalysts in Vacuum Gas Oil Hydrocracking Process. Int. J. Chem. React. Eng. 16, (2018)

VITAE

Name : Tareq Ali Salem Al-Attas

Date of Birth : 11/14/1993

Email : tareq.attas@gmail.com

Address : Al-Ahsa (Hofuf) 31982, Saudi Arabia

Academic Background :

Master of Science, Chemical Engineering (2016-2018)
King Fahd University of Petroleum and Minerals

Bachelor of Science, Chemical Engineering (2012-2016)
King Fahd University of Petroleum and Minerals

Journal Publications :

- **T.A. Al-Attas**, M.H. Zahir, S.A. Ali, S.A. Al-Bogami, Z.O. Malaibari, S.A. Razzak, M.M. Hossain, Novel (Co-, Ni)-*p-tert*-Butylcalix[4]arenes as Dispersed Catalysts for Heavy Oil Upgrading: Synthesis, Characterization and Performance Evaluation, Energy & Fuels. 33 (2018) 561-573. doi:10.1021/acs.energyfuels.8b03619.
- **T.A. Al-Attas**, M.H. Zahir, S.A. Ali, S.A. Al-Bogami, Z. Malaibari, S.A. Razzak, M.M. Hossain, Kinetics of the synergy effects in heavy oil upgrading using novel Ni-*p-tert*-butylcalix[4]arene as a dispersed catalyst with a supported catalyst, Fuel Process. Technol. 185 (2019) 158–168. doi:10.1016/j.fuproc.2018.12.003.
- **T.A. Al-Attas** and Hossain MM. (2019). Apparent Kinetics of Co-Gasification of Biomass and Vacuum Gas Oil (VGO). *To be submitted*.
- Ahmed Al-Rashidy, **T.A. Al-Attas**, Ali SA, Al-Bogami SA, Razzak SA, Hossain MM. (2019). Water-Soluble (Fe-Mo and Ni-Mo) and Oil-Soluble (Ni-LTM and Co-LTM) as Dispersed Catalysts for Hydrocracking of LVGO: Activity and Kinetics. *To be submitted.*

Conference Publications :

- **Al-Attas Tareq A.**, Bdwi EAS, Ali SA, Al-Bogami SA, Hossain MM. (Nov 12-13, 2018). Oil-Soluble Dispersed Catalysts for Slurry-Phase Hydrocracking of Heavy VGO. The 28th Annual Saudi-Japan Symposium, KFUPM, Dhahran, Saudi Arabia.
- **Al-Attas Tareq A.**, Bdwi EAS, Ali SA, Al-Bogami SA, Hossain MM. (May 2018). Promotional Effects of Oil-Soluble Dispersed Metal-Based Catalyst on Hydrocracking of VGO. The 9th Annual KFUPM Students Scientific Forum, KFUPM, Dhahran, Saudi Arabia.

Patents :

- Mohammad M. Hossain, Md Hasan Zahir, **Tareq A. Al-Attas**. Catalytic Hydrocracking of vacuum gas oil (VGO) over Metal-Based *p-tert*-Butylcalix[4]arenes. *Submitted in May 2018. Patent pending.*
- Mohammad M. Hossain and **Tareq A. Al-Attas**. Co-Gasification of Biomass and Vacuum Gas Oil (VGO). *Submitted in March 2018. Patent pending.*